AD-A032 368 NAVAL POSTGRADUATE SCHOOL MONTEREY CALIF F/G 8/3

NUMERICAL INVESTIGATION OF THE DYNAMICS OF SEA OF MARMARA.(U)

SEP 76 H YUCE

UNCLASSIFIED NL

1 OF 2

AD A032368

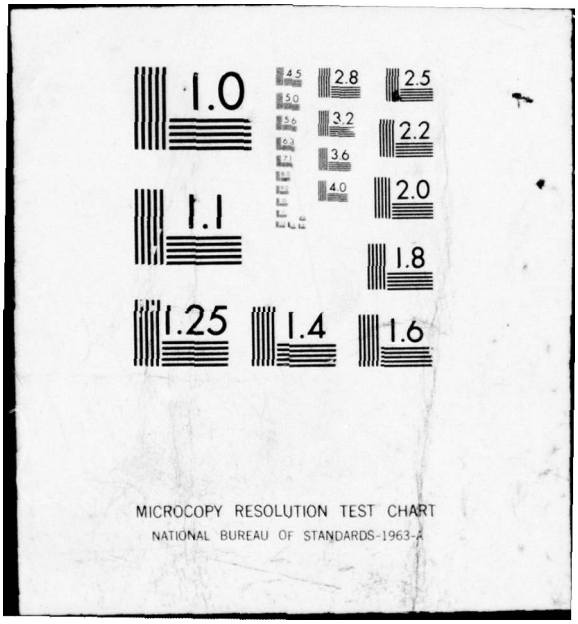
1.0
1.1
1.25
1.4
1.6
1.8
2.0
2.2
2.5
2.8
3.2
3.6
4.0
4.5
5.0
5.6
MICROCOPY RESOLUTION TEST CHART
NATIONAL BUREAU OF STANDARDS-1963-A

(2)

N.U

NAVAL POSTGRADUATE SCHOOL
Monterey, California

THESIS

NUMERICAL INVESTIGATION OF
THE
DYNAMICS OF SEA OF MARMARA

by

Huseyin Yuce

September 1976

Thesis Advisor: J. B. Wickham

SECURITY CLASSIFICATION OF THIS PAGE (When Data Entered)

REPORT DOCUMENTATION PAGE		READ INSTRUCTIONS BEFORE COMPLETING FORM
1. REPORT NUMBER	2. GOVT ACCESSION NO.	3. RECIPIENT'S CATALOG NUMBER (9)
4. TITLE (and Subtitle) (6) Numerical Investigation of the Dynamics of Sea of Marmara.		5. TYPE OF REPORT & PERIOD COVERED Master's Thesis, September 1976
		6. PERFORMING ORG. REPORT NUMBER
7. AUTHOR(s) (10) Huseyin Yuce		8. CONTRACT OR GRANT NUMBER(s)
9. PERFORMING ORGANIZATION NAME AND ADDRESS Naval Postgraduate School Monterey, California 93940		10. PROGRAM ELEMENT, PROJECT, TASK AREA & WORK UNIT NUMBERS (12) 123p.
11. CONTROLLING OFFICE NAME AND ADDRESS (11) Naval Postgraduate School Monterey, California 93940		12. REPORT DATE September 1976 13. NUMBER OF PAGES 124
14. MONITORING AGENCY NAME & ADDRESS(if different from Controlling Office) Naval Postgraduate School Monterey, California 93940		15. SECURITY CLASS. (of this report) Unclassified 15a. DECLASSIFICATION/DOWNGRADING SCHEDULE

16. DISTRIBUTION STATEMENT (of this Report)

Approved for public release; distribution unlimited.

17. DISTRIBUTION STATEMENT (of the abstract entered in Block 20, if different from Report)

18. SUPPLEMENTARY NOTES

19. KEY WORDS (Continue on reverse side if necessary and identify by block number)

Sea of Marmara
Turkish Straits
Regional Circulation Models

20. ABSTRACT (Continue on reverse side if necessary and identify by block number)

Dynamics of the circulation in the Sea of Marmara are investigated with a time dependent, three dimensional numerical model. The empirically inferred hydrologic regimes of the sea and connective straits are discussed.

A baroclinic model based on the primitive equations is solved by direct integration of an initial value problem. → (cont'd p 2)

DD FORM 1 JAN 73 1473 (Page 1) EDITION OF 1 NOV 65 IS OBSOLETE S/N 0102-014-6601 |

251 450

SECURITY CLASSIFICATION OF THIS PAGE (When Data Entered)

(cont'd from p 1)

The circulation in the sea is driven by surface forces that simulate wind stress and horizontal pressure gradient forces related to internal stratification.

The predicted density field, in sigma-t units, is compared with data. Detailed three dimensional horizontal velocity patterns and vertical velocity patterns in horizontal planes are given.

Bottom friction, irregular bottom topography, non-linear terms in the momentum equation and vertical mean part of the horizontal velocity have been omitted. For simplicity density is predicted in place of temperature and salinity.

DD Form 1473
1 Jan 73
S/N 0102-014-6601

Numerical Investigation of the Dynamics of Sea of Marmara

by

Huseyin Yuce
Lieutenant, Turkish Navy
Turkish Navy Academy, 1970

Submitted in partial fulfillment of the requirements for the degree of

MASTER OF SCIENCE IN OCEANOGRAPHY

from the

NAVAL POSTGRADUATE SCHOOL
September 1976

Author Hüseyin Yüce

Approved by: J. B. Wickham
Thesis Advisor

Robert C. Harney
Second Reader

Dale F. Leipper
Chairman, Department of Oceanography

J. R. Borsting
Academic Dean

ABSTRACT

Dynamics of the circulation in the Sea of Marmara are investigated with a time dependent, three dimensional numerical model. The empirically inferred hydrologic regimes of the sea and connective straits are discussed.

A baroclinic model based on the primitive equations is solved by direct integration of an initial value problem. The circulation in the Sea is driven by surface forces that simulate wind stress and horizontal pressure gradient forces related to internal stratification.

The predicted density field, in sigma-t units, is compared with data. Detailed three dimensional horizontal velocity patterns and vertical velocity patterns in horizontal planes are given.

Bottom friction, irregular bottom topography, non-linear terms in the momentum equation and vertical mean part of the horizontal velocity have been omitted. For simplicity density is predicted in place of temperature and salinity.

TABLE OF CONTENTS

LIST OF TABLES

LIST OF FIGURES

Figure

ACKNOWLEDGEMENTS

The author wishes to express his appreciation for the guidance and assistance given by Professor J. B. Wickham. He is also indebted to Professor R. L. Haney who generously shared his experience in the field of modelling in numerous invaluable discussions and timely encouragement throughout the entire study.

He is grateful to Lieutenant Commander Mustafa Dogusal, Turkish Navy, who made available all data for use in this study.

Thanks go to the staff of the W. R. Church Computer Center whose patience and understanding was greatly appreciated.

Finally, thanks to his wife, Fatos, for her faith, encouragement and understanding, to his young boys, Kerem, Erhan, for all their efforts which made this study possible.

I. INTRODUCTION

There is an intense growing interest in recent years in the development of simulation of hydrological conditions in coastal waters and smaller adjacent seas. Advancement in modern technology requires much greater accuracy than can be obtained by the use of classical instrumentation and measurement techniques only. Due to the discontinuous nature of such observations these measurements can provide the basis for analysis of the current system, temperature, salinity and other variables on a climatological basis. But climatological conditions are not accurate enough in coastal waters for uses such as construction, navigation, tracing of pollutants, mining effluent, oil spills, search and rescue operations, agriculture, etc. It is also true that sampling the ocean adequately whether for exploratory or research purpose is a major problem. Great short-term variability of conditions in coastal waters makes it even more difficult to make adequate representative measurements.

As a result, in addition to the classical methods of analyses of current systems, determination of salinity and temperature distributions etc., new simulation techniques which were applied long before synoptic numerical weather prediction received much more attention (T. Levastu, S. Larson and K. Rabe, 1976).

The objective of this study is to develop a regional circulation model of the Sea of Marmara. The circulation and density distribution, in sigma-t units, in that sea are simulated by a nine-level numerical model with an horizontal flat bottom at 1000 m depth. The motion is driven by prescribed wind stress and horizontal pressure gradient forces due to internal stratification.

II. PHYSICAL GEOGRAPHY AND HYDROLOGY OF THE SEA OF MARMARA

The Sea of Marmara is a small sea located between Asia Minor and Europe and occupies the main part of the Turkish straits system (210 km). The Strait of Canakkale (Dardanelles) (60 km) connects the Sea of Marmara to the Mediterranean and through the Strait of Istanbul (Bosporus) (30 km) it is connected to the Black Sea at the North. (Figure 1)

The structure of the basin which is small in area (about 11000 km^2) is associated with the Anatolicin fault which lies along its bottom to the North. The trough passing along the Northern deep slope consists of three depressions (max. 1380 m). These three basins are separated by low connecting sills. A shallow trough lies at the foot of the continental slope which is well pronounced only in the easternmost part of the sea. At the South it becomes shallower having depths of the order 60–80 m. Minimum depths at the Strait of Canakkale and Strait of Istanbul are 57 and 37 m; they have mean widths 4.5 km and 0.7 km and average lengths 60 and 30 km, respectively.

The climate of the Sea of Marmara is influenced by the regional atmospheric circulation system of the Eastern Mediterranean, the Black Sea and Asia Minor Peninsula. During the summer, the Eastern Mediterranean basin is under the

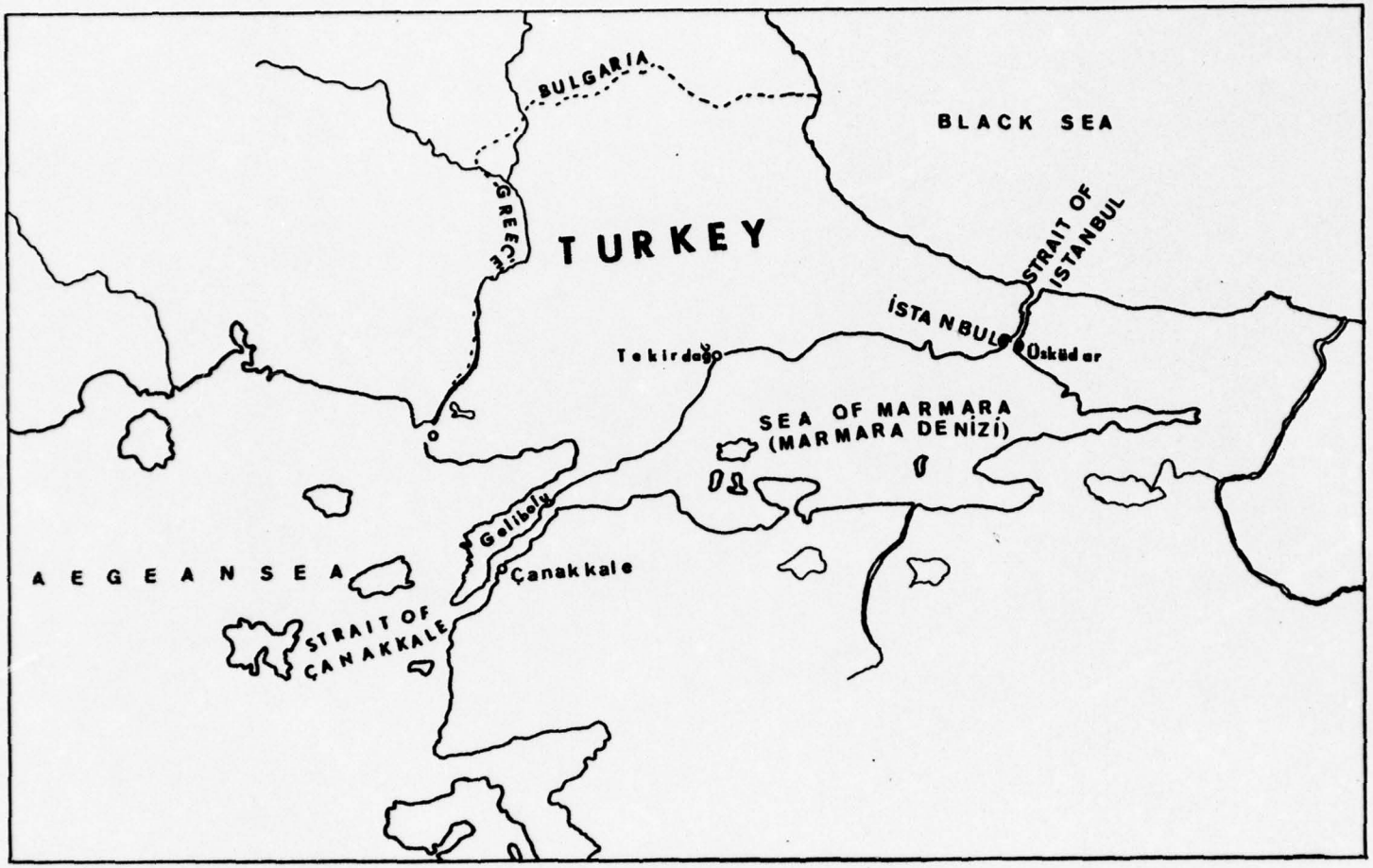

Figure 1. Location map of the Sea of Marmara.

influence of a stable wind system which is called "Etesian" wind. Etesians are monsoon-like and associated with a quasi-stationary cyclonic circulation above the Asia Minor Peninsula during summer. The active period of the Etesian winds falls almost entirely within the summer season (approximately from May to October). There are two maximums, which are pronounced during July and August. These Etesian winds, which are dry winds and generally northerly or northeasterly from the Black Sea, have diurnal variability.

Southerly winds bring warm and humid air to the area during winter. When these southerly winds are sufficiently strong, they produce storm waves and surges along the coast of Marmara and at the entrance to the Strait of Istanbul (Gunnerson and Ozturgut, 1974).

The hydrological regime of the Sea of Marmara is largely determined by the water exchange between the Mediterranean and Black Seas through the connective straits, Strait of Canakkale, and Strait of Istanbul. Problems of water exchange, vertical mixing and hydrological characteristics of the currents in these straits and in the Sea of Marmara have been the subject of many extensive studies conducted by the Turkish Navy Hydrographic Office and by the University of Istanbul. In addition to these fundamental and frequent studies there were some investigations conducted by German, Russian and English investigators at the end of the 19th and beginning of the 20th century. Recent studies and observations, if connected to old data and observations, can give

a better understanding of the complete regional oceanographic condition.

These studies are mainly concentrated on the Strait of Istanbul and the vicinity of this strait. This is due to the importance of this strait as a link in the connection between the Black Sea and the Mediterranean Sea through the Sea of Marmara. This makes it an important factor controlling Black Sea chemistry, biology, sedimentation, etc.

Based on the first detailed survey of Makarov and Merz 1917–18, in Moller (1928), and subsequent studies of Ullyott and Ilgaz (1946), Pektas (1956), A. K. Bogdanova (1961, 1965), C. G. Gunnerson and E. Ozturgut (1974) and others, the main properties of this straits' system and its vicinities are fairly well understood.

One of the main characteristics of these straits is a two–layer structure of the current, which is determined by the differences between the relatively fresh water of the Black Sea and saline water from the Mediterranean which occupies the depths of the Sea of Marmara and forms the bottom water of two connective straits (Figure 2). Other external factors such as wind, water level drop along the straits, water balance, topographic influences and the depth and width of the straits also must be considered. The scale of the motion and complexity of these factors make it difficult to determine the current system mathematically.

Another main characteristic of these straits is the two–layer stratification of water which is associated with the

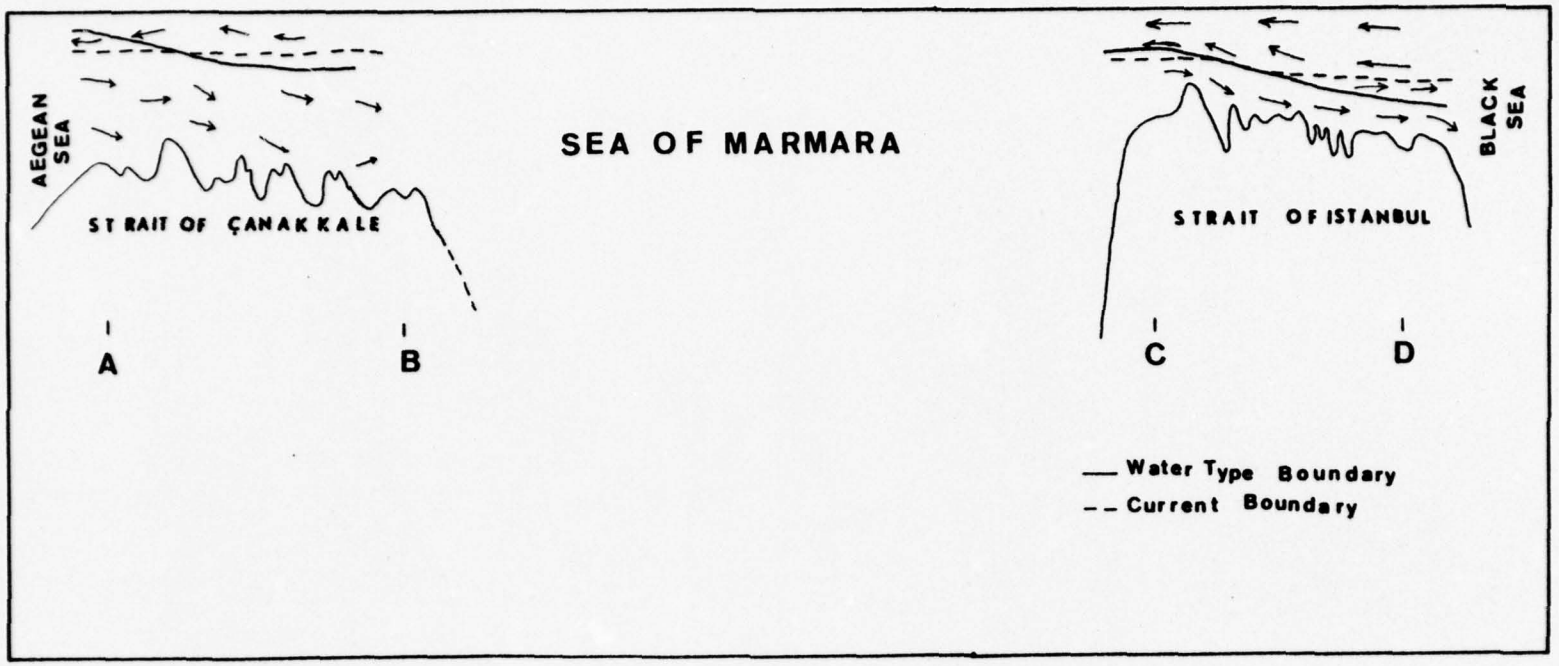

Figure 2. Schematic diagram of water stratification and current system at two connective straits which are important in determining the hydrological condition of Sea of Marmara.

two-layer current system. This stratification is also a consequence of the water mass differences at the two ends of the straits.

Detailed observations of temperature and salinity distributions indicate certain features of the diffusion of the Mediterranean water into the Black Sea. This water flows North through the Strait of Istanbul from the Sea of Marmara. It is shown by Bogdanova (1961, 1965) that this underflow of Mediterranean water into the Black Sea is present throughout the year and descends to significant depths in the Black Sea.

This water exchange through the straits system fluctuates according to seasons, years and periods. This is very important for the hydrologic regimes of the Sea of Marmara and the Black Sea. Water level differences, given with the following expression, are mainly due to excess precipitation over evaporation and river runoff in the Black Sea.

$$\Delta h = Z_B - Z_M \tag{1.1}$$

Δh : sea level differential between Black Sea and Mediterranean

Z_B : water level of Black Sea

Z_M : water level of Mediterranean

Sea level differential (Δh) is always positive and fluctuates with time. It can be expressed in two components

$$\Delta h = \overline{\Delta h} + (\Delta h)' \tag{1.2}$$

where

$\overline{\Delta h}$: average sea level differential

$(\Delta h)'$: fluctuating part of sea level differential [$(\Delta h)' \propto f(t)$]

According to Bogdanova (1965) $\overline{\Delta h}$ has a value 42 cm based on the long term observations. The fluctuating part of the sea level differential and total level differential are given in Table I.

TABLE I.

Monthly average fluctuation sea level differential and sea level differential.[1]

Month	I	II	III	IV	V	VI	VII	VIII	IX	X	XI	XII
$(\Delta h)'$(cm)	1	0	3	7	11	15	6	0	−5	−7	−7	−4
Δh (cm)	43	42	45	49	53	57	48	42	37	35	35	38

([1]Based on the data given by Bogdanova, 1965)

The maximum change is

$$\frac{\partial}{\partial t} (\Delta h)_{max} = \frac{\partial}{\partial t} (\Delta h')_{max} = - 9 \text{ cm/month},$$

observed during approximately June. This falls approximately in a period when continental runoff begins to decrease. The fluctuating sea level differential increases from March to July. As a consequence during this period the upper current becomes stronger and the lower current becomes weaker. From

August to November sea level fluctuation decreases and begins to increase again from August to February. The upper current of the Strait of Istanbul becomes weaker and the lower current becomes stronger.

According to Bogdanova's (1965) observations the maximum Δh value is observed during June and has a value 57 cm; the minimum Δh value 35 cm is observed during October and November.

The average sea level differential between the Black Sea and the Sea of Marmara is about 35 cm which is six times Moller's (1928) estimate (Gunnerson and Ozturgut, 1974).

There is a characteristic stratification with a sharp density transition layer over the whole area. The sharpness is more pronounced at the North at the Strait of Istanbul. A cross section of sigma-t values for the Strait of Istanbul is shown in Figure 3. Fresh warm water of the Black Sea lies in a surface layer 15-20 m thick at Istanbul. This water which is mainly river runoff and excess precipitation overrides the Mediterranean water which is cold and dense. The wedge form of the upper water shows clearly in this strait, but this is not true for the Strait of Canakkale. On the other hand, the wedge form of the lower water is comparatively stronger and more pronounced in the Strait of Canakkale due to the downward sloping of the sea bed toward the North in the Strait of Istanbul. Average sigma-t values for surface and bottom water are 13.5 and 27.5. (Defant, 1961)

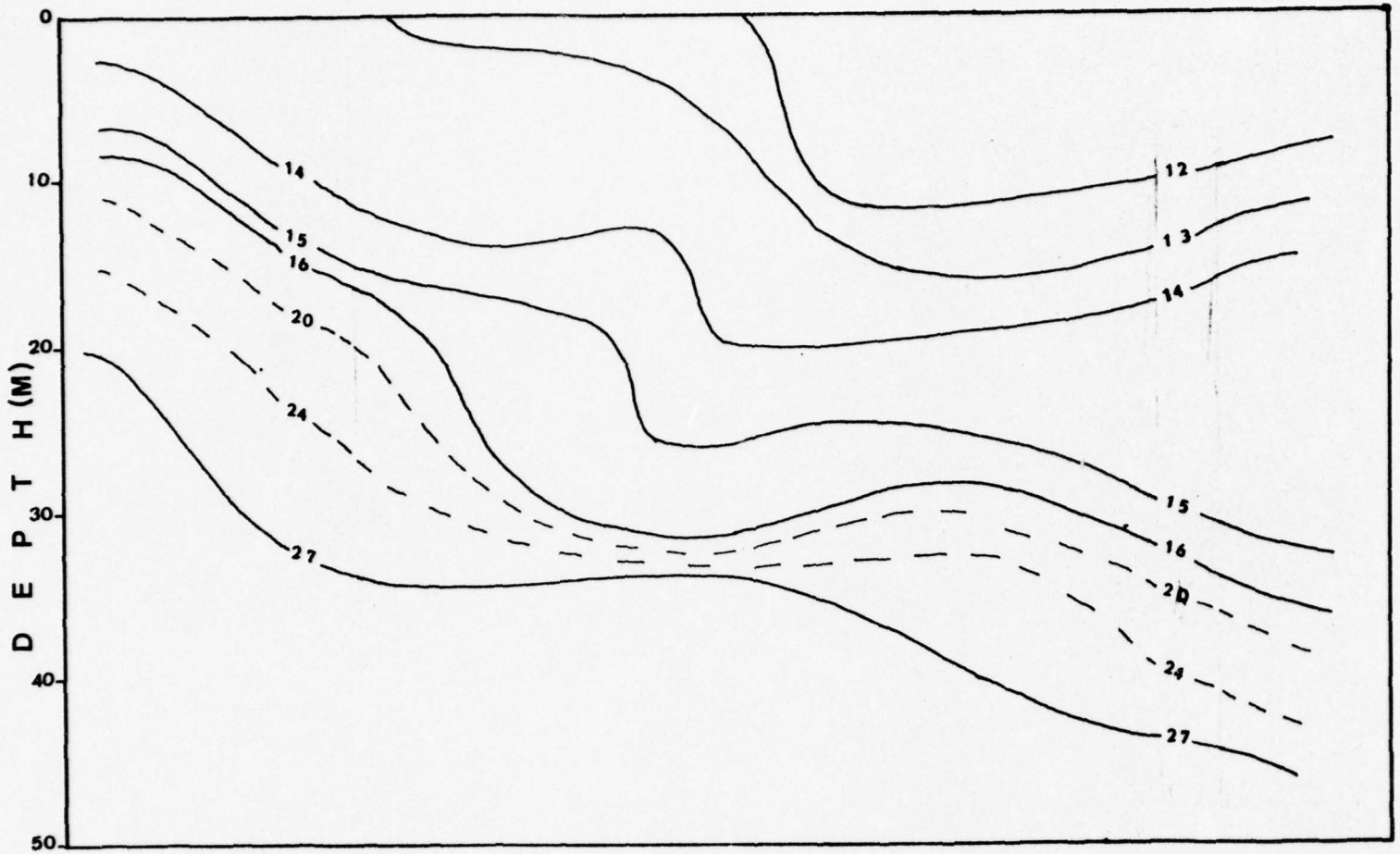

Figure 3. Sigma–t cross section of Strait of Istanbul (between C–D points).

According to Gunnerson and Ozturgut (1974), the average salinity of Black Sea waters at a station 9 km from the Northern entrance of the Strait of Istanbul was approximately 17.5 °/oo for an observation period July 1966 to December 1967. Lower values were observed (16–17 °/oo) from July 17 to August 23, 1967. This lower surface salinity reflects maximum discharge of rivers into the Black Sea. Higher average surface salinities (17.5 – 19.0 °/oo) were observed for the rest of the year and extreme values (as high as 25 °/oo) during winter months. These were due to the favorable conditions for Mediterranean water to flow northward. These conditions include small differences between the levels of the Black Sea and the Mediterranean and southerly or southwesterly winds over the Sea of Marmara and Strait of Istanbul. At the midpoint the average salinity in the lower layer is approximately 38.5 °/oo and in the surface layer 17.5 °/oo. A salinity cross section is given in Figure 4.

Warm and fresh Black Sea water can be identified easily from the temperature cross-section which is given in Figure 5. Below this warm fresh water of the Black Sea cold intermediate water of Sea of Marmara can be observed. Mediterranean water occupies the deep bottom layer of the Strait of Istanbul.

The dynamics of the processes occurring in these two straits is determined by the wind stress over the straits and the drop of the sea levels and densities at the end of the straits. The main driving forces are gradient of water

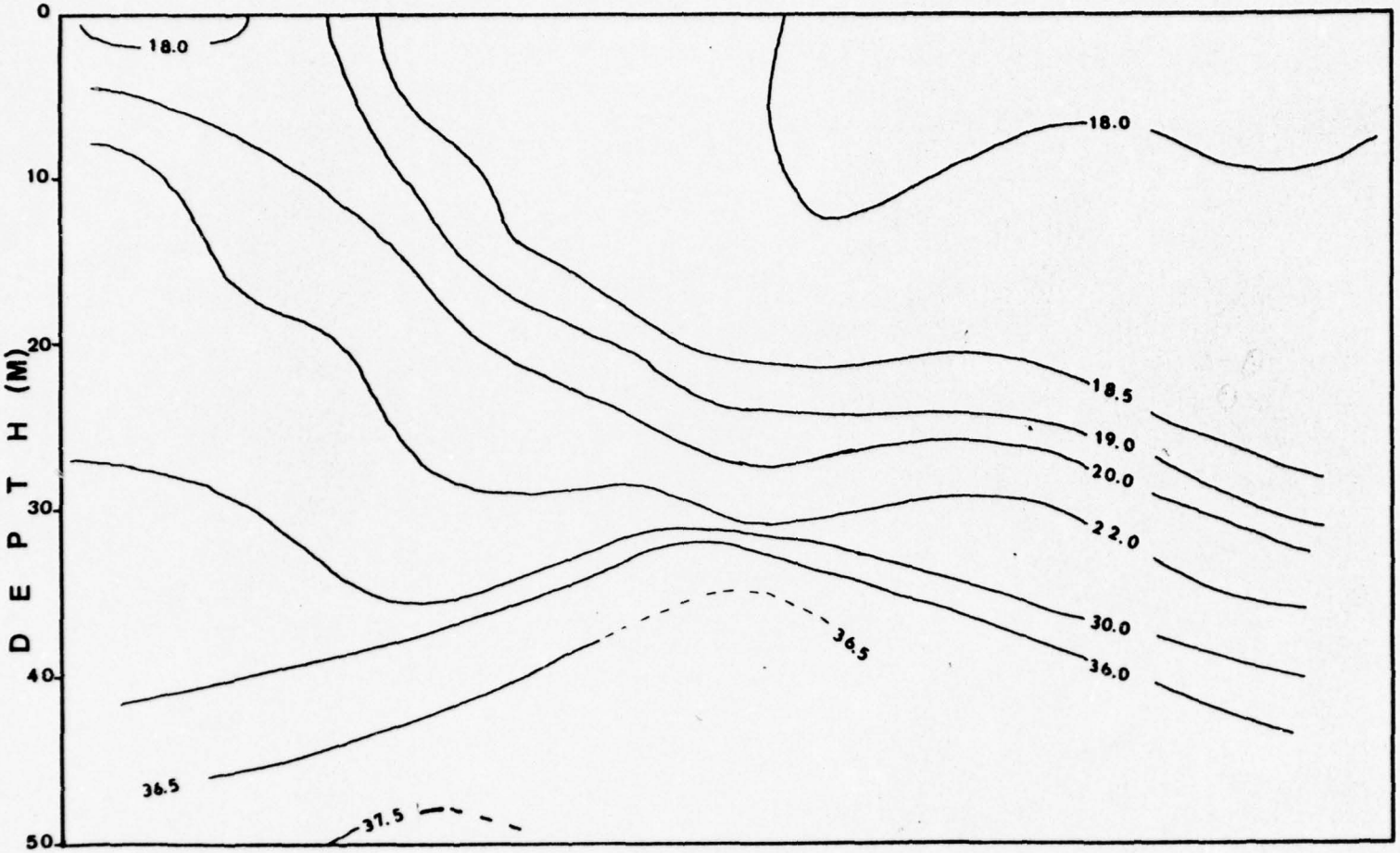

Figure 4. Salinity cross section of Strait of Istanbul (between C–D points).

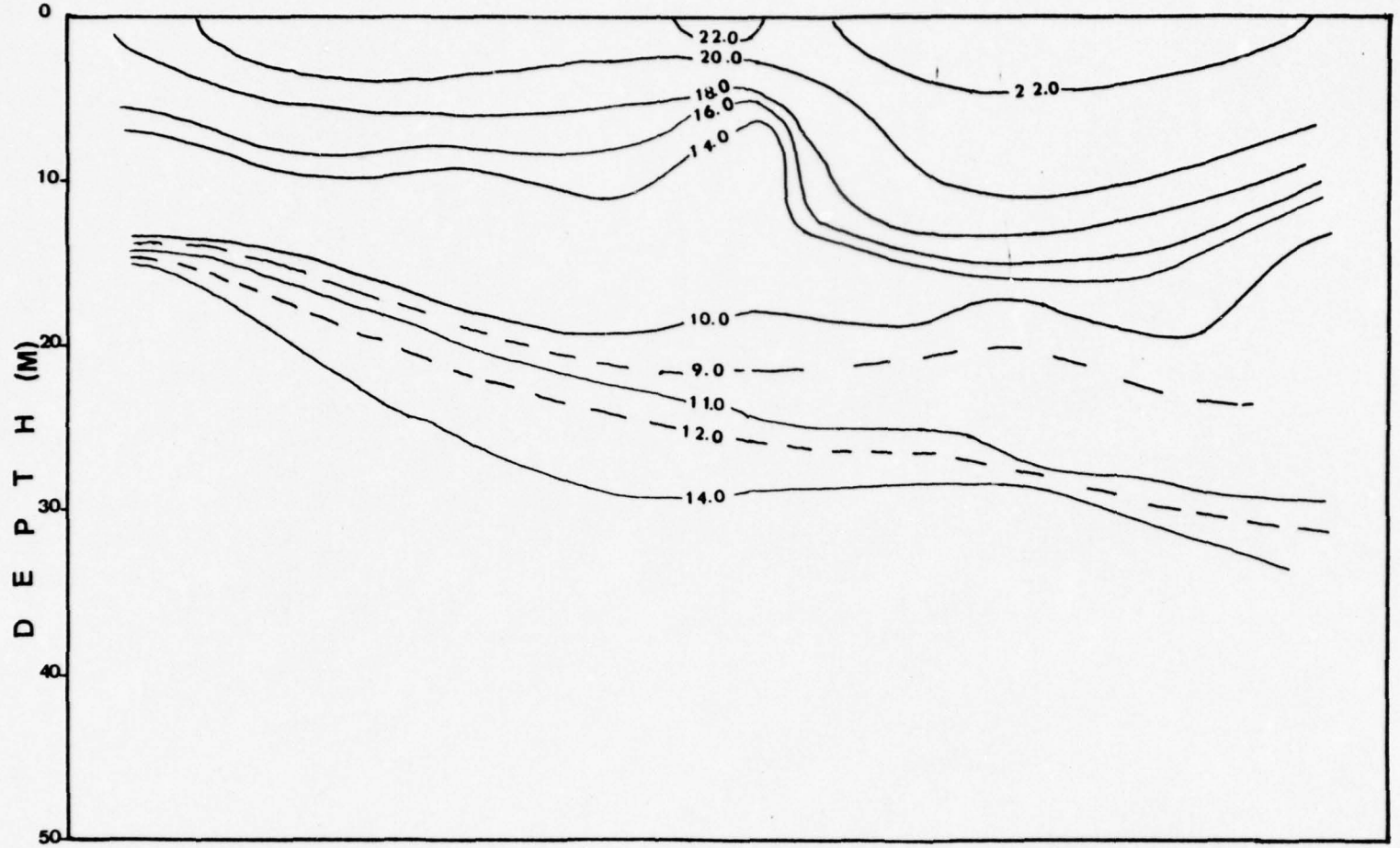

Figure 5. Temperature cross section of Strait of Istanbul (between C–D points).

level, thermohaline forcing, wind force exerted on the surface and coriolis force.

According to observations the boundary between the water masses generally does not coincide with the boundary between currents. The boundary between water masses has a greater slope than the boundary between currents (Defant, 1961). This is probably due to diffusion processes occurring at the current boundary and to the nature of the current (Figure 2).

The average Black Sea inflow and outflow through the Straits of Istanbul according to the analysis of Moller (1928) are 6,100 and 12,600 m^3/sec, respectively (Gunnerson and Ozturgut, 1974). Velocity is greatest at the sea surface and decreases rapidly with depth and laterally; it increases from North to South. Under normal conditions it is 40–50 cm/sec at the entrance of the strait and 150 cm/sec at the South end. The lower current is strongest in the central part of the lower water which is at about 16 m from the bottom in the Strait of Istanbul and 45 m in the Strait of Canakkale. These velocities are 100–150 cm/sec and 25 to 10 cm/sec respectively (Defant, 1961).

In general in the Sea of Marmara there is Black Sea water at the surface and Mediterranean water at the bottom. This is the normal state. Except for times when very strong southerly winds bring bottom water to the surface and cause wind mixing these two main water types are both present with a very thin intermediate water layer. The Black Sea water extends to a depth of 15–20 m in the vicinity of the Strait

of Istanbul and becomes shallower farther south. There is intermediate water between these two water types which extends at most to about 50–60 m. Below this the basin is filled with Mediterranean water as shown in Figures 6,7 and 8. This water has a temperature 14.9°C, salinity 38.55 °/oo and sigma–t 28.75, approximately in June.

Surface water has a large annual variability. On the other hand bottom water does not. Due to the described oceanographic conditions bottom water is almost isolated from surface processes and has a large time–scale of variability compared to surface water. Average inflow and outflow rates at the straits give approximately 30 years for "turnover" time or "flushing" time for bottom water and 200 days for surface water.

Based on the same rates a typical value for the vertical mean current $|\bar{u}|$ is 10^{-2} cm sec^{-1}. A characteristic magnitude for horizontal velocity $|u|$ using the thermal wind relation is 4 cm sec^{-1}. Due to the large isolated reservoir of Mediterranean water of almost uniform characteristics in the lower part of the basin, the thermohaline circulation is confined to the upper 50–60 m.

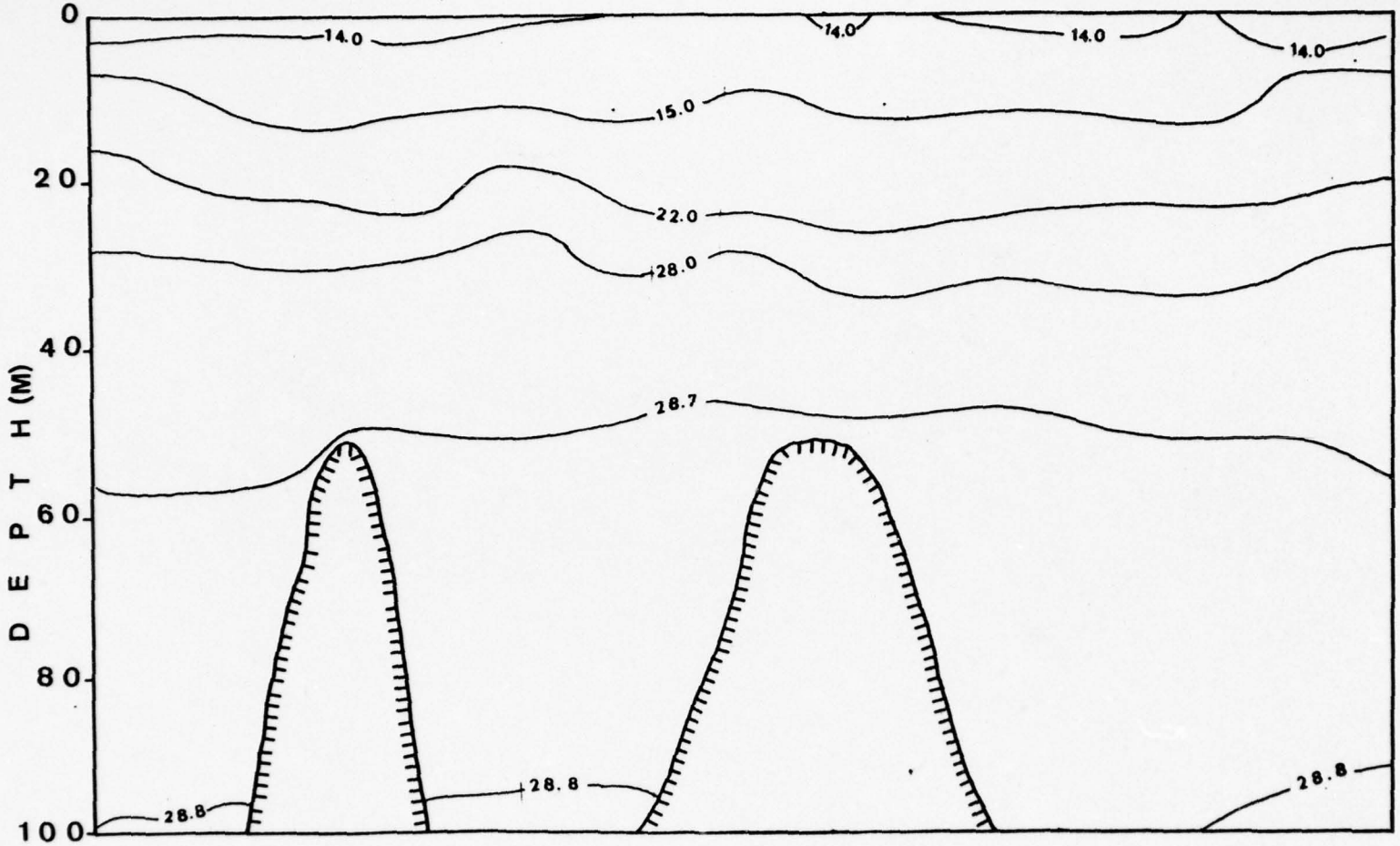

Figure 6. Sigma-t cross section of Sea of Marmara for upper 100 meters. Section is taken between Strait of Canakkale and Strait of Istanbul (approximately B-C point in figure 2).

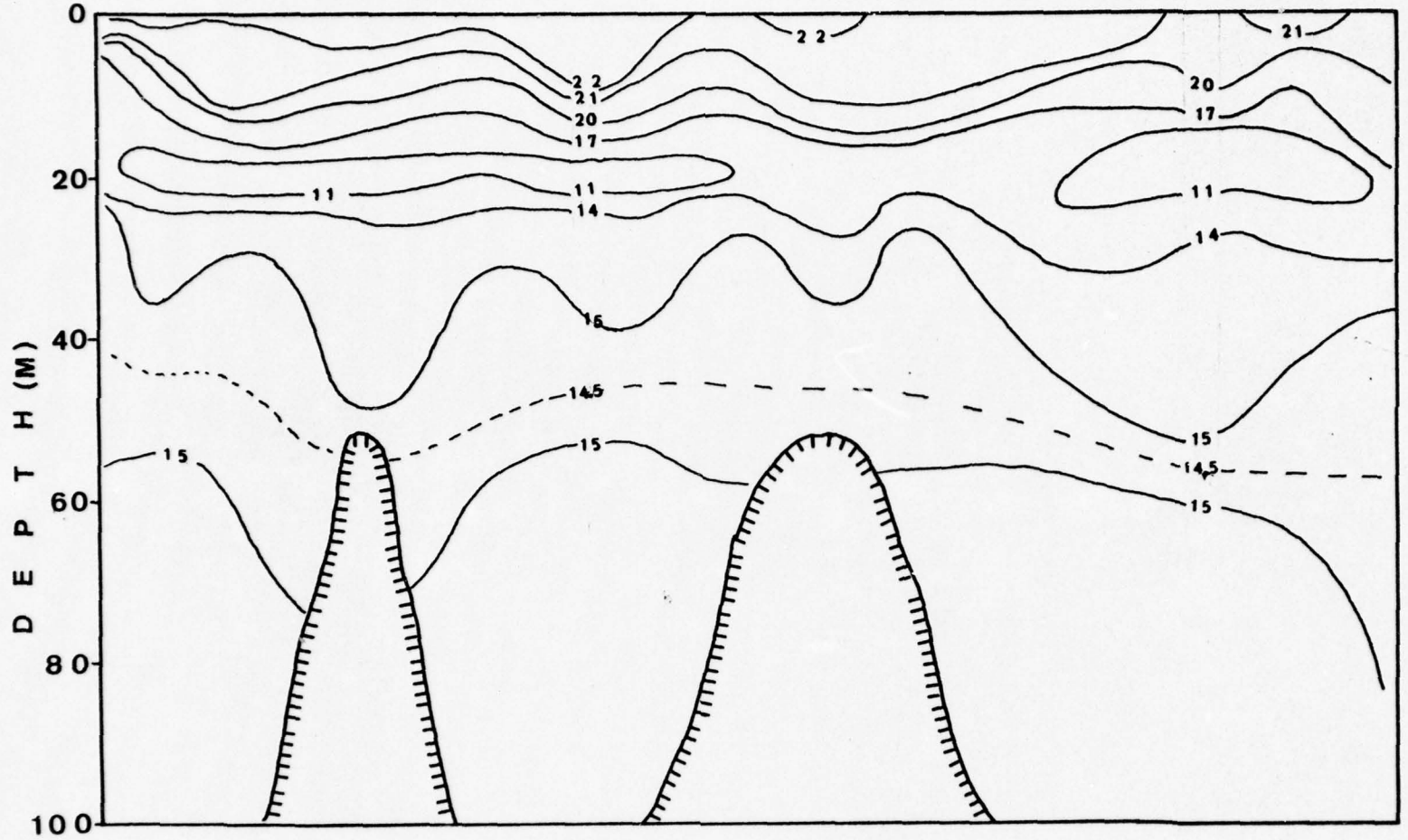

Figure 7. Temperature cross section of Sea of Marmara for upper 100 meters. (Same section as Figure 6.)

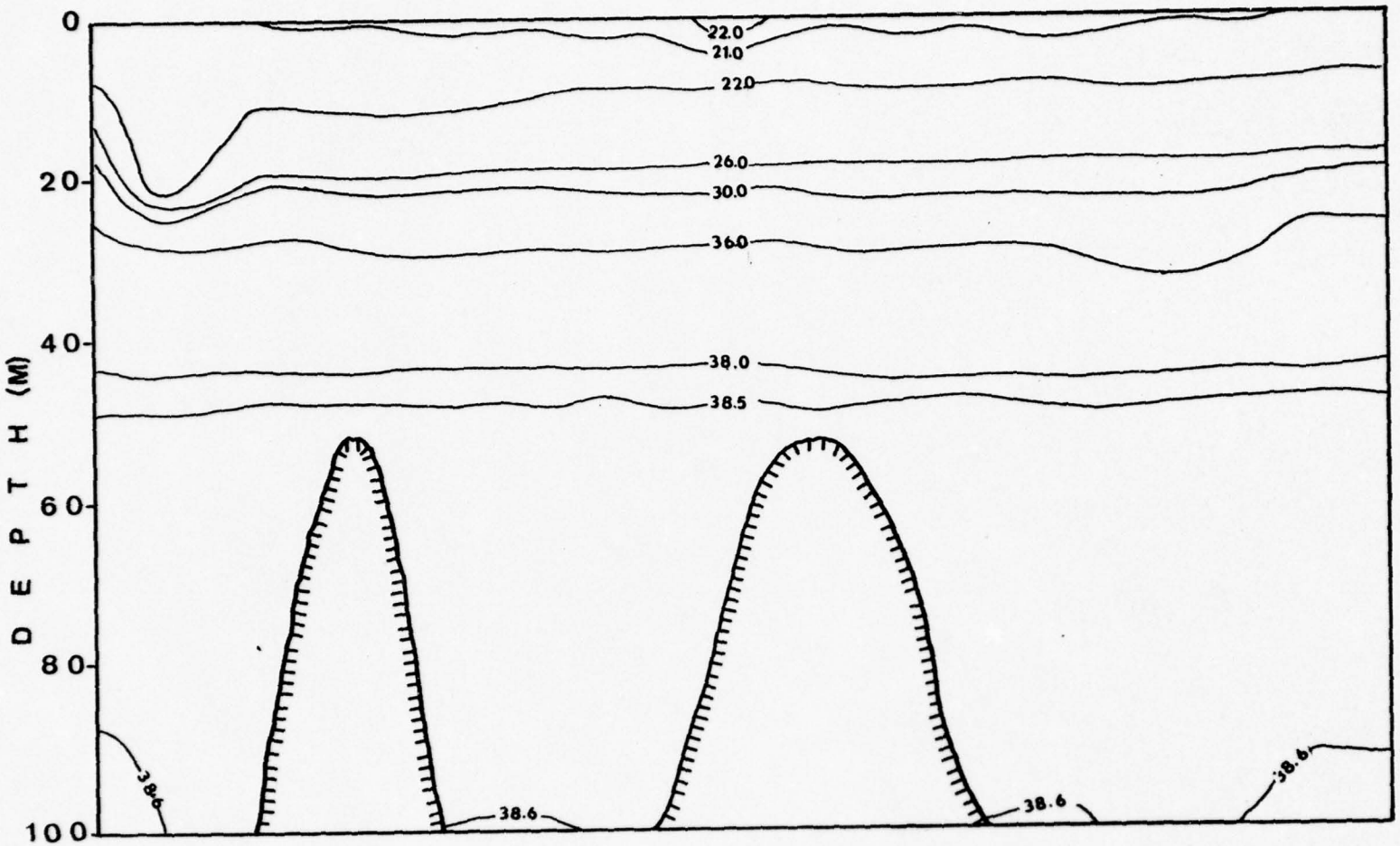

Figure 8. Salinity cross section of Sea of Marmara for upper 100 meters. (Same section as Figure 5.)

III. SELECTION OF THE NUMERICAL MODEL

Regional circulation models may be separated into two categories. One type of regional circulation model is a diagnostic density model. This approach is based on an observed density field and wind stress distribution. These quantities, however, are not observed continuously and in an evenly distributed way. But based on average values of these quantities a velocity field is calculated diagnostically. A diagnostic model, which seems at first easier, has drawbacks mainly of two types. First, it requires taking into account actual configuration of the basin geometry and, second, it requires sufficient representative observations. These two factors make this approach complicated and expensive.

A second type of approach to study regional circulation models is to use a predictive model with an idealized topography and basin area. But this becomes more complex by the inclusion of more dynamical processes.

At first glance it seems that diagnostic models are a better way of simulation of dynamical processes. But these observations on which such models depend are generally gathered by land based stations (e.g., wind data) and extrapolated to the area of concern. Furthermore, using average values brings up the question of how representative the

result is. Further, it is difficult to get a continuous view of the dynamical process and long-term quantative analyses.

On the other hand, although prognostic models are complex due to the dynamical processes involved, they are less expensive and can give a continuous view of variables, which is generally based on an initial density field. At least as a first approximation it seems reasonable and economical to study a regional circulation simulation. Present data are still used to estimate the initial density field and wind stress distribution in this kind of model.

Due to the uneven distribution of density and wind stress observations it was mandatory to use the prognostic approach at the beginning. The procedure adopted is to use present data as efficiently as possible to estimate a realistic initial density field and a constant wind stress distribution throughout the integration period.

IV. DESCRIPTION OF THE DYNAMIC MODEL

A. BASIC EQUATIONS OF THE MODEL

Basic assumptions which lead to important simplifications are: (1) the hydrostatic assumption, (2) the Boussinesq assumption with respect to density variations (density variation is neglected except where it appears as a coefficient of the gravitational constant), and (3) an implicit treatment of the mixing process by eddy diffusion. In addition, the non-linear terms are neglected in the momentum equation.

With these, the sea is assumed incompressible, and density is replaced by a constant value everywhere except in the hydrostatic equation.

The governing equations based on these assumptions are:

$$\frac{\partial u}{\partial t} = -\frac{\partial}{\partial x}\left(\frac{P}{\rho_o}\right) + A_M \nabla^2 u + K_v \frac{\partial^2 u}{\partial z^2} + fv \tag{4.1}$$

$$\frac{\partial v}{\partial t} = -\frac{\partial}{\partial y}\left(\frac{P}{\rho_o}\right) + A_M \nabla^2 v + K_v \frac{\partial^2 v}{\partial z^2} - fu \tag{4.2}$$

$$\frac{\partial P}{\partial z} = -(\rho - \rho_o)g \tag{4.3}$$

$$\frac{\partial u}{\partial x} + \frac{\partial v}{\partial y} + \frac{\partial w}{\partial z} = 0 \tag{4.4}$$

$$\frac{d\rho}{dt} = A_H \nabla^2 \rho + K \frac{\partial^2 \rho}{\partial z^2} + \delta_c(\rho) \tag{4.5}$$

where the symbols have the following meanings:

t	time
x	horizontal coordinate measures positive eastward
y	horizontal coordinate measures positive northward
z	vertical coordinate measures positive upward with an origin at mean water level
u	eastward velocity component
v	northward velocity component
w	vertical velocity component
ρ	density
ρ_o	reference constant density
P	departure, from reference pressure which is
P_o	pressure at reference density ($= -\rho_o gz$)
g	acceleration of gravity
f	coriolis parameter ($= 2\Omega \sin\phi$)
Ω	angular speed of earth rotation
ϕ	latitude
A_M	coefficient of horizontal diffusion for momentum (constant)
K_v	coefficient of vertical diffusion for momentum (constant)
A_H	coefficient of horizontal diffusion for density (constant)
K	coefficient of vertical diffusion for density (constant)
$\frac{d()}{dt}$	material derivative $[= \frac{\partial()}{\partial t} + u\frac{\partial()}{\partial x} + v\frac{\partial()}{\partial y} + w\frac{\partial()}{\partial z}]$
δ_c	introduces the effect of convective process when the stratification is unstable

The sea is driven by wind and thermohaline forcing, these effects being introduced with surface boundary conditions in the momentum and density equations, respectively. The boundary conditions specified at the sea surface are

$$\left.\begin{aligned} K\frac{\partial \rho}{\partial z} &= 0 \\ K_v\frac{\partial u}{\partial z} &= 0 \\ K_v\frac{\partial v}{\partial z} &= \frac{\tau_s^y}{\rho_o} \\ w &= 0 \end{aligned}\right\} \quad z = 0 \qquad (4.6)$$

Heating or cooling at the sea surface is neglected over the period of integration. A linear north–south density gradient is specified in the uppermost level in the model and held constant during calculations. The x component of surface stress is taken to be zero and calculations are carried out with a uniform meridional wind stress.

The boundary conditions specified at the flat horizontal bottom are

$$\left.\begin{aligned} K\frac{\partial \rho}{\partial z} &= 0 \\ u=v=w &= 0 \end{aligned}\right\} \quad z = -H \qquad (4.7)$$

The boundary conditions at the side walls of the basin are

$$\left.\begin{aligned} A_H \frac{\partial \rho}{\partial y} = u = v = 0 \qquad & \\ A_H \frac{\partial \rho}{\partial x} = u = v = 0 \qquad & \end{aligned}\right\} \quad \begin{aligned} y &= 0, Ly \\ x &= 0, Lx \end{aligned} \tag{4.8}$$

where Ly : width of the basin (50 km)

Lx : length of the basin(200 km)

Boundary conditions at the straits are based on specified density and velocity fields which were taken from available data and annual average inflow and outflow rates respectively.

B. DESCRIPTION OF THE SOLUTION TECHNIQUES

Since the model sea has a horizontal flat bottom and "rigid lid" approximation, vertical velocity vanishes at the surface and bottom. Following the method used by Bryan and Cox (1967–1968a–b), Haney (1974) and others, the ocean surface was considered a balanced surface at which w = 0. In this approach the height of the sea surface is not obtained from the continuity equation; therefore, external gravity waves are eliminated. This also removes the vertical mean divergence from all scales of motion. Elimination of external gravity waves allows the use of a longer time step. In the case of long–term integration this is an important gain compared to the loss of the prediction for height of the sea

surface. Filtering external gravity waves has a negligible effect on the density-driven part of the current.

Due to the conditions on vertical velocity, integration of the continuity equation from bottom to surface requires the following condition:

$$\frac{\partial \bar{u}}{\partial x} + \frac{\partial \bar{v}}{\partial y} = 0 \tag{4.9}$$

where the meaning of the overbar is

$$(\bar{\ }) \text{ vertical mean } \left[= \frac{1}{H} \int_{-H}^{0} (\ )\, dz\right]$$

and

$(\ )'$ indicates departure from vertical mean of any quantity.

Also for some basic integral constraints this is a required relation to be consistent with boundary conditions.

The "rigid lid" approximation, and (4.9), are accomplished by vertically integrating equations (4.1), (4.2) and subtracting the result from equations (4.1) and (4.2) respectively. Using present boundary conditions, the new sets of equations are

$$\frac{\partial u'}{\partial t} = -\frac{\partial P'}{\rho_o \partial x} + A_M \nabla^2 u' + K_v \frac{\partial^2 u'}{\partial z^2} + fv'$$

$$\frac{\partial v'}{\partial t} = -\frac{\partial P'}{\rho_o \partial y} + A_M \nabla^2 v' + K_v \frac{\partial^2 v'}{\partial z^2} - \frac{\tau_s^y}{\rho_o H} - fu' \tag{4.10}$$

where

u' eastward shear velocity component

v' northward shear velocity component

P' departure of P from its vertical average

$$[= \int_z^0 (\rho-\rho_o)g d\eta - \frac{1}{H}\int_{-H}^0 \left(\int_z^0 (\rho-\rho_o)g d\eta \right) dz] \qquad (4.11)$$

The relation between shear current and total current for horizontal components is

$$u'(x,y,z,t) = u(x,y,z,t) - \bar{u}(x,y,t)$$

$$v'(x,y,z,t) = v(x,y,z,t) - \bar{v}(x,y,t) \qquad (4.12)$$

since

$$|u| >> |\bar{u}| \quad \text{and} \quad |v| >> |\bar{v}| \qquad (4.13)$$

equation (4.12) takes the form

$$u'(x,y,z,t) \cong u(x,y,z,t)$$

$$v'(x,y,z,t) \cong v(x,y,z,t) \qquad (4.14)$$

Thus total u, v component of horizontal velocity can be represented by vertical shear currents u', v'. In the following part primes of u' and v' are dropped.

The equations are non-dimensionalized by making the following substitutions for new non-dimensional variables

$$
\begin{aligned}
(x,y) &= (x,y)/L \\
\rightarrow (z) &= (z)/h \\
(u,v) &= (u,v)/V_1 \\
\rightarrow (w) &= (w)/\frac{V_1 h}{L} \\
(P,P') &= \frac{(P,P')}{\rho_o f L V_1} \\
(t) &= \frac{(t)}{\frac{L}{V_1}} \\
(\tau) &= \frac{(\tau)}{\tau_M} \\
(\sigma) &= \frac{(\sigma)}{(\sigma_N - \sigma_S)}
\end{aligned}
\qquad (4.15)
$$

where

V_1 scale velocity associated with density driven current

h scale depth, taken equal to a characteristic thermocline depth

L length scale

τ_M wind stress [= MAX($\tau^x(x,y)$, $\tau^y(x,y)$]

σ sigma-t [= $(\rho-1) \times 10^3$]

σ_N surface sigma-t at northern part of the basin

σ_S surface sigma-t at southern part of the basin

A scale velocity associated with the density driven current is defined by using geostrophic and hydrostatic scaling which were introduced by Bryan and Cox (1968a). When the geostrophic relation is differentiated with respect to z and the hydrostatic equation is used, the result is

$$\frac{g}{\rho_o} \frac{\partial \rho}{\partial y} = f \frac{\partial u}{\partial z} \tag{4.16}$$

A scale velocity connected with the density distribution may be defined by

$$V_1 = \frac{g \Delta \rho}{\rho_o f L} h \tag{4.17}$$

where

$\Delta \rho$ north–south surface density differences

$(= \rho_N - \rho_S)$

A scale velocity for wind driven current is defined by

$$V_2 = \frac{\tau_M}{\rho_o f h L_r} \tag{4.18}$$

where

τ_M wind stress

L_r relative characteristic length scale for wind stress [= L/R] and L is a length scale for wind stress and R radius of the earth

Substitution of these non-dimensional variables into (4.10), (4.11), (4.4) and (4.5) with some rearrangement, gives these equations in terms of non-dimensional variables of the form

$$\frac{\partial u}{\partial t} = -\frac{1}{Ro}\frac{\partial P'}{\partial x} + \frac{E_H}{Ro}\nabla^2 u + \frac{E_V}{Ro}\frac{\partial^2 u}{\partial z^2} + \frac{1}{Ro}v \tag{4.19}$$

$$\frac{\partial v}{\partial z} = -\frac{1}{Ro}\frac{\partial P'}{\partial y} + \frac{E_H}{Ro}\nabla^2 v + \frac{E_V}{Ro}\frac{\partial^2 v}{\partial z^2} - \frac{V_r}{Ro}\frac{1}{L_r H_r}\tau_s{}^y - \frac{1}{Ro}u \tag{4.20}$$

$$p' = \int_z^0 (\sigma-\sigma_o)\,d\eta - \frac{1}{H}\int_{-H}^0 \left(\int_z^0 (\sigma-\sigma_o)\,d\eta\right) dz \tag{4.21}$$

$$w = \int_z^0 \nabla\cdot V\, d\eta \tag{4.22}$$

$$\frac{\partial \sigma}{\partial t} + u\frac{\partial \sigma}{\partial x} + v\frac{\partial \sigma}{\partial y} + w\frac{\partial \sigma}{\partial z} = \frac{1}{Pe}\nabla^2\sigma + \left(\frac{K}{K_v}\right)\frac{E_V}{Ro}\frac{\partial^2 \sigma}{\partial z^2} + \delta_c(\sigma) \tag{4.23}$$

where

Ro Rossby number which shows the relative importance of local time change term in the equation of motion with respect to that of the coriolis term $\left[= \frac{V_1}{fL}\right]$

E_H horizontal Ekman number which shows relative importance of lateral diffusion and coriolis terms

$$\left[= \frac{A_M}{fL^2}\right]$$

E_V vertical Ekman number, gives the ratio of vertical diffusion of momentum to the coriolis term

$$\left[= \frac{E_V}{fh^2}\right]$$

Pe Peclet number, shows importance of advection compared to diffusion of density

$$[= \frac{V_1 L}{A_H}]$$

V_r relative velocity, ratio of barotropic velocity to baroclinic velocity

$$[= \frac{V_2}{V_1}]$$

H_r relative depth, ratio of basin depth to thermocline depth

$$[= \frac{H}{h}]$$

The model is governed by these six parameters assuming a value for L_r is defined. All the parameters of the resultant run and constants of the model are given in table 2.

Equations (4.19) – (4.23) are solved for variables u, v, P', w and σ. The variables u, v, and σ are predicted from (4.19), (4.20) and (4.23). P' and w are calculated diagnostically from equations (4.21) and (4.22), respectively.

TABLE 2. PARAMETERS AND CONSTANTS

Ro	4.255×10^{-3}	Rossby number
E_H	0.532×10^{-2}	Horizontal Ekman number
E_V	0.851×10^{-2}	Vertical Ekman number
Pe	10.0	Péclet number
H_r	50.0	Relative depth
V_r	0.1	Relative velocity
Δx	10×10^5 cm	Zonal grid spacing
Δy	5×10^5 cm	Meridional grid spacing
Δt	8 minute	Time step
t	28.9 day	Time scale
ϕ	40°	Reference latitude
Ω	2π day^{-1}	Rotation rate of the earth
R	6.37×10^8 cm	Radius of the earth
g	1000 cm sec^{-2}	Gravity acceleration
ρ_o	1.012 gm cm^{-3}	Reference density
H	1×10^5 cm	Depth of the sea
L_r	10	Curl factor or relative length scale for wind stress
K	1.6 cm^2 sec^{-1}	Eddy diffusivity
K_v	3.2 cm^2 sec^{-1}	Eddy viscosity
V_1	4 cm sec^{-1}	Characteristic baroclinic velocity
L	1×10^7 cm	Characteristic length scale
A_M	0.5×10^8 cm^2 sec^{-1}	Lateral eddy viscosity
A_H	0.4×10^7 cm^2 sec^{-1}	Lateral eddy diffusion coefficient

V. DESCRIPTION OF THE NUMERICAL MODEL

A. SPACE AND TIME DIFFERENCING TECHNIQUES

The space and time differencing schemes are similar to the schemes used by Haney (1974) for a general circulation model.

In the integration of the primitive equations a staggered grid and centered space differencing scheme are utilized. The main concern in choosing the staggered grid was avoidance of a computational mode which appears when a centered space differencing scheme is used with an unstaggered grid. This computational mode in space is not present for a staggered grid. The staggered grid also has advantage in saving computing time due to the presence of variables at alternate grid points.

A leapfrog scheme is used for time integration. The starting scheme is a combination of forward and leapfrog scheme as shown below

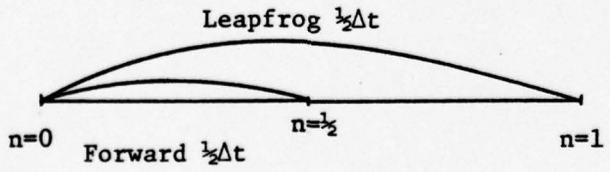

($\frac{1}{2}$ time step forward) + ($\frac{1}{2}$ time step leapfrog) → Time step 1.

where

n represents a time step

In most circulation models Matsuno scheme (Matsuno, 1966) is used as a starting scheme and to remove the solution separation which is present when a leapfrog scheme utilized exclusively for time integration. Since time integration in this model is not long enough to cause solution separation a cheme such as Matsuno is not used here.

Each term in the momentum and sigma–t equations is evaluated at a different time step to ensure linear computational stability.

Neglecting coefficients, the time differencing of the equation of motion corresponding to (4.20) is given by

$$v^{n+1)} = v^{(n-1)} + 2\Delta t[PT^{(n)} + FT^{(n-1)}] - 2\Delta t\, f[C1\, u^{(n+1)} + C2\, u^{(n-1)}] \qquad (5.1)$$

where

PT pressure term

FT friction term, which is composed of lateral diffusion of momentum and vertical eddy stress

A trapezoidal implicit scheme is utilized for the coriolis term. Then, to satisfy consistency and linear computational stability, coefficients C1 and C2 must satisfy the relation.

$$C1 + C2 = 1$$

$$\frac{1}{2} \leq C1 \leq 1 \qquad (5.2)$$

The values C1 = 0.55 and C2 = 0.45 are commonly accepted for these constants which produce very slight damping of

inertial oscillations. Equation (5.1) and an analogous equation for $u^{(n+1)}$ are solved simultaneously for the two unknowns $u^{(n+1)}$, $v^{(n+1)}$. The time differencing form of the sigma-t equation has the form

$$\sigma^{(n+1)} = \sigma^{(n-1)} + 2\Delta t[ADV^{(n)} + HD^{(n-1)} + VD^{(n-1)}] + \delta_c(\sigma^{n+1}) \tag{5.3}$$

where

ADV advection term

HD horizontal diffusion term

VD vertical diffusion term

The leapfrog scheme is conditionally stable and the time step must satisfy the relation (for two dimensional wave propagation)

$$C\frac{\Delta t}{\Delta x} \leq \frac{1}{\sqrt{2}} \tag{5.4}$$

where

C maximum phase speed of the waves present in the system.

External gravity waves are removed and inertial oscillations are rendered neutral by (5.1) and (5.2). Therefore only internal gravity waves are present to determine C. The phase speed of the internal gravity waves is

$$C = \sqrt{g'H} \tag{5.5}$$

where

g' is modified acceleration of gravity and given by the relation

$$g' = g \frac{\Delta\rho}{\rho_o} \tag{5.6}$$

where

g acceleration of gravity

$\Delta\rho$ a typical value for the vertical density differences

ρ_o reference density

Assuming $g = 1000$ cm sec^{-2}, $\Delta\rho = 10 \times 10^{-3}$ gm cm^{-3} and $\rho_o = 1.012$ gm cm^{-3} gives a value for $g' \cong 9.88$ cm sec^{-2}. Integrations are carried out with an 8-minute time step for a grid spacing of 5 km, without any stability problem.

B. THE FINITE DIFFERENCE EQUATIONS

The numerical method is set down in terms of the non-dimensional variables. The finite difference scheme is based on a three-dimensional array of points with indices i,j,k. Time step is indicated by (n) as a superscript. In the notation the letters i,j,k are always integers.

Horizontal spacing is such that $\Delta x = 10$ km and $\Delta y = 5$ km, and uniform in the x and y directions. The horizontal grid pattern is shown in figure 9. Where horizontal velocity components (u,v) are defined at circled points, vertical velocity (w) and sigma-t (σ) are defined at dot points.

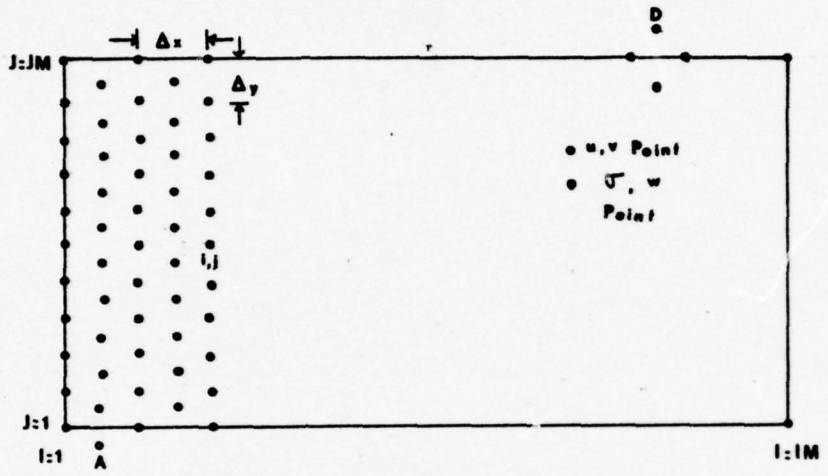

Figure 9. Placement of variables on horizontal grid plane. The open circles denote the definition points of the horizontal velocity components (u,v) and dots denote definition points of (σ,w). The distance between adjacent grid point is Δx = 10 km and Δy = 5 km in x and y direction, respectively. IM and JM have values 21 and 11 respectively.

For an arbitrary interior point, where (u,v) are stored longitude (x) and latitude (y) are defined by

$$x_i + \frac{1}{2} = \frac{\Delta x}{2}\,[1 + (i-1)] \qquad i = 1,2,\ldots, IM-1$$

$$y_j + \frac{1}{2} = \frac{\Delta y}{2}\,[1 + (j-1)] \qquad j = 1,2,\ldots, JM-1 \tag{5.7}$$

The vertical pattern of variables is shown in figure 10. The vertical index indicated with k and the vertical velocity w are given along the surface and bottom and along the layer boundaries. The variables (u,v,σ) are located at the kth level. Depth of each level is defined as

$$z_1 = -\frac{\Delta z_1}{2}$$

$$z_k = z_1 - \sum_{m=2}^{m=k} (\Delta z_m + \Delta z_{m-1})/2 \quad k = 2,3\ldots KM \tag{5.8}$$

Layer thicknesses for each level are given in table 3.

Table 3. LAYER THICKNESSES

k	1	2	3	4	5	6	7	8	9
$\frac{\Delta z_k}{h}$	0.25	0.25	0.3125	0.6875	1.0	1.5	6.0	15.0	25.0

To resolve the surface layer more accurately, four levels are located within 20 meters. Close to the bottom a coarser grid is used. Resolution in the surface layer is greater than in the bottom layer.

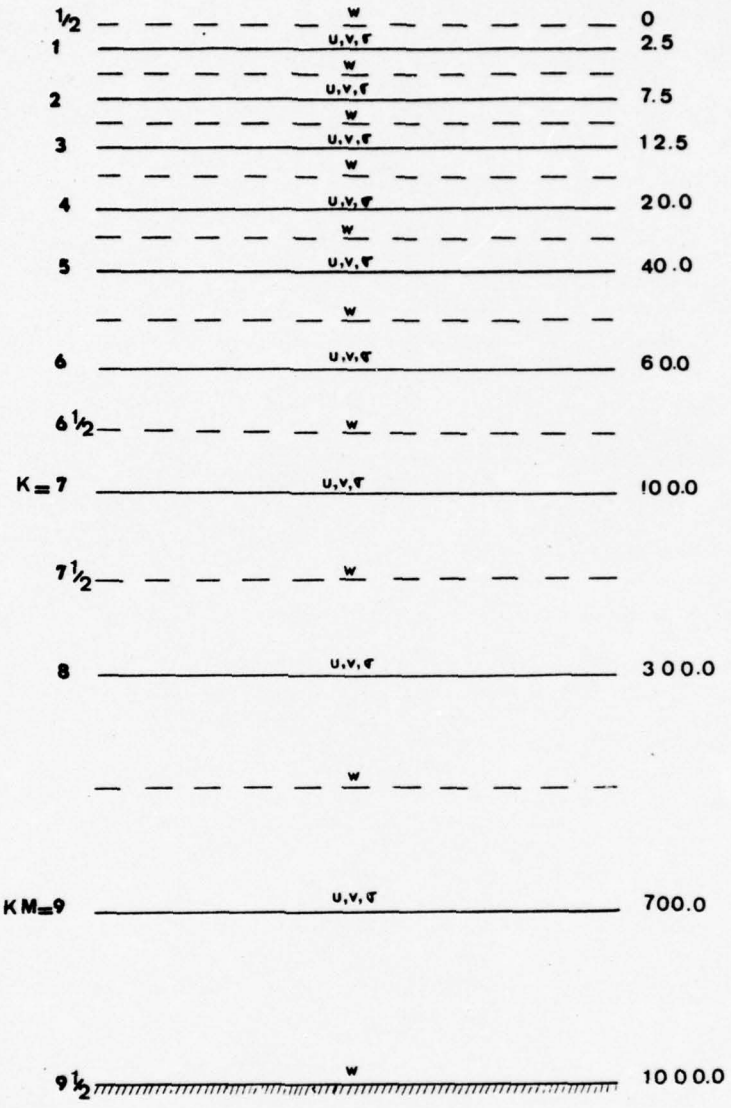

Figure 10. Vertical structure of the model (u,v,σ) are defined at integer K values and w is defined along the layer boundaries.

The finite difference form of the hydrostatic equation has the form

$$P_{ij1} = (\sigma-\sigma_o)_{i,j,\frac{1}{2}} \ \Delta Z_{\frac{1}{2}}$$

$$P_{ijk} = P_{ij,k-1} + (\sigma-\sigma_o)_{ijk-\frac{1}{2}} \cdot \Delta Z_{k-\frac{1}{2}} \quad k=2,3,KM \tag{5.9}$$

and the vertical average of the departure pressure is calculated with the relation

$$\overline{P}_{ij} = \sum_{k=1}^{k=KM} P_{ijk} \ \Delta Z_k \tag{5.10}$$

The departure P' is calculated from

$$P'_{ijk} = P_{ijk} - \overline{P}_{ij} \tag{5.11}$$

which is the finite difference analog of (4.23).

The finite difference approximation of the continuity equation, in which the vertical velocity between the levels is calculated, has the form

$$w_{ijk+\frac{1}{2}} = w_{ijk-\frac{1}{2}} + [U_x + V_y]_{ijk} \ \Delta Z_k \tag{5.12}$$

where

$$U_{x\ ijk} = \tfrac{1}{2}(u_{x\ j+\frac{1}{2}} + u_{x\ j-\frac{1}{2}})_{ik}$$

$$V_{y\ ijk} = \tfrac{1}{2}(v_{y\ i+\frac{1}{2}} + v_{y\ i-\frac{1}{2}})_{jk} \tag{5.13}$$

and

$$u_{x\ ij+\frac{1}{2}k} = \frac{1}{\Delta x}(u_{i+\frac{1}{2}} - u_{i-\frac{1}{2}})_{j+\frac{1}{2}k}$$

$$v_{y\ i+\frac{1}{2}jk} = \frac{1}{\Delta y}(v_{j+\frac{1}{2}} - v_{j-\frac{1}{2}})_{i+\frac{1}{2}k} \tag{5.14}$$

which are analogs of $(\frac{\partial u}{\partial x})$ and $(\frac{\partial v}{\partial y})$ respectively. Gradients of horizontal velocity components u_x and v_y are defined at half-integer grid points west and south of the u and v storage points shown in figure 11a.

Integration from the surface downward, using surface boundary condition w=0, is done by

$$w_{ijk+\frac{1}{2}} = \sum^{k}{}' (U_x + V_y)_{ij} \, \Delta Z \tag{5.15}$$

The formula for the finite difference approximation of the equation (4.19) by which u is predicted is

$$\left[\frac{u^{n+1} - u^{n-1}}{2\Delta t}\right]_{i+\frac{1}{2}j+\frac{1}{2}k} = -\frac{1}{2Ro}\left[\frac{P'_{i+1\ j+1} - P'_{i\ j+1}}{\Delta x}\right.$$

$$\left. + \frac{P'_{i+1\ j} - P'_{ij}}{\Delta x}\right]^{n}_{k} + \frac{E_H}{Ro}\left[\frac{u_{x\ i+1\ j+\frac{1}{2}} - u_{x\ i\ j+\frac{1}{2}}}{\Delta y}\right.$$

$$\left. + \frac{u_{y\ i+\frac{1}{2}\ j+1} - u_{y\ i+\frac{1}{2}j}}{\Delta y}\right]^{n-1}_{k} + \frac{E_V}{Ro}\left[\frac{u_{z\ k-\frac{1}{2}} - u_{z\ k+\frac{1}{2}}}{\Delta Z_k}\right]^{n-1}_{i+\frac{1}{2}\ j+\frac{1}{2}}$$

$$+ \frac{1}{Ro}\left[C1\ v^{n+1} + C2\ v^{n-1}\right]_{i+\frac{1}{2}\ j+\frac{1}{2}k} \tag{5.16}$$

where $$u_{yj+1} = \frac{u_{j+1\frac{1}{2}} - u_{j+\frac{1}{2}}}{\Delta y})_{i+\frac{1}{2}k} \tag{5.17}$$

and $$u_{zk-\frac{1}{2}} = \frac{u_{k-1} - u_k}{\Delta Z_{k-\frac{1}{2}}})_{i+\frac{1}{2}j+\frac{1}{2}} \tag{5.18}$$

Equations (5.16) and (5.17) represent $(\frac{\partial u}{\partial y})$ and $(\frac{\partial u}{\partial z})$ and are located half grid distance south and above the velocity (u) storage points, respectively, as shown in figure 11 a–b.

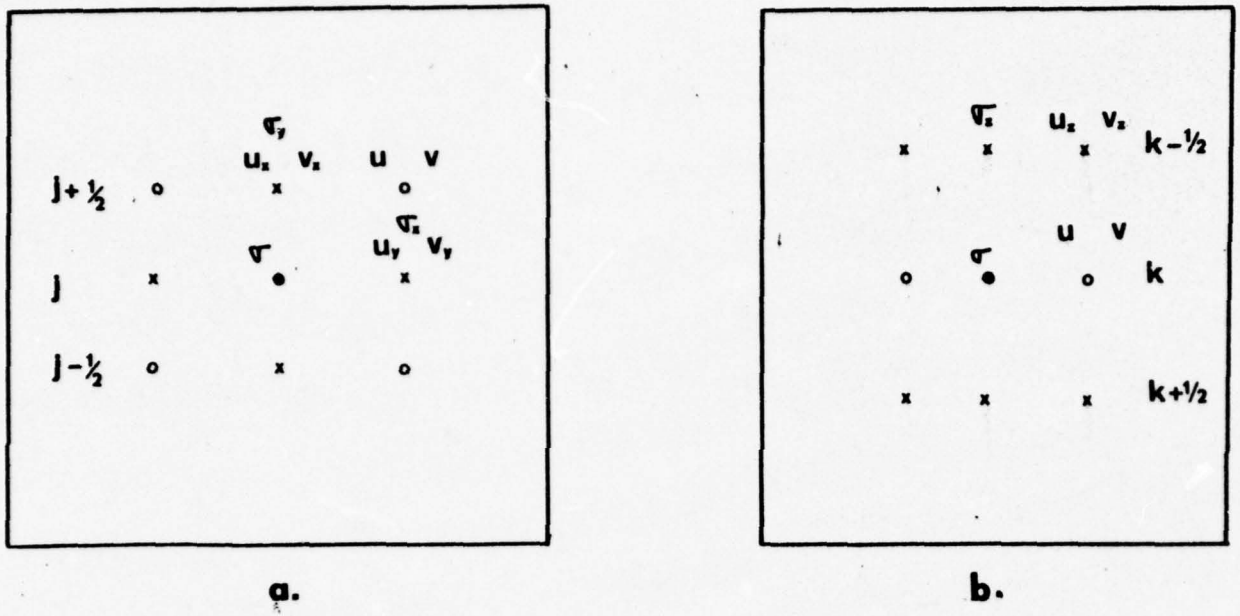

Figure 11 a. Horizontal locations of variables which define the horizontal gradients of u,v, and σ. (u), (v) are located at open circles, dots represent locations of σ. At x points gradients of these variables are defined.

b. Vertical locations of variables which define the gradients of u, v and σ. u_z and v_z are at half grid points above the (u,v) storage point. σ_z^z is defined at half grid distances above the σ storage points.

The formula for the finite difference approximation of the equation (4.20) in which v is predicted has the form

$$\left[\frac{v^{n+1} - v^{n-1}}{2\Delta t}\right]_{i+\frac{1}{2}j+\frac{1}{2}k} = -\frac{1}{2Ro}\left[\frac{P'_{i+1\ j+1} - P'_{i+1j}}{\Delta y}\right.$$

$$\left. + \frac{P'_{ij+1} - P_{ij}}{\Delta y}\right]^{n}_{k} + \frac{E_H}{Ro}\left[\frac{v_{x\ i+1\ j+\frac{1}{2}} - v_{x\ ij+\frac{1}{2}}}{\Delta x}\right.$$

$$\left. + \frac{v_{y\ i+\frac{1}{2}j+1} - v_{y\ i+\frac{1}{2}j}}{\Delta y}\right]^{(n-1)}_{k}$$

$$+ \frac{E_V}{Ro}\left[\frac{v_{z\ k-\frac{1}{2}} - v_{z\ k+\frac{1}{2}}}{\Delta Z_k}\right]_{i+\frac{1}{2}j+\frac{1}{2}}$$

$$+ \frac{V_r}{Ro}\frac{L_r}{H_r}\tau^{y}_{i+\frac{1}{2}} - \frac{1}{Ro}\left[C1u^{n+1} + C2u^{n-1}\right]_{i+\frac{1}{2}j+\frac{1}{2}k} \qquad (5.19)$$

where

$$v_{x\ i+1} = \frac{v_{i+1\frac{1}{2}} - v_{i+\frac{1}{2}}}{\Delta x})_{j+\frac{1}{2}k} \qquad (5.20)$$

$$v_{z\ k-\frac{1}{2}} = \frac{v_{k-1} - v_k}{\Delta Z_{k-\frac{1}{2}}})_{i+\frac{1}{2}j+\frac{1}{2}} \qquad (5.21)$$

Equations (5.20) and (5.21) are analogues of $(\frac{\partial v}{\partial x})$ and $(\frac{\partial v}{\partial z})$ and are stored south and above the velocity storage points, as shown in figure 11a–b.

The finite difference approximation of the sigma-t equation has the following form,

$$\left[\frac{\sigma^{n+1} - \sigma^{n-1}}{2\Delta t}\right]_{ijk} = -A_{ijk}^{(n)} + \frac{1}{Pe}\left(\frac{\sigma_{x\ i+\frac{1}{2}j+\frac{1}{2}} - \sigma_{x\ i-\frac{1}{2}j+\frac{1}{2}}}{\Delta x}\right.$$

$$\left. + \frac{\sigma_{y\ i+\frac{1}{2}j+\frac{1}{2}} - \sigma_{y\ i+\frac{1}{2}j-\frac{1}{2}}}{\Delta y}\right)_k^{n-1}$$

$$+ \frac{K}{K_v}\frac{1}{Ro}E_v\left(\frac{\sigma_{z\ k+\frac{1}{2}} - \sigma_{z\ k-\frac{1}{2}}}{\Delta Z_k}\right)_{i+\frac{1}{2}j+\frac{1}{2}}^{n-1}$$

$$+ \delta_c(\sigma^{n+1})_{ijk} \qquad (5.22)$$

where

$$A_{ijk} = \frac{1}{4\Delta x}[(u_{i+\frac{1}{2}j+\frac{1}{2}} + u_{i+\frac{1}{2}j-\frac{1}{2}})\cdot(\sigma_{ij} + \sigma_{i+1j})_k$$

$$- (u_{i-\frac{1}{2}j+\frac{1}{2}} + u_{i-\frac{1}{2}j-\frac{1}{2}})\cdot(\sigma_{i-1j} + \sigma_{ij})_k]$$

$$+ \frac{1}{4\Delta y}[(v_{i+\frac{1}{2}j+\frac{1}{2}} + v_{i-\frac{1}{2}j-\frac{1}{2}})\cdot(\sigma_{ij-1} + \sigma_{ij})_k$$

$$- (v_{i+\frac{1}{2}j-\frac{1}{2}} + v_{i-\frac{1}{2}j-\frac{1}{2}})\cdot(\sigma_{ij-1} + \sigma_{ij})_k]$$

$$+ \frac{1}{2\Delta Z_k}[(w_{ijk-\frac{1}{2}})\cdot(\sigma_{ijk} + \sigma_{ijk-1})$$

$$- (w_{ijk+\frac{1}{2}})\cdot(\sigma_{ijk} + \sigma_{ijk+1})] \qquad (5.23)$$

and

$$\sigma_{x\ i+\frac{1}{2}jk} = \frac{1}{\Delta x}\ (\sigma_{i+1} - \sigma_i)_{jk}$$

$$\sigma_{y\ ij+\frac{1}{2}k} = \frac{1}{\Delta y}\ (\sigma_{j+1} - \sigma_j)_{ik} \qquad (5.24)$$

$$\sigma_{z\ ijk+\frac{1}{2}} = \frac{1}{\Delta Z_{k+\frac{1}{2}}}\ (\sigma_{zk} - \sigma_{zk+1})_{ij}$$

As shown in figure (11 a-b) $\sigma_{x\ i-\frac{1}{2}}$ and $\sigma_{y\ j-\frac{1}{2}}$ and $\sigma_{Zk-\frac{1}{2}}$ are defined at half grid distances south, east and above the sigma-t storage points.

Before proceeding to a new time step convective adjustment is applied. It is difficult to state the convective adjustment mechanism. With this mechanism the density structure is forced to remain stable. It may be expressed by

$$\delta_c = \begin{pmatrix} 0 \\ \infty \end{pmatrix} \qquad \begin{matrix} \sigma_Z < 0 \\ \sigma_Z > 0 \end{matrix} \qquad (5.25)$$

In case of unstable stratification, vertical mixing becomes effectively infinite. At each time step this infinite mixing is included in numerical solution by testing sigma-t profile for unstable lapse rate ($\sigma_{k-1} > \sigma_k$). If this condition exists new values of sigma-t for those two layers are set equal to the vertical average sigma-t of the two layers instantaneously. This process is repeated until complete stability is reached for the entire layer.

C. SPECIFICATION OF BOUNDATION CONDITIONS

As shown in Figure 3-1 σ,w are variables which are defined at lateral boundaries; also horizontal gradients of (u,v) are defined at these lateral boundaries. The boundary conditions are satisfied by the following relations which are given for eastern and western boundaries. Similar conditions exist for north and south boundaries with the exception of open boundaries.

Normal components are set equal to zero by

$$u_{x\ i=1} = \frac{2u}{\Delta x})_{i=\frac{1}{2}}$$

$$u_{x\ i=IM} = \frac{2u}{\Delta x})_{i=IM-\frac{1}{2}} \qquad (5.26)$$

In the momentum equation zero-slip condition is applied to the valocity tangent to the boundary. On the other hand, when computing the advection term in the density equation free slip condition exists for the velocity tangent to the boundary. This implies the following conditions

$$u_{i=1} = u_{i=1\frac{1}{2}}$$

$$u_{i=IM} = u_{IM-\frac{1}{2}} \qquad (5.27)$$

Definition of vertical gradients of (u,v) allows the writing of the vertical stress term in flux form easily. Boundary conditions at the surface and bottom are defined in the following manner:

$$u_z \quad k = \frac{1}{2} = 0 \tag{5.28}$$

Zonal wind stress is assumed zero and only a constant meridional wind stress is defined.

$$v_z \; k = \frac{1}{2} = \frac{V_r L_r}{E_v} \tau_s{}^y \tag{5.29}$$

On the other hand it is assumed that horizontal velocities vanish at the bottom. The following conditions force velocities (u,v) to reach zero at the bottom

$$u_{z\; k=KM+\frac{1}{2}} = \frac{2u}{\Delta Z}\Big|_{k=KM}$$

$$v_{z\; k=KM+\frac{1}{2}} = \frac{2v}{\Delta Z}\Big|_{k=KM} \tag{5.30}$$

The boundary conditions of zero mass fluxes across the side walls and bottom are satisfied by imposing the following conditions:

$$(\sigma u)_{i=\frac{1}{2}} = -(\sigma u)_{i=3/2]jk}$$

$$(\sigma u)_{i=IM+\frac{1}{2}} = -(\sigma u)_{i=IM-\frac{1}{2}]jk} \tag{5.31}$$

Similar conditions exist at north and south boundaries.

In the diffusion term zero flux and insulation are satisfied by the following conditions:

$$\sigma_{x_{i=\frac{1}{2}}} = -\sigma_{x_{i=3/2}}$$

$$\sigma_{x_{i=IM+\frac{1}{2}}} = -\sigma_{x_{i=IM-\frac{1}{2}}} \qquad (5.32)$$

where σ_x is defined at half grid distances west of the sigma-t storage points, as shown in figure 11a. Similar conditions exist at north and south for meridional gradients of sigma-t, with the exception of open boundaries where sigma-t is defined outside the domain.

At the sea surface downward flux is absent.

$$\sigma_z \; k = \frac{1}{2} = 0 \qquad (5.33)$$

The sigma-t equation is solved for only the upper six levels. It is assumed that sigma-t for the rest of the depth range has a value σ_c, which is held constant during integration. This enters the system in the calculation of the vertical gradient of sigma-t one half grid distance below the sixth level,

$$\sigma_{z_{k=6\frac{1}{2}}} = \frac{\sigma - \sigma_c}{\Delta z})_{k=6} \qquad (5.34)$$

and σ_c has a value 28.5 in sigma-t units.

VI. RESULTS

Computations are carried out for different values of the parameters with an integration period of 24 hours. Parameters of these runs are given in Table 2. Results of the model are given for the fields of horizontal velocity components (u,v), vertical velocity (w) and density (sigma-t) in dimensional form.

The horizontal velocity field at z = -2.5 m is given in Figure 12. The horizontal stress exerted on the sea surface by southerly wind causes the surface water to move in a generally North-east direction. This is a consequence of movement of surface water as an Ekman layer, drifting to the right of the wind stress in the Northern Hemisphere. Since the curl of the wind is zero divergence of the Ekman drift is also zero. But horizontal velocity is strongly convergent and divergent near the boundaries. Northeastward drift takes place over the entire basin at this depth. The strongest flow has a magnitude 20 cm/sec in the central part of the basin and diminishes toward the boundaries. Near open boundaries velocities are smaller compared to the velocities at neighboring grid points. The southward flow at these points represents the exchange with the Black Sea water at the north and Mediterranean water at the south. The magnitudes of these currents are 5 cm/sec and 2 cm/sec at grid points just near the entrances of the Straits of Canakkale and the Strait of Istanbul. The applied meridional wind stress has a value of

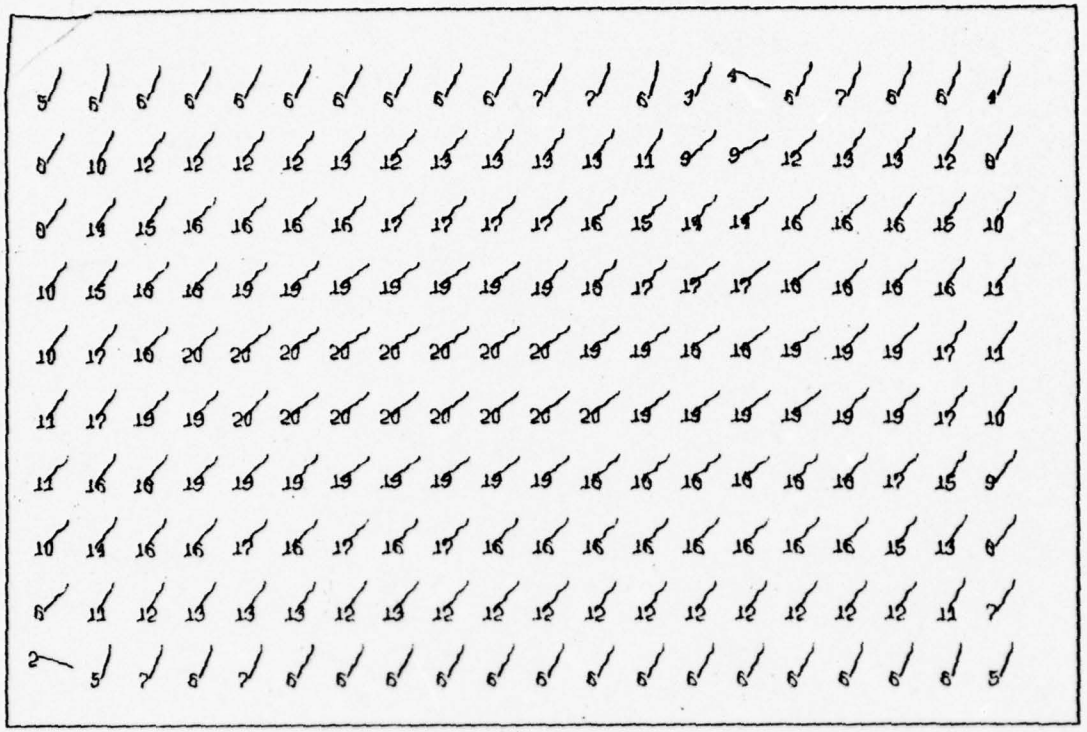

Figure 12. Horizontal velocity vectors for first level, (2.5 meter).

0.3 dyn cm^{-2} which is not strong enough to move surface water to the north as it does at neighboring grid points.

In the second layer z = −7.5 m the horizontal velocity changes direction to the right and becomes weaker. Horizontal velocities at that level are shown in figure 13w; they have a magnitude 5 cm sec^{-1}. Flow adjacent to the straits is still southerly and has a magnitude 5 cm sec^{-1} and 3 cm sec^{-1} at the vicinities of the Straits of Istanbul and Canakkale respectively.

The circulation pattern at lower levels differs from the upper level flows both in magnitude and direction. These differences can be observed in the circulation pattern at the z = −40.0 m level (Figure 14). The pattern is not irregular compared to the upper layers.

The northeastward surface drift in the first layers is accompanied by a westward and partly southwestward flow in the bottom layers. A northward flow adjacent to the Strait of Canakkale brings Mediterranean water into the basin. A similar northward flow of Mediterranean water does not appear at the northern strait due to the shallow sill depth at that point.

Flow in the layers close to the bottom becomes weaker. The influence of the circulation at the straits on the general pattern is small. The circulation pattern at a depth 700.0 m is shown in figure 15. The maximum magnitude is 0.033 cm sec^{-1}.

One advantage of the numerical modeling study is that it gives estimates of important oceanographic variables that

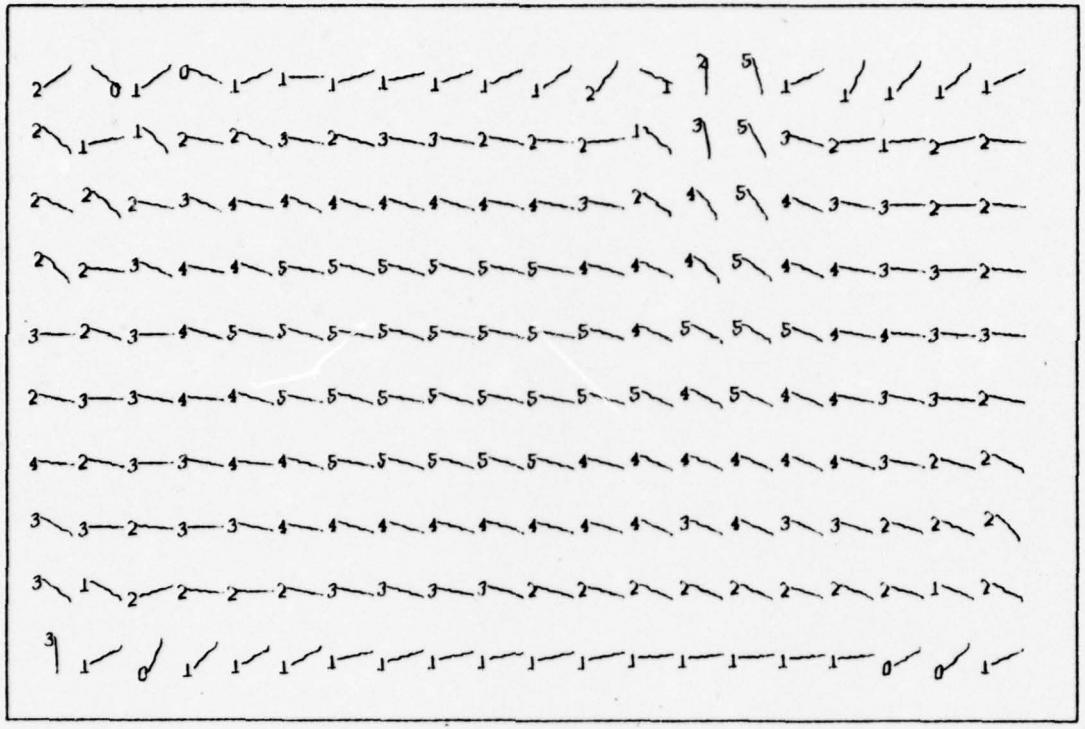

Figure 13. Horizontal velocity vectors for second level, 7.5 meter).

Figure 14. Horizontal velocity vectors for fifth level, (40.0 meter).

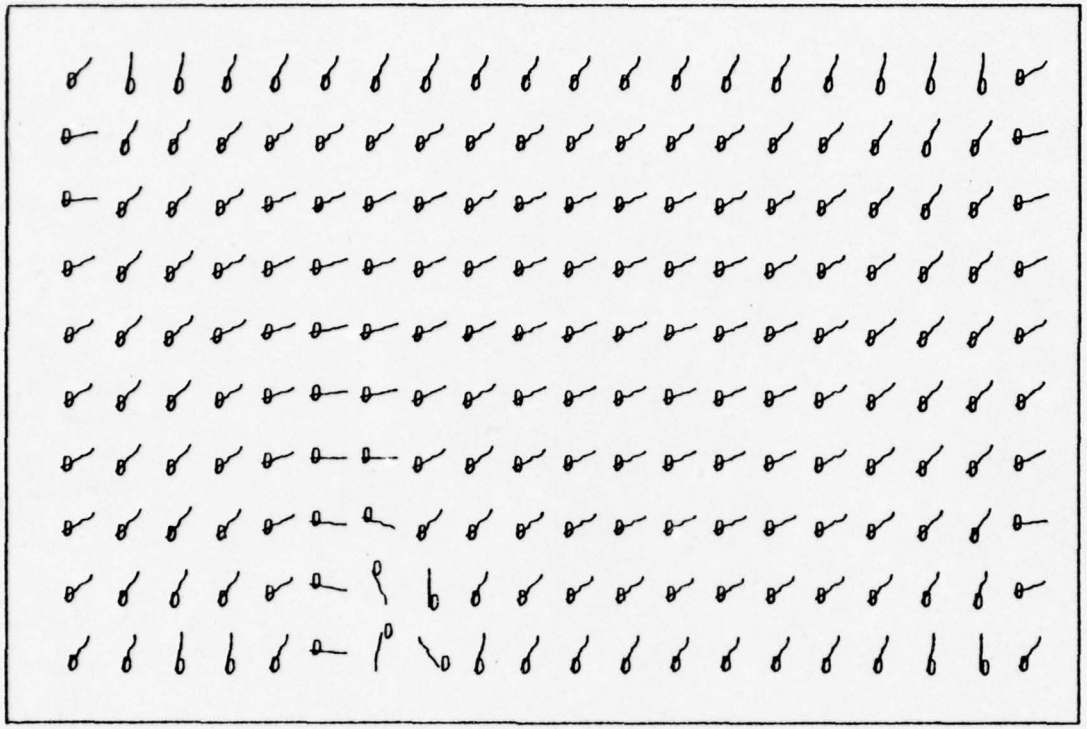

Figure 15. Horizontal velocity vectors for ninth level, (700.0 meter).

cannot be obtained by measurements. One such variable is the vertical velocity. The vertical velocity at the base of the first layer is given in Figure 16. The magnitude of the vertical velocity differs markedly between the boundaries and the interior. Rising motion (upwelling) is taking place in the south and southwest and sinking motion (downwelling) is taking place in the north-northeast. Vertical velocity is mainly determined by the Ekman drift current intersecting the boundaries. Southerly wind stress produces upwelling and downwelling at the south and north, respectively. Upwelling extends to the north on the western side and downwelling to the south on the eastern side. The maximum magnitude of the vertical motion is 358 cm day^{-1}. Strong upwelling and downwelling take place adjacent to the straits. This is consistent with the nature of the horizontal current system in the vicinity of the straits.

Vertical velocity at the bottom of the second layer, $z = -7.5$ m, is shown in Figure 17. The general pattern is similar to the vertical velocity at the base of the first layer. Strong vertical velocity is present along the lateral walls to the southwest and northeast where it has a magnitude $\pm$ 300 cm day^{-1}. With depth the effect of wind on vertical velocity decreases due to the vertical stability. The vertical velocity pattern at the base of the eighth level is shown in Figure 18.

The sigma-t pattern at the first level, 2.5 m is shown in Figure 19. This pattern at $z = -2.5$ m is specified by

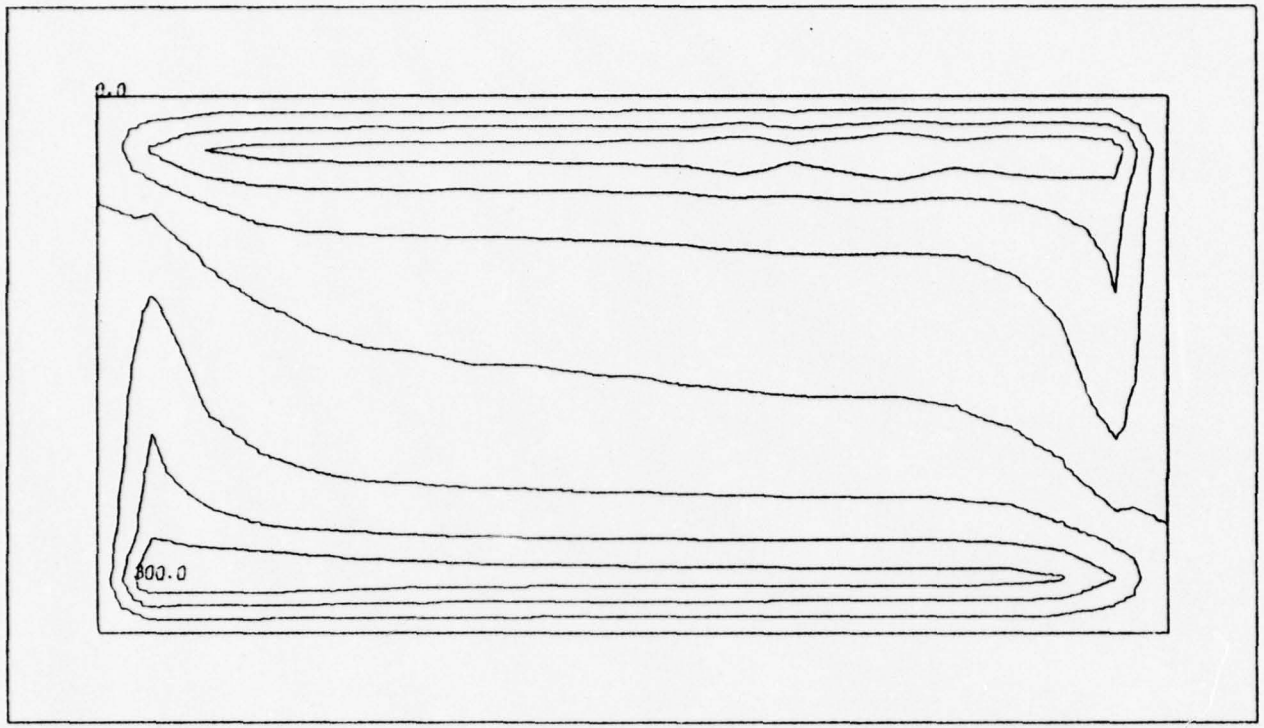

Figure 16. Vertical velocity at the base of the first layer (5.0 meter).

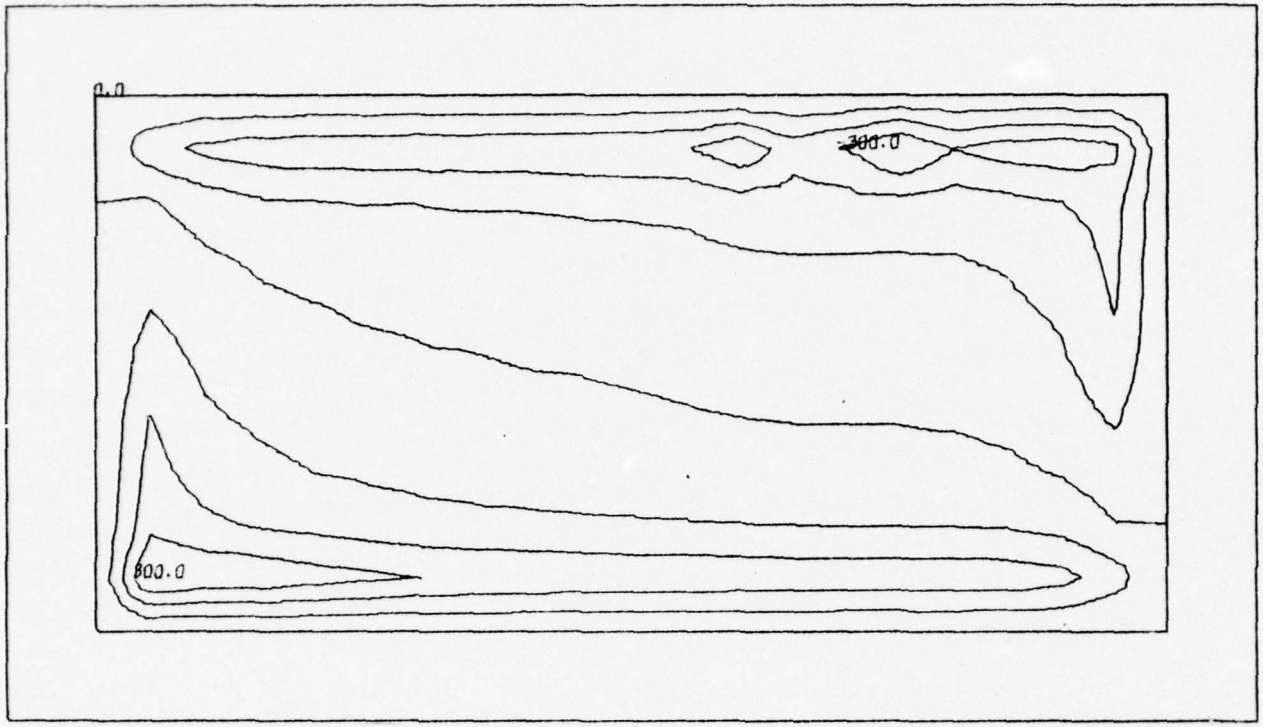

Figure 17. Vertical velocity at the base of the second layer (10.0 meter).

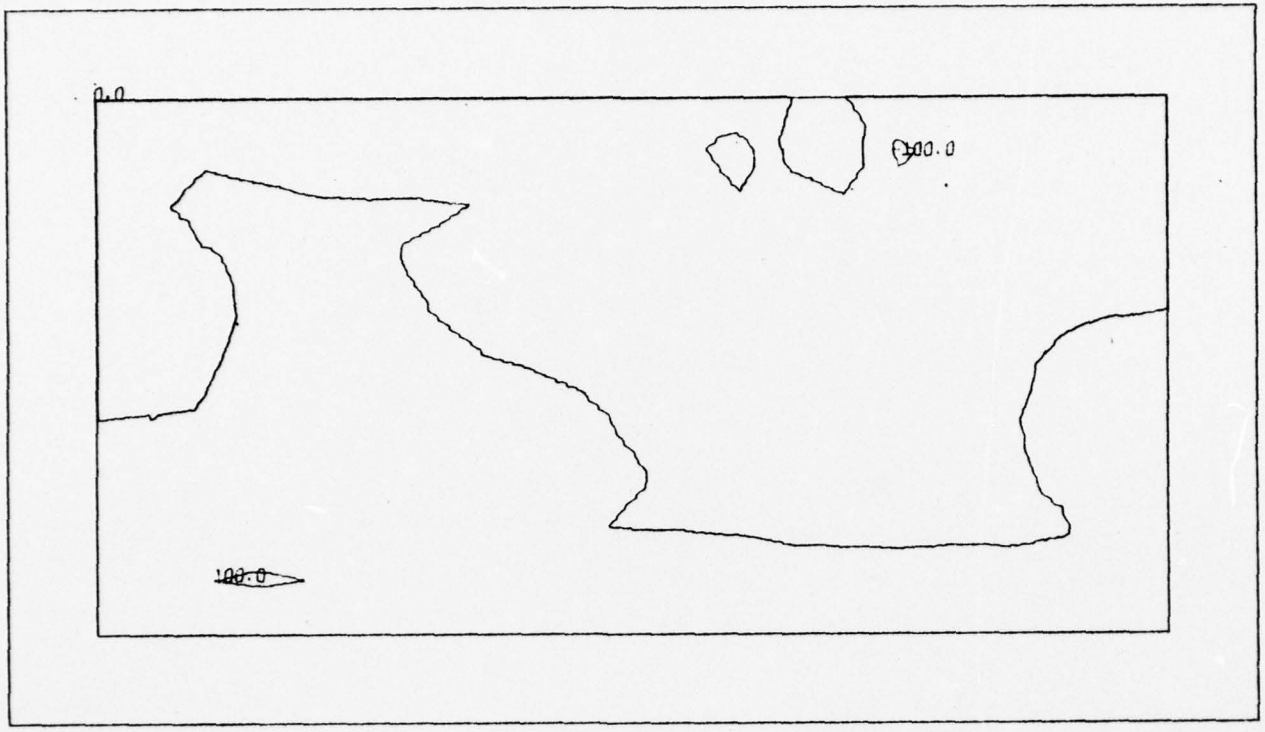

Figure 18. Vertical velocity at the base of the eighth layer (500 meter).

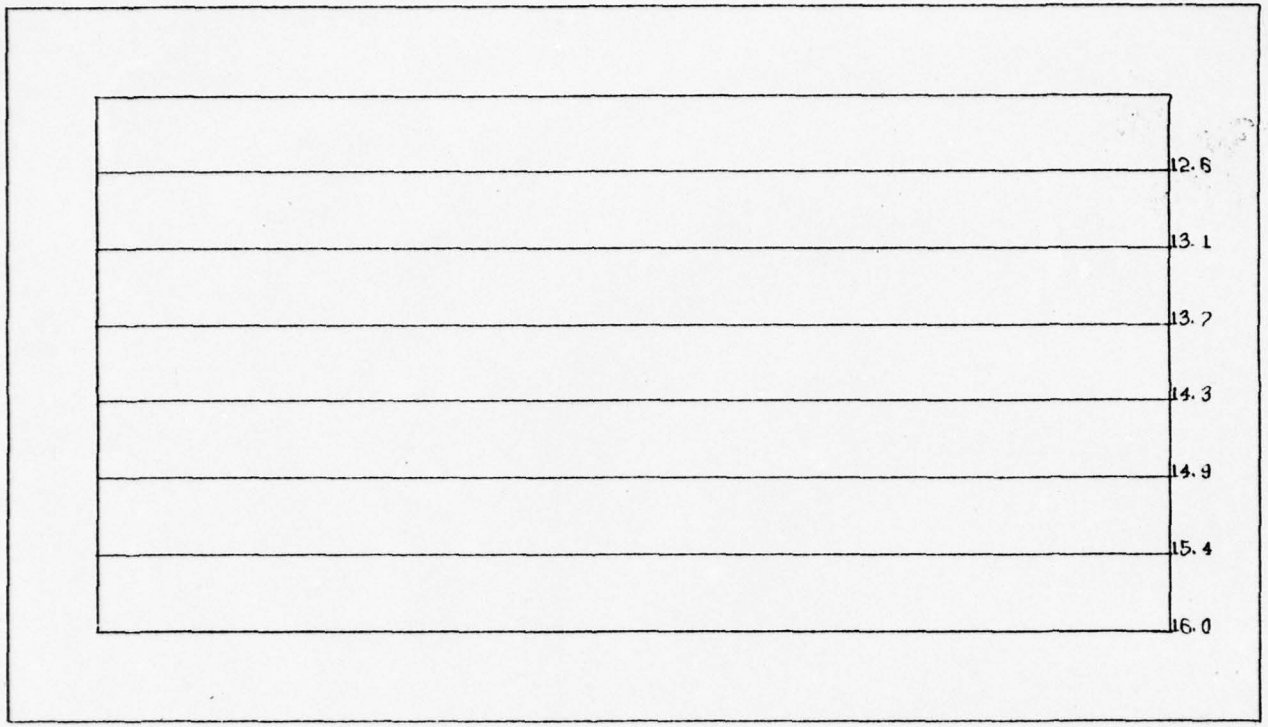

Figure 19. Horizontal sigma-t pattern at first level, (2.5 meter).

the surface boundary condition. At this level the surface sigma-t is a function of latitude only and held constant during the integration period.

Deviations from the surface pattern begin to appear just below the first level at 7.5m. The sigma-t pattern for the second level is shown in Figure 20. A close relationship is present between this sigma-t pattern and the vertical velocity field shown in Figure 17. At the north and northeast sinking motion brings in low density and water and at the south rising motion brings in high density water to this depth. This pattern is more strongly tied to the surface boundary conditions on sigma-t than at other levels. There is a low density water pool at the north. As a consequence of upwelling a high dense water pool is present at the south extending in an east-west direction. Magnitudes of sigma-t are 16.5 and 18.0 at north and south respectively.

The sigma-t pattern at the fourth level $z = -20$ m is shown in Figure 21. The effect of vertical motion appears as a low density water pool at the northeast. Below this level $z = -40$ (not shown), sigma-t is uniform and has a value 28.5. This is consistent with the sigma-t pattern given in Figure 6.

Further insight into these results may be gained by examining the meridional and east-west cross sections of sigma-t and the (u,v) components of the horizontal velocity. There is also the possibility of comparing the predicted sigma-t pattern to the observations.

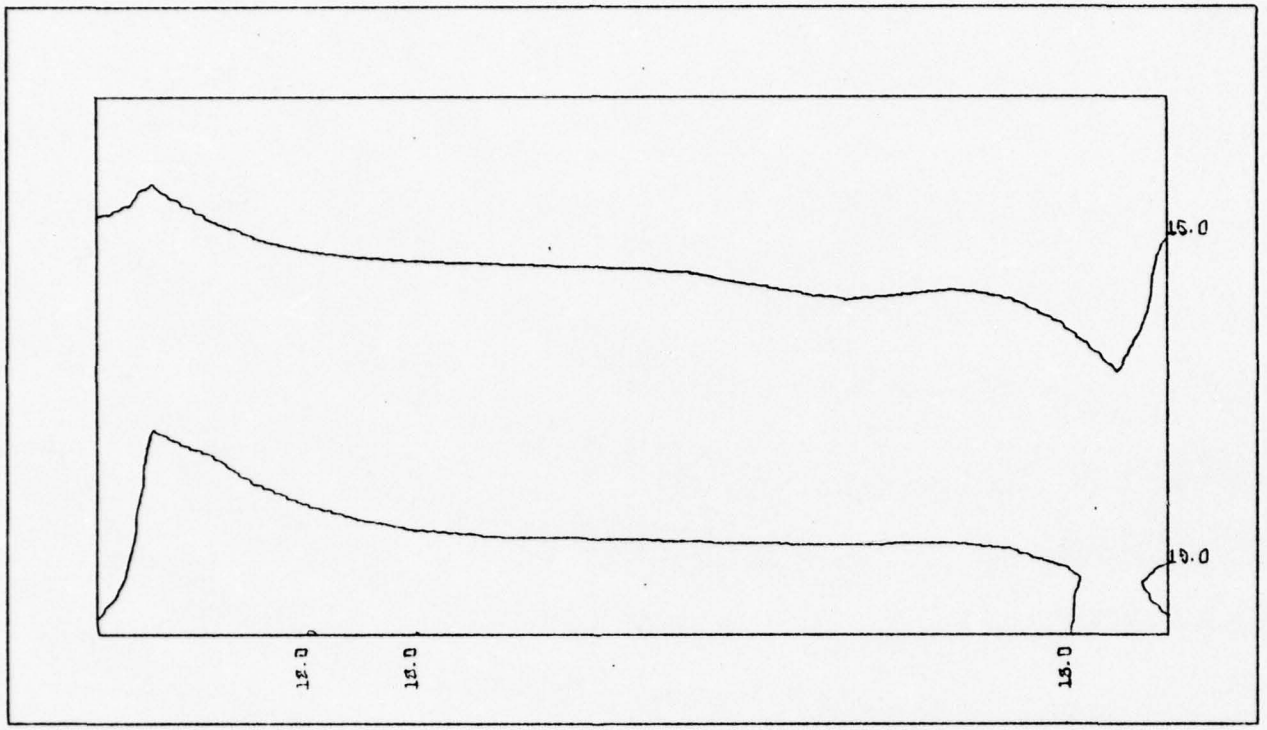

Figure 20. Horizontal sigma-t pattern at second level, (7.5 meter).

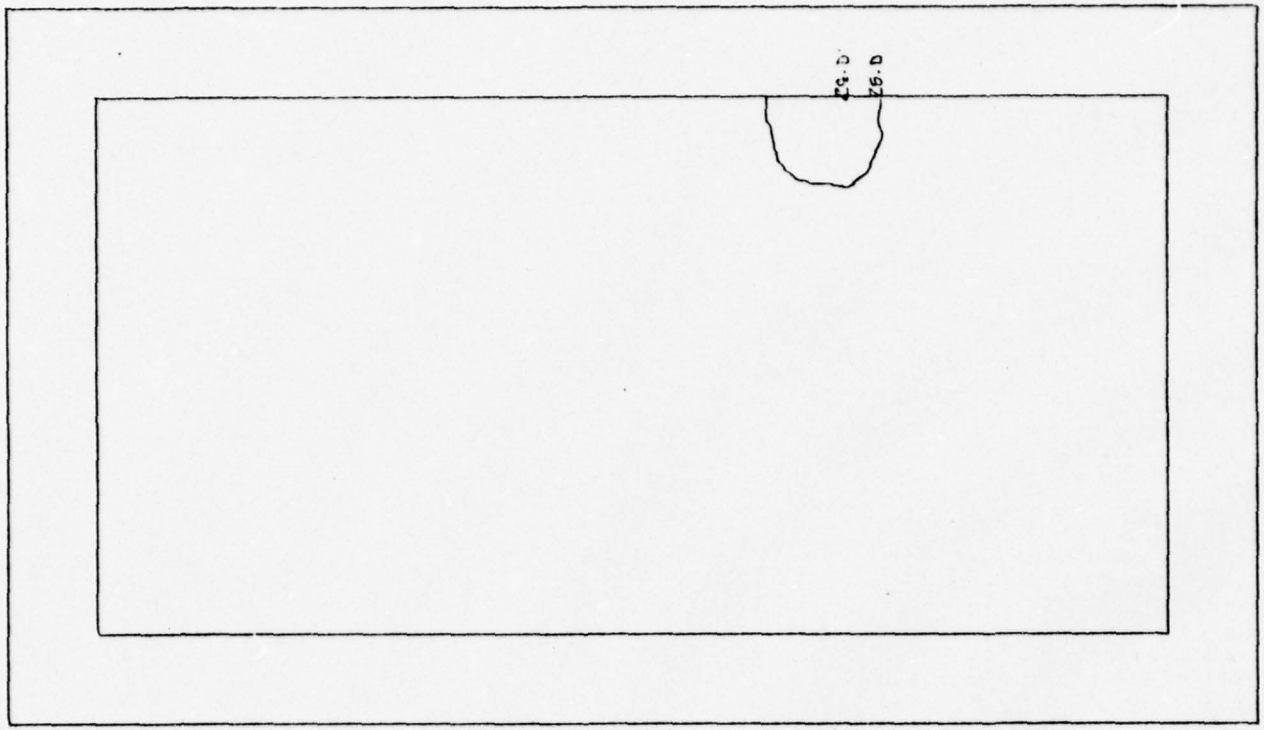

Figure 21. Horizontal sigma-t pattern at fourth level, (20 meter).

Meridional cross sections of sigma-t at different longitudes are shown in Figures 22-24. The general patterns are similar. High density water rises to the surface and stratification becomes shallower further south. Below 40 m density is constant. This is consistent with the observed sigma-t field. At the west and south very strong upwelling and weak downwelling at north are shown in Figure 22. In the central region there is upwelling in the south and downwelling in the north as shown in Figure 23. Further east the effect of strong downwelling is shown by the rate of tilting of the isopycnals at the north compared to the south in Figure 24.

Meridional cross sections of zonal velocity in the east, central and western parts of the basin are shown in Figures 25-27. The zonal flow at the surface is eastward and changes direction with depth. Zonal flow is westward at greater depths. Strong flow is present at the surface and decreases rapidly with depth. Variation with longitude can be observed by comparing the figures. In the central part zonal velocity has a magnitude 16.0 cm/sec at the surface and decreases both laterally and vertically. Below 20 meters flow is westward and has a magnitude 0.6 cm sec^{-1}.

East-west cross sections of sigma-t patterns for three latitudes are shown in Figures 28-30. A regular stratification is deformed by upwelling and downwelling of the eastern and western sides of the basin (Figure 29). Departures are present in the north and south, as shown in Figures 28 and 29 respectively. Intrusion of less dense Black Sea water can be identified in Figure 30.

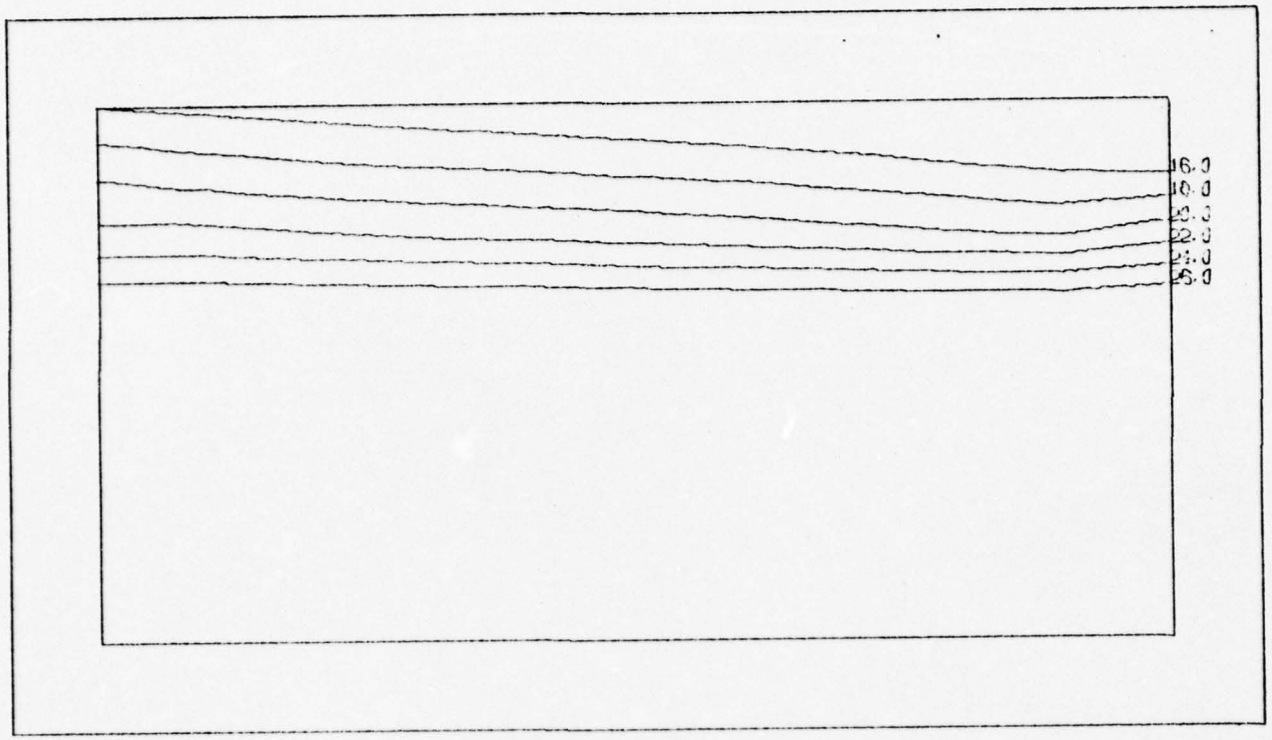

Figure 22. Meridional cross section for sigma-t at the western part of the basin.

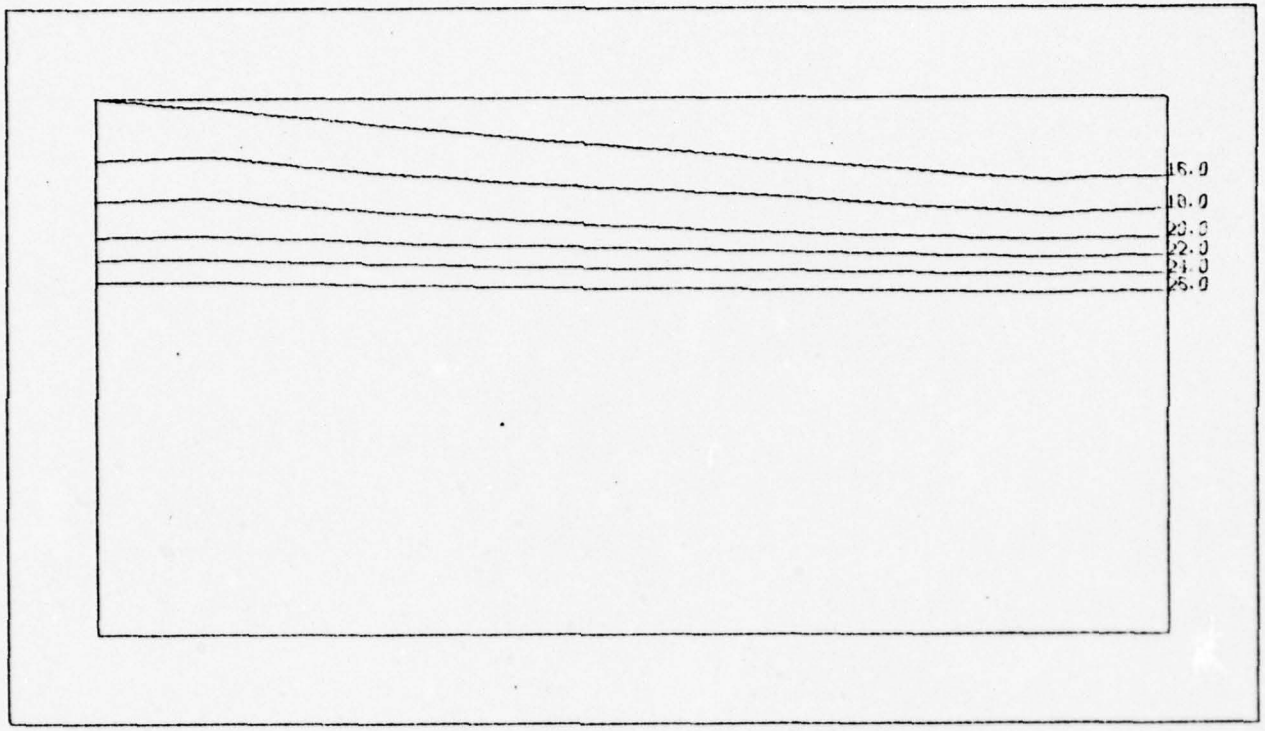

Figure 23. Meridional cross section for sigma-t at the central part of the basin.

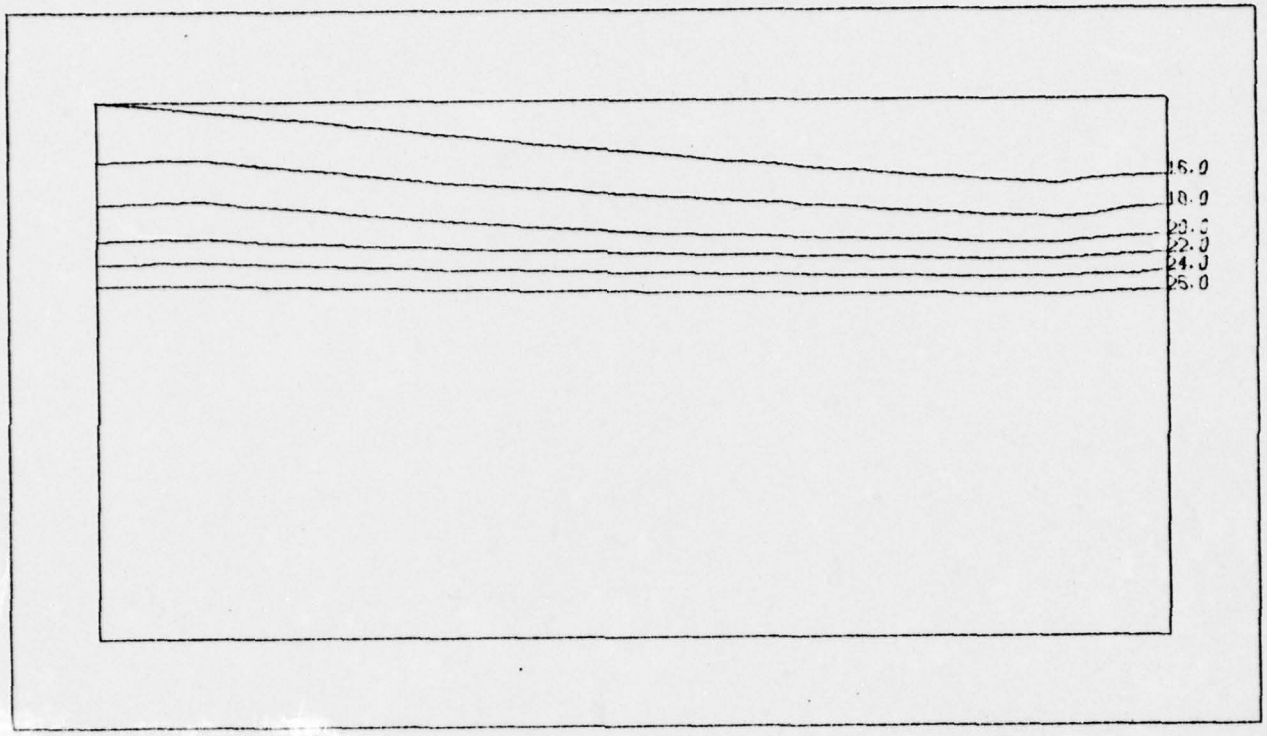

Figure 24. Meridional cross section for sigma-t at the eastern part of the basin.

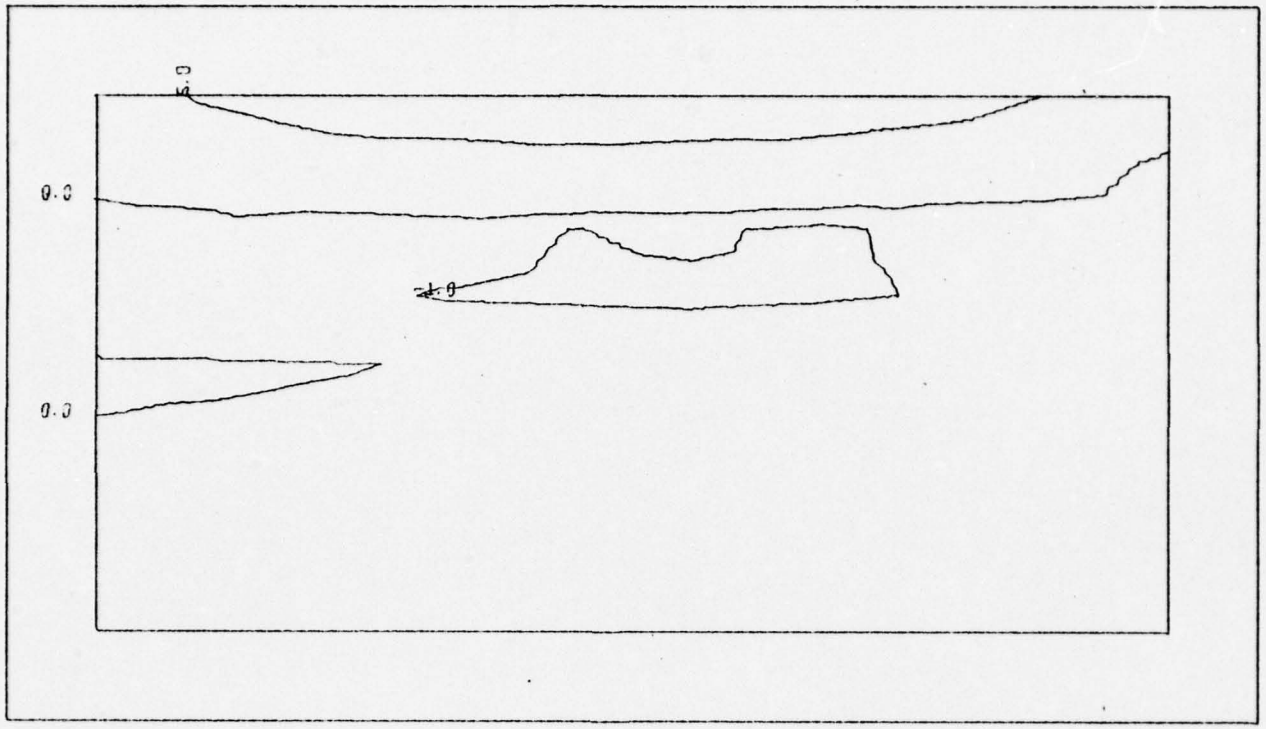

Figure 25. Meridional cross section of the zonal velocity, (u), at the western part of the basin.

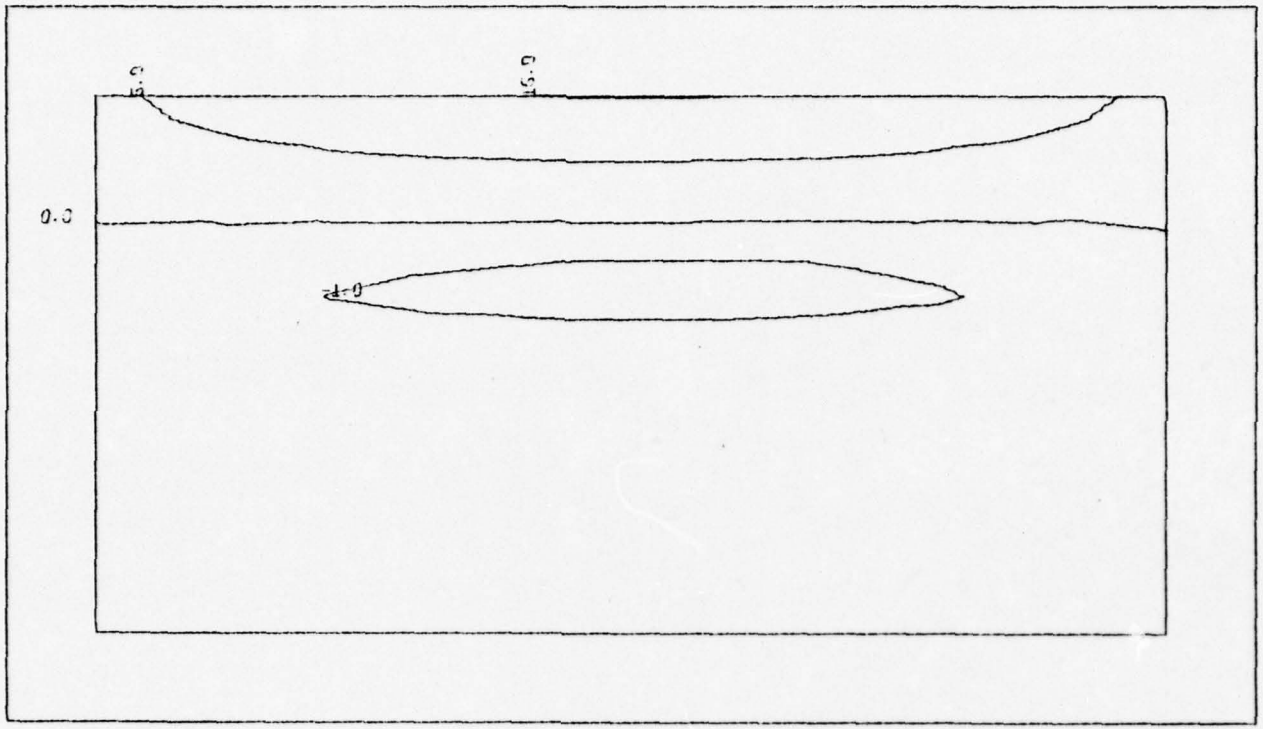

Figure 26. Meridional cross section of the zonal velocity, (u), at the central part of the basin.

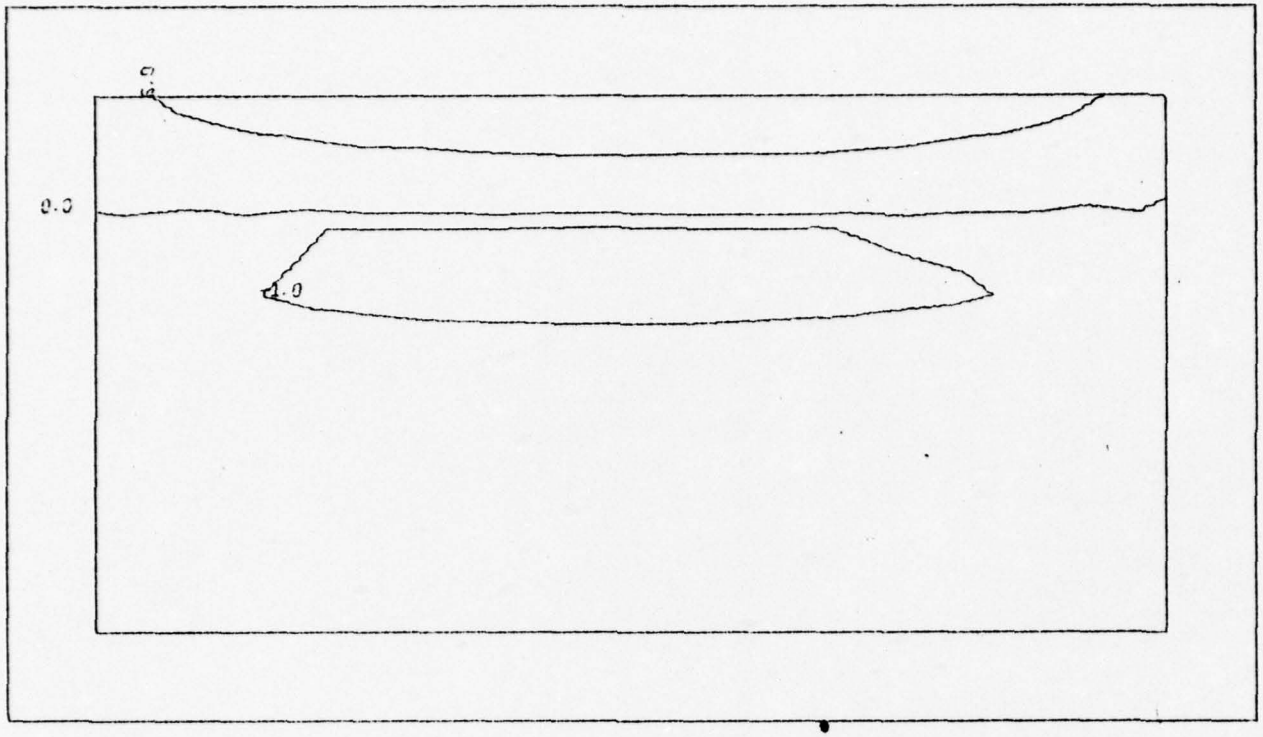

Figure 27. Meridional cross section of the zonal velocity, (u), at the eastern part of the basin.

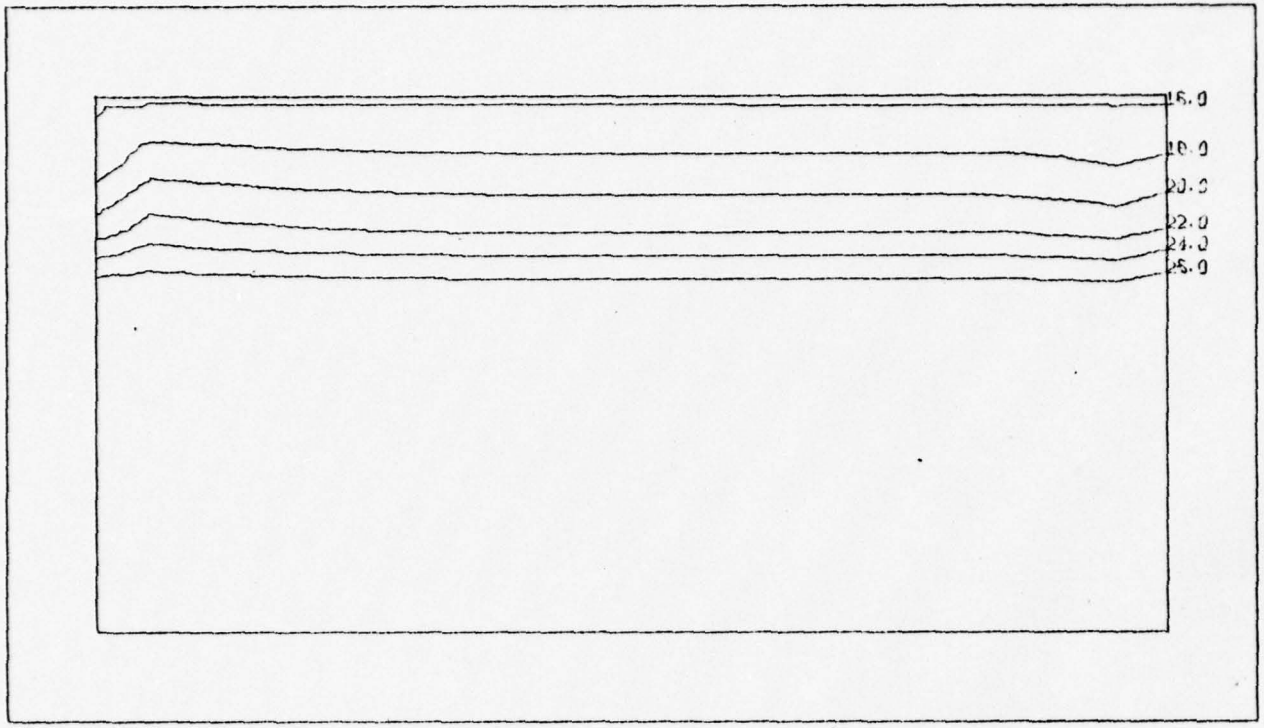

Figure 28. East–west sigma–t cross section for the southern part of the basin.

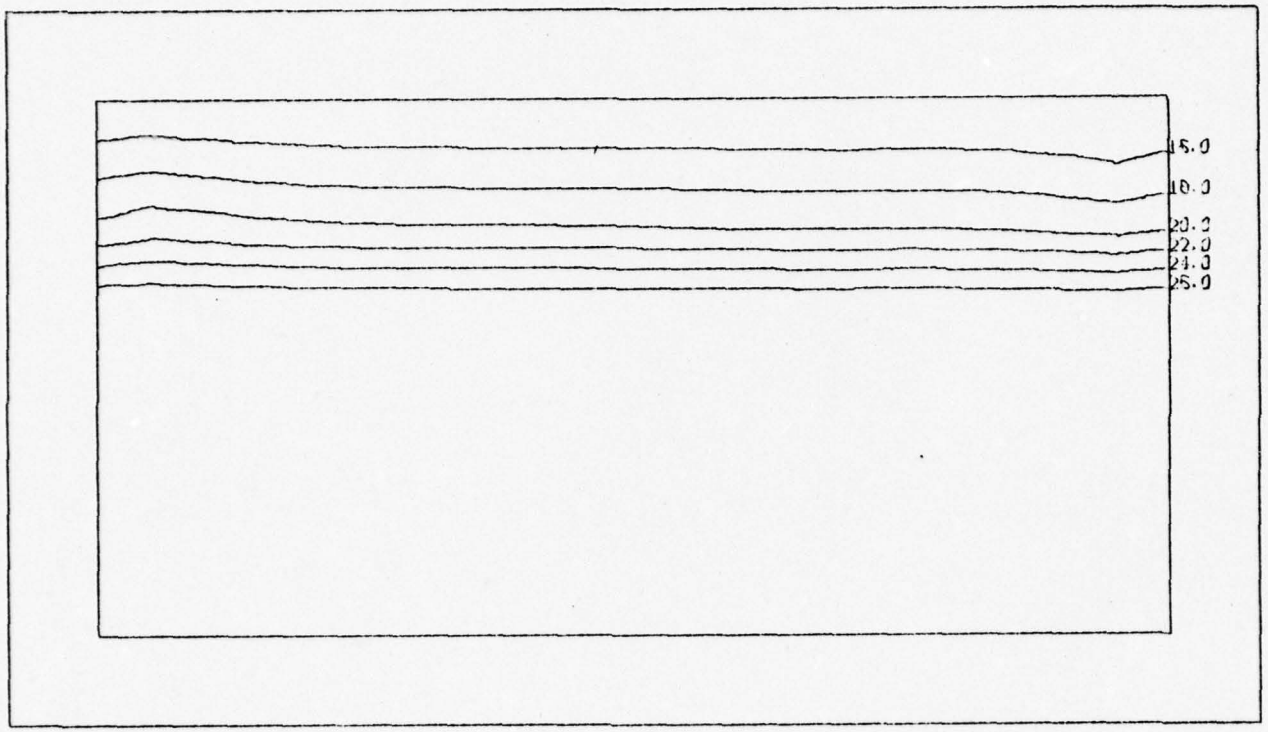

Figure 29. East–west sigma–t cross section for the central part of the basin.

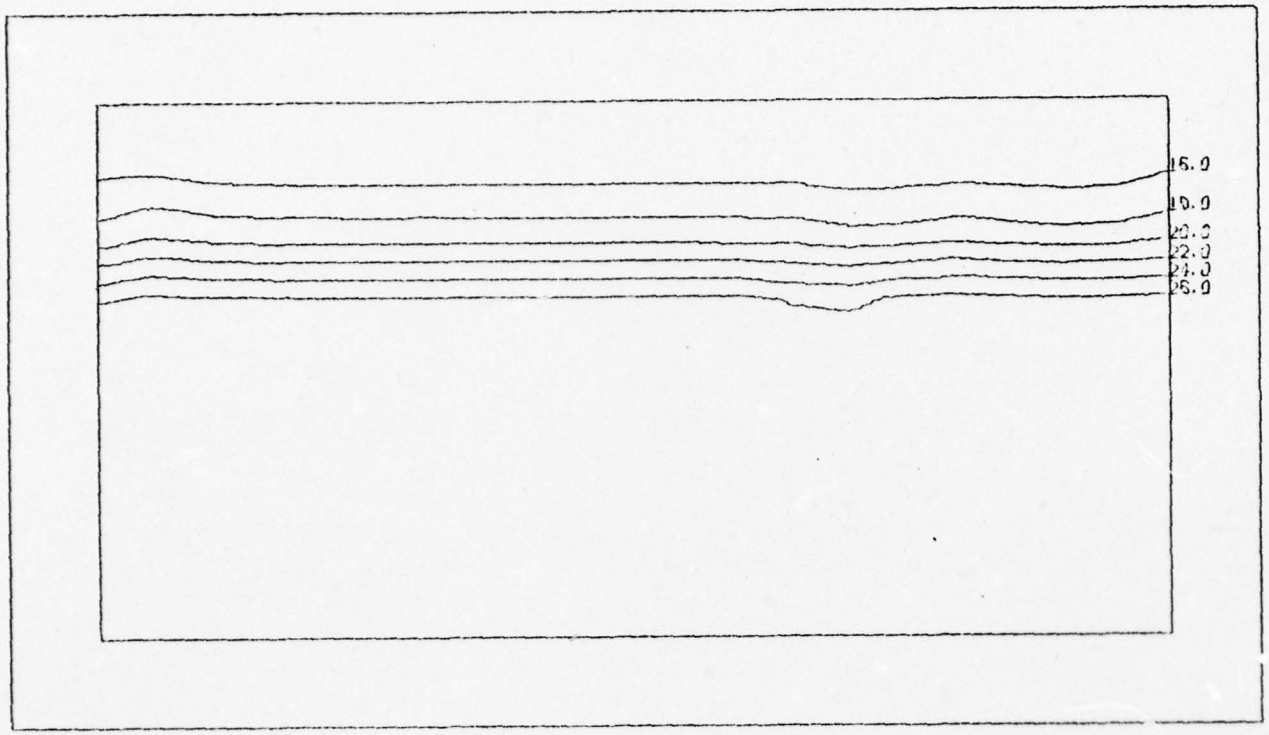

Figure 30. East–west sigma–t cross section for the northern part of the basin.

The vertical cross sections of the meridional velocity which correspond to the previous sigma-t sections, are given in Figures 31-33. There is a northward flow at the surface in each section. The cross section near the southern boundary shows a southerly flow below the surface layer. Flow changes direction at about 20 meters. In the vicintiy of the Strait of Istanbul the effect of the open boundary is indicated by a weak northerly flow. There is a southerly flow below that and at depth about 30 m another reversal takes place. Weak northward flow is associated with the southerly wind. The southward and northward flows at depth are consistent with observations.

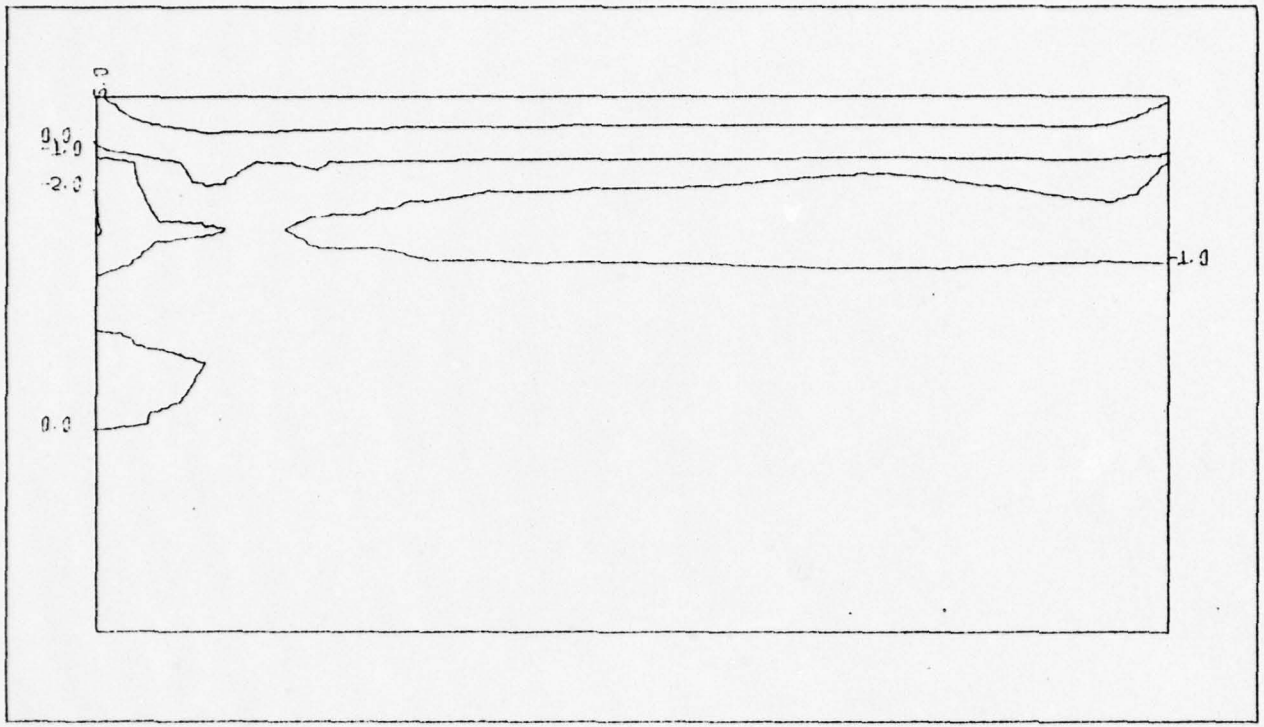

Figure 31. East–west cross section of the meridional velocity, (v), at the southern part of the basin.

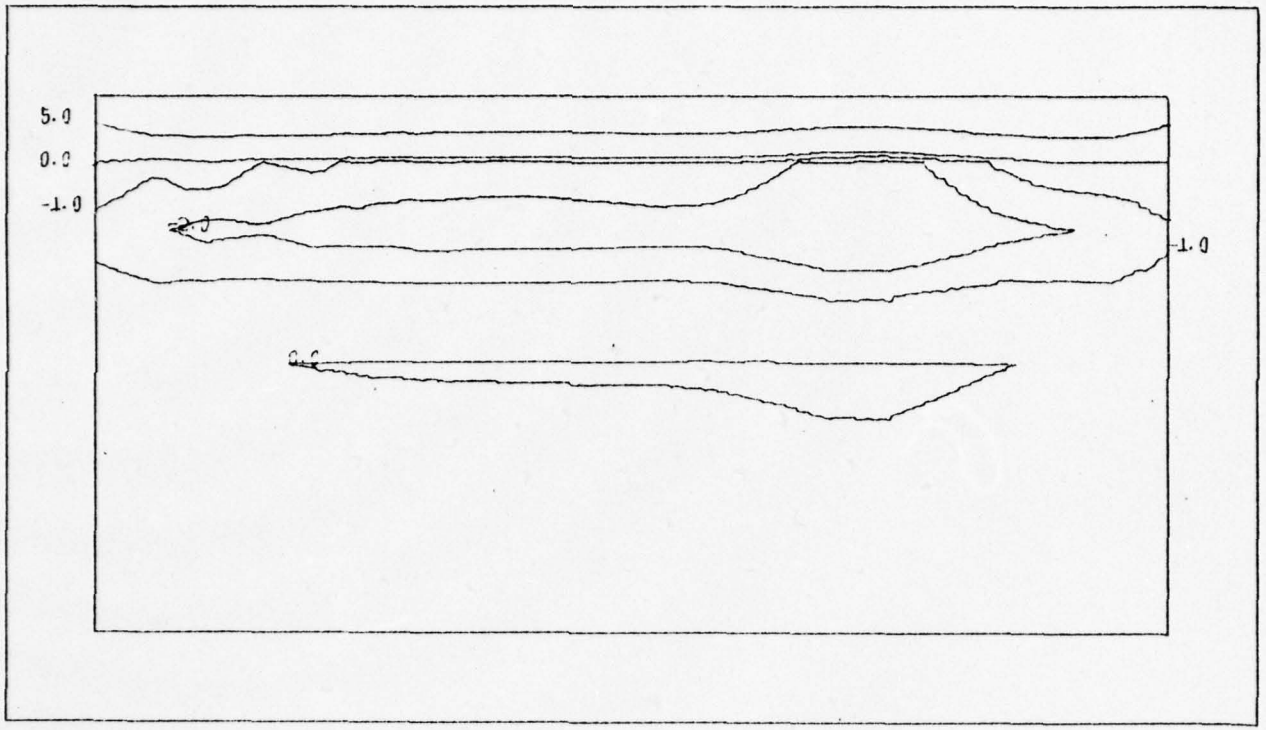

Figure 32. East-west cross section of the meridional velocity, (v), at the central part of the basin.

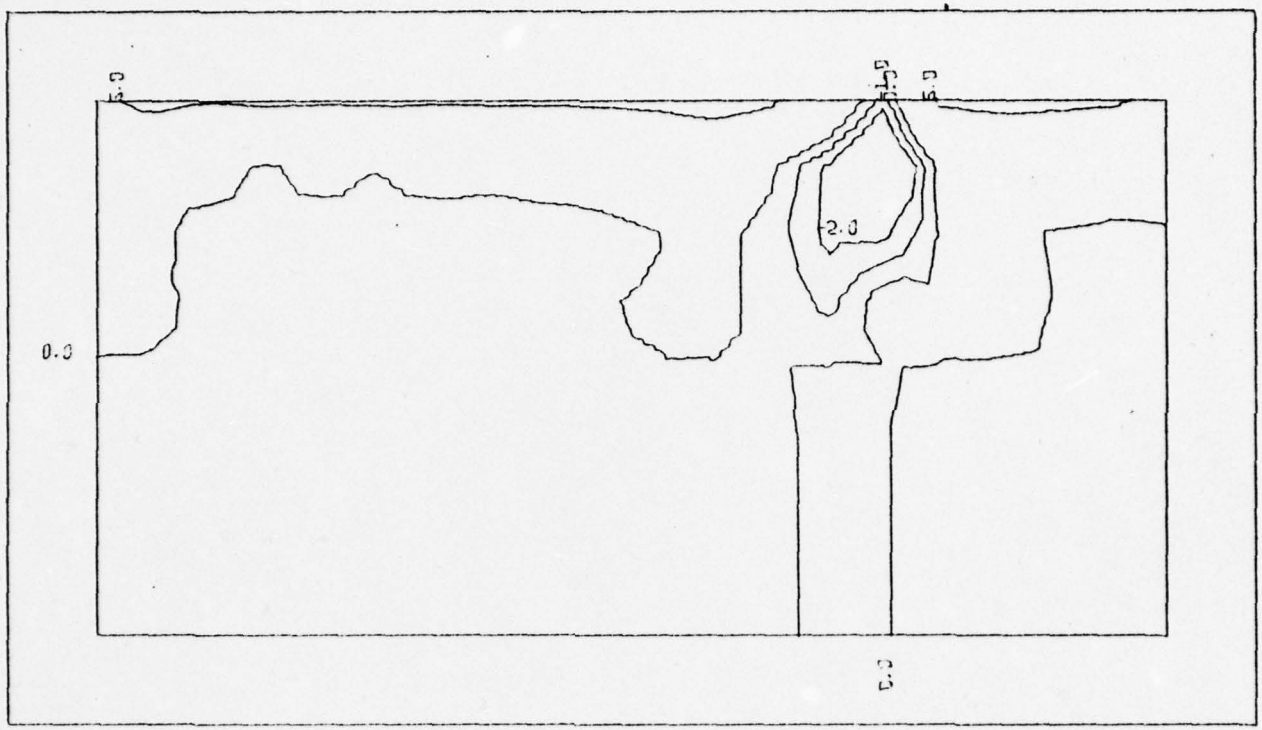

Figure 33. East-west cross section of the meridional velocity, (v), at the northern part of the basin.

VII. CONCLUSIONS

In order to investigate the dynamics of the Sea of Marmara a circulation model is formulated based on the hydrostatic and Boussinesq approximations. Since very little is known about the turbulence characteristics of the ocean or adjacent seas, viscosity and conductivity are replaced by new terms representing the contributions of the smaller scale motions to the exchange of momentum and density. Horizontal eddy transfer of momentum is accomplished using a constant eddy viscosity and diffusivity coefficient. For the exchange of momentum and density in the vertical a constant vertical diffusion coefficient also is used. The vertical mixing of density is enhanced by the use of an instantaneous adjustment mechanism to eliminate unstable lapse rates. A lateral mixing coefficient for density is less than that used for momentum. These coefficients should be sufficiently small so as not to obscure lateral transfer of the quantities, and a non zero momentum coefficient is needed to satisfy the zero slip boundary condition. In this study constant values of the coefficients are

$$A_H = .4 \times 10^7 \ \ cm^2 sec^{-1} \ \text{(density)}$$

and

$$A_M = \ 5 \times 10^7 \ \ cm^2 sec^{-1} \ \text{(momentum)}$$

The vertical diffusion coefficient which is difficult to evaluate either by measurement or in principle, is assigned 1.6 and 3.2 $cm^2 sec^{-1}$ for density and momentum respectively. Other parameters and constants are given in Table II.

Further study of thermocline penetration, water exchange, vertical mixing processes and current gradients might provide a better possibility for matching these coefficients.

Although many important factors, such as the irregular bottom topography, bottom friction and non-linear terms in the equation of motion have been omitted, the results from the model are generally encouraging. More realistic results may be achieved by incorporating these effects systematically in further studies.

Integration in the model is carried out with a constant southerly wind stress which was chosen arbitrarily. Although the scale of the motion is small compared to a characteristic length scale for meteorological features, wind stress may be significantly variable over the sea due to the geographic location of the sea. Also seasonal variations of the wind may have a considerable effect on the vertical mean part of the current which is neglected during this study.

The model does not separately predict temperature and salinity which are sometimes important quantities. Diagnostic calculation of the density with the aid of predicted temperature and salinity fields can be done with a very simple modification of the model. This would require a calculation of the heat and salt fluxes at the surface and meridional

salt and heat separately in the model. It would be more difficult, however, to define boundary conditions for these quantities at the open boundaries. It is also difficult to simulate seasonal variations of these quantities at the open boundaries. Once these are defined properly, based on accurate observations, there are no inherent difficulties in simulating the dynamical processes in the sea using the general principles involved in this model. Even though this model depends on the particular hypothesis used for horizontal and vertical eddy transport of heat, salt and momentum, it is clear that valuable studies on small scale water bodies can be made.

APPENDIX A

COMPUTER PROGRAM DESCRIPTION

The computer program is written in FORTRAN IV and was used with the IBM 360/67 computer system at the W. R. Church Computer Center, Naval Postgraduate School.

The overall program is divided into two basic subprograms (1) the main program and associated subroutines (2) an access program which draws and writes the results of the first program.

The main program consists of nine subroutines which calculate different terms of the equation of motion and the density equation, pressure, vertical velocity and changes variables for next time step.

FORTRAN IV symbols for the primary program and a brief description of the subroutines are given below:

UMI	Zonal velocity component at n-1 time step
U	Zonal velocity component at n time step
UA1	Zonal velocity component at n+1 time step
VM1	Meridional velocity component at n-1 time step
U	Meridional velocity component at n time step
UA1	Meridional velocity component at n+1 time step
SGM1	Sigma-t at n-1 time step
SGMT	Sigma-t at n time step
SGMT	Sigma-t at n+1 time step

ADV	Total advection term in density equation
ADV	Local rate of change of sigma-t
ADV	Pressure
A	Surface pressure
PBAR	Vertical average pressure
W	Vertical velocity
UXG	Gradient of zonal velocity in x direction
UYG	Gradient of zonal velocity in y direction
UZG	Gradient of zonal velocity in vertical
VXG	Gradient of meridional velocity in x direction
VYG	Gradient of meridional velocity in y direction
VZG	Gradient of meridional velocity in vertical
SGX	Gradient of sigma-t in x direction
SGY	Gradient of sigma-t in y direction
SGZ	Gradient of sigma-t in vertical
TX	Meridional wind stress
TY	Zonal wind stress
DZ	Layer depth
DZ	Layer
BB	Depth dependent velocity at the Northern fictitious boundary
CA	Depth dependent velocity at the Southern fictitious boundary
BO	fictitious boundary Sigma-t defined outside the domain at North
CD	Sigma-t defined outside the domain at South
DX	Horizontal grid spacing in x direction
DY	Horizontal grid spacing in y direction
RO	Rossby number

EH	Horizontal Ekman number
EV	Vertical Ekman number
PEl	Péclet number
VVl	Relative velocity
AK	Vertical eddy diffusivity
AKV	Vertical eddy viscosity
RL	Curl factor
HH	Depth of the basin
DT	Time step

SUBROUTINE PRES	Calculates pressure
SUBROUTINE VERW	Calculates vertical velocity
SUBROUTINE ADVEC	Calculates advection term in the density equation
SUBROUTINE HDGRD	Calculates gradients of the sigma-t
SUBROUTINE DIFFO	Calculates local time rate of the change sigma-t by subtracting advection term from the diffusion term
SUBROUTINE SIGEQ	Calculates new sigma-t and makes convective adjustment for unstable lapse rates.
SUBROUTINE HVGRD	Calculates gradients of the horizontal velocities
SUBROUTINE HORV	Calculates horizontal velocity components, u,v.

A descriptive flow diagram of the program is shown in Figure 34.

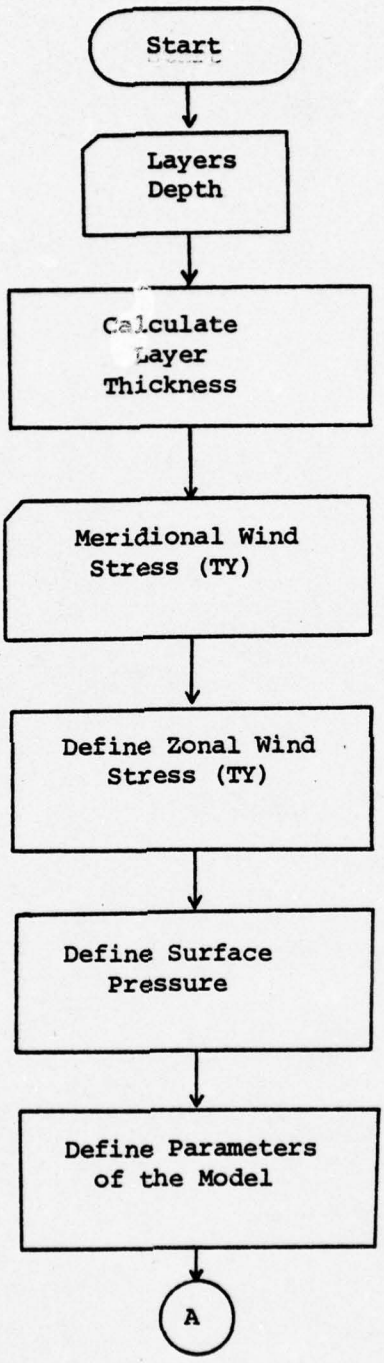

Figure 34. Descriptive flow diagram of the program.

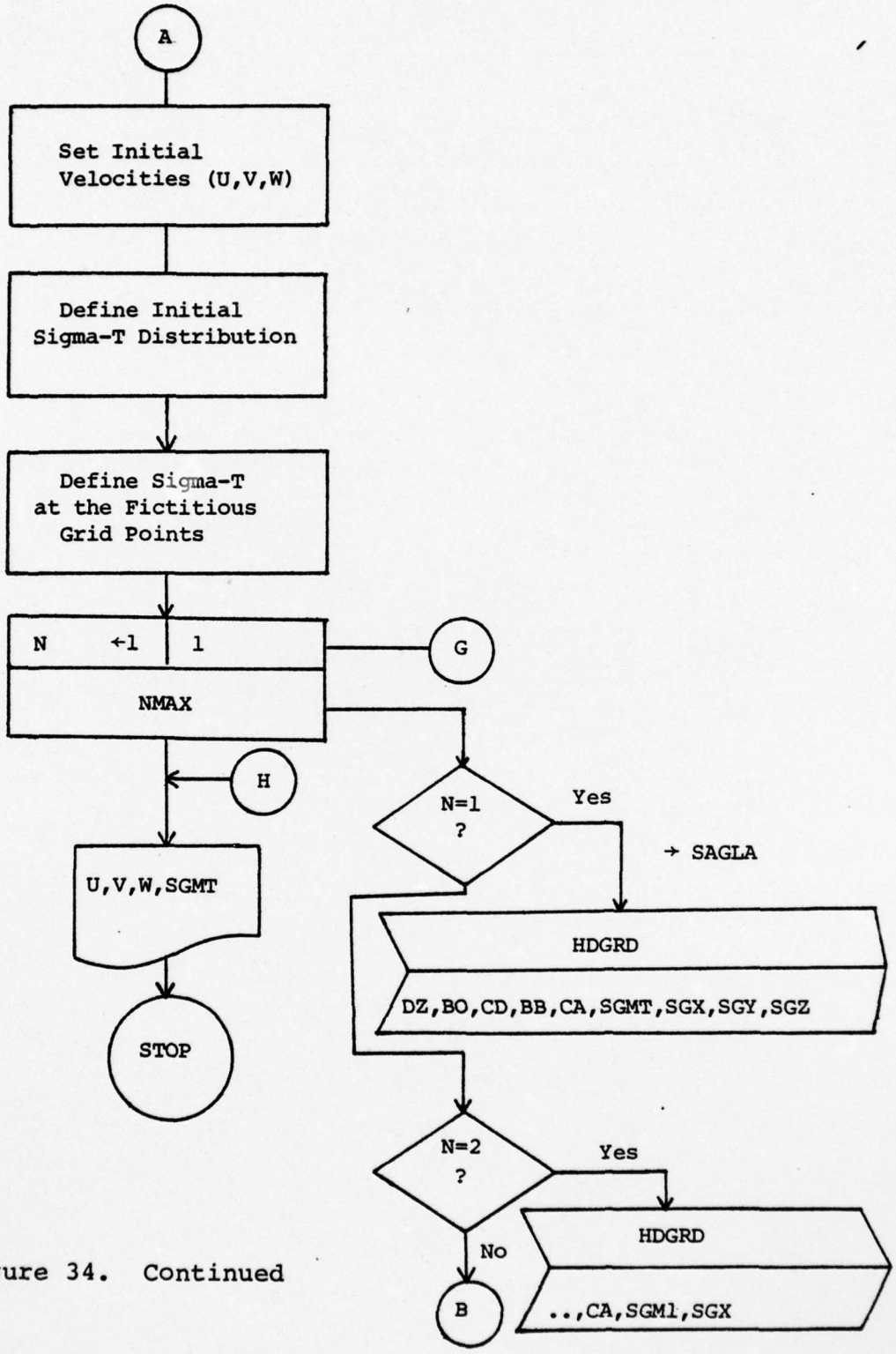

Figure 34. Continued

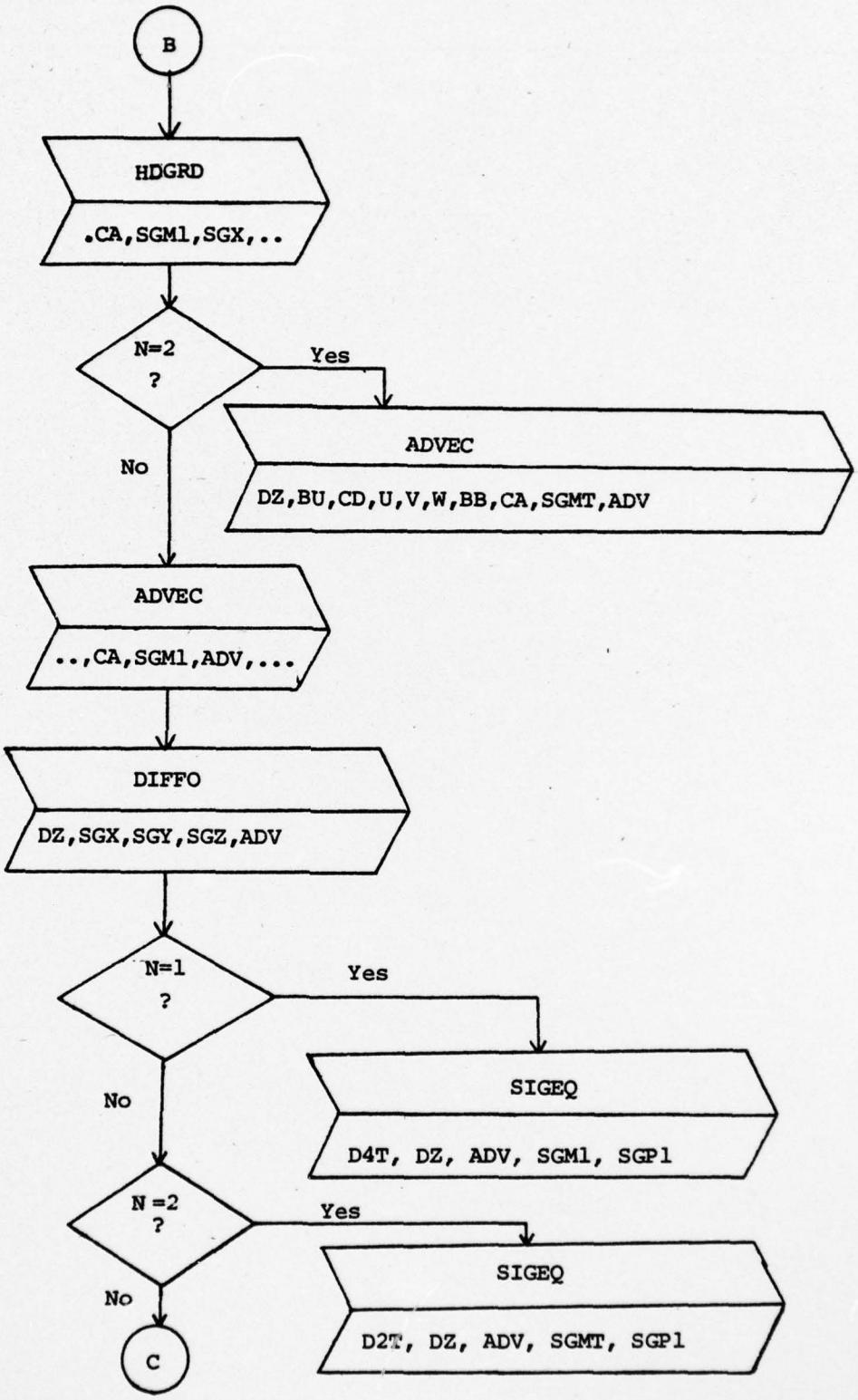

Figure 34. Continued

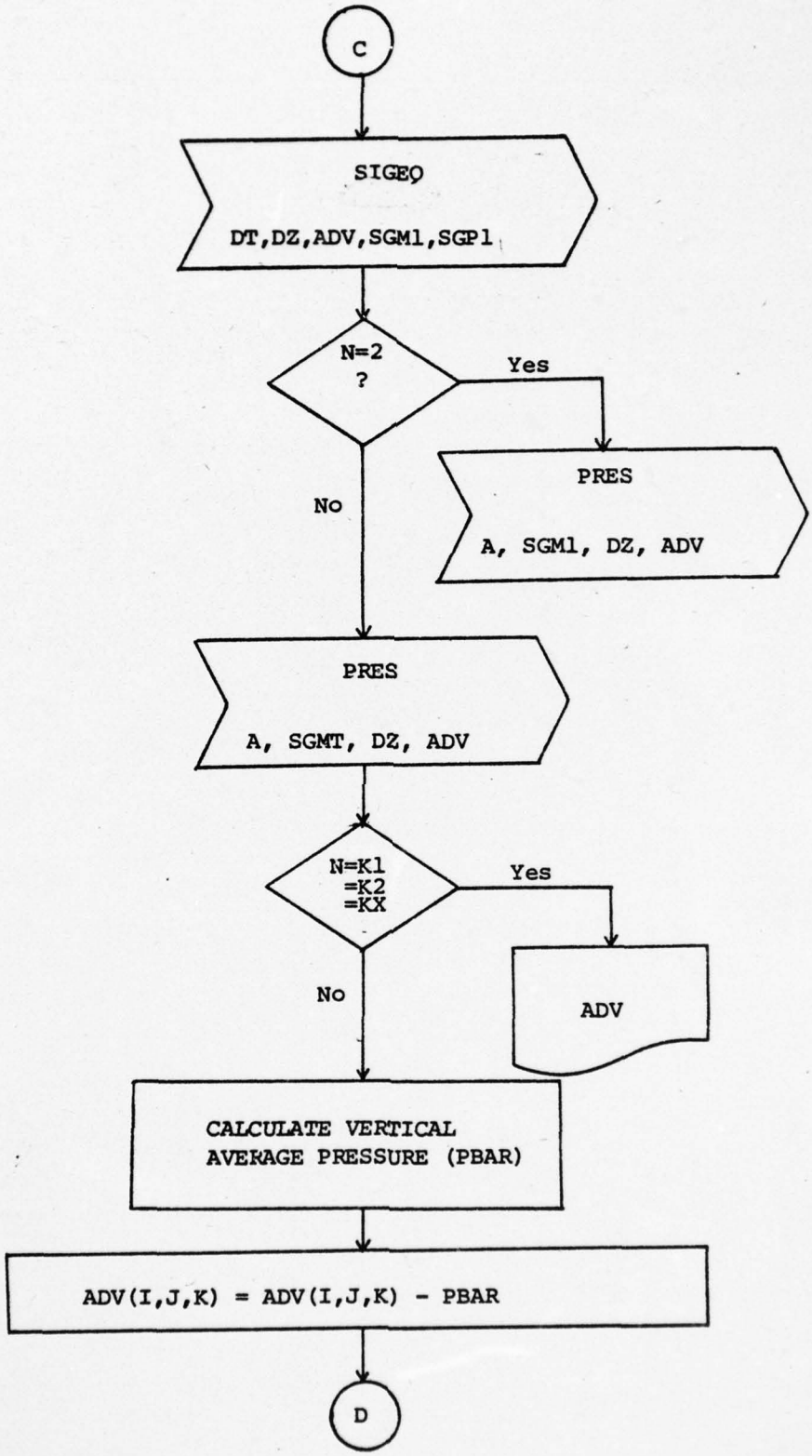

Figure 34. Continued

AD-A032 368 NAVAL POSTGRADUATE SCHOOL MONTEREY CALIF F/G 8/3

NUMERICAL INVESTIGATION OF THE DYNAMICS OF SEA OF MARMARA.(U)

SEP 76 H YUCE

UNCLASSIFIED NL

2 OF 2

AD A032368

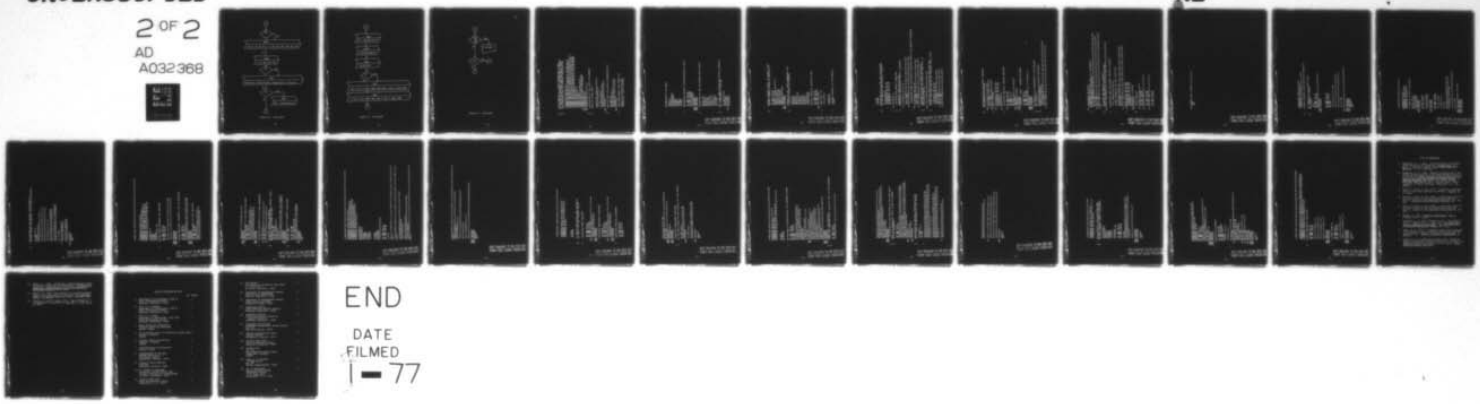

END

DATE FILMED 1-77

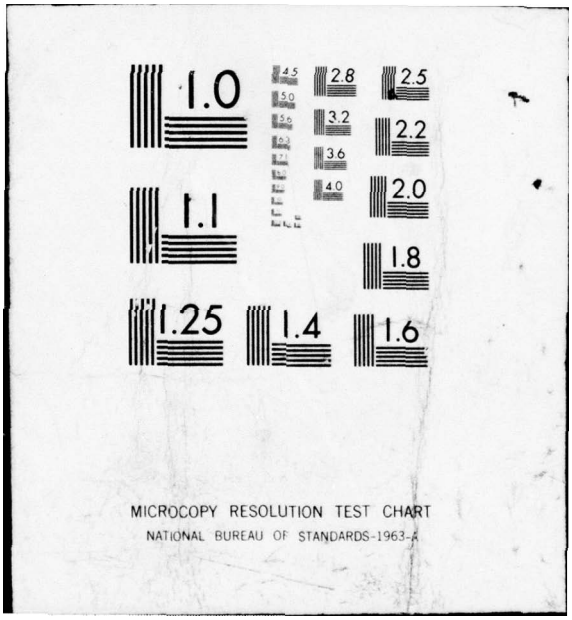
1.0
1.1
1.25
1.4
1.6
1.8
2.0
2.2
2.5
2.8
3.2
3.6
4.0
4.5
5.0
5.6
MICROCOPY RESOLUTION TEST CHART
NATIONAL BUREAU OF STANDARDS-1963-A

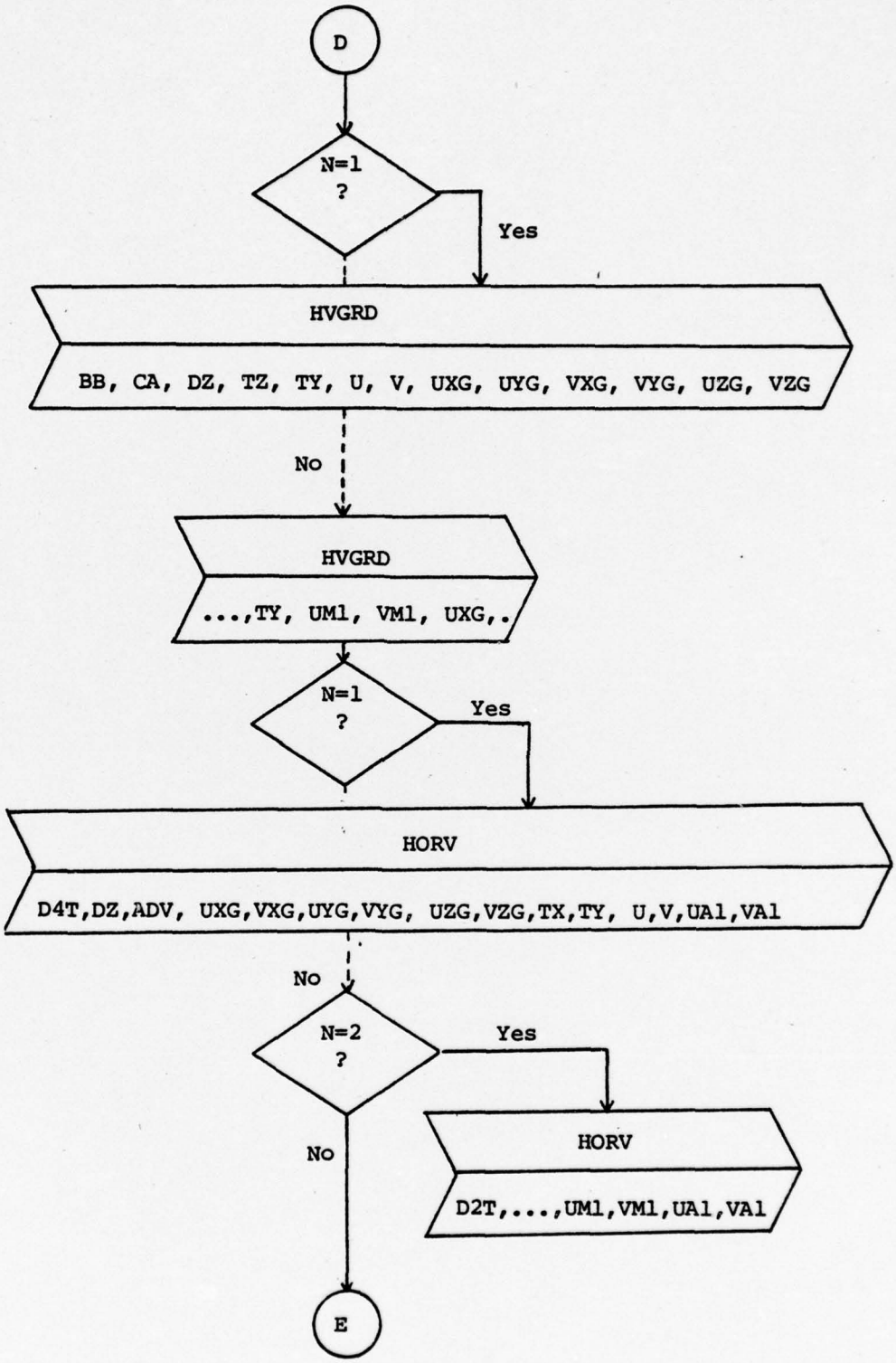

Figure 34. Continued

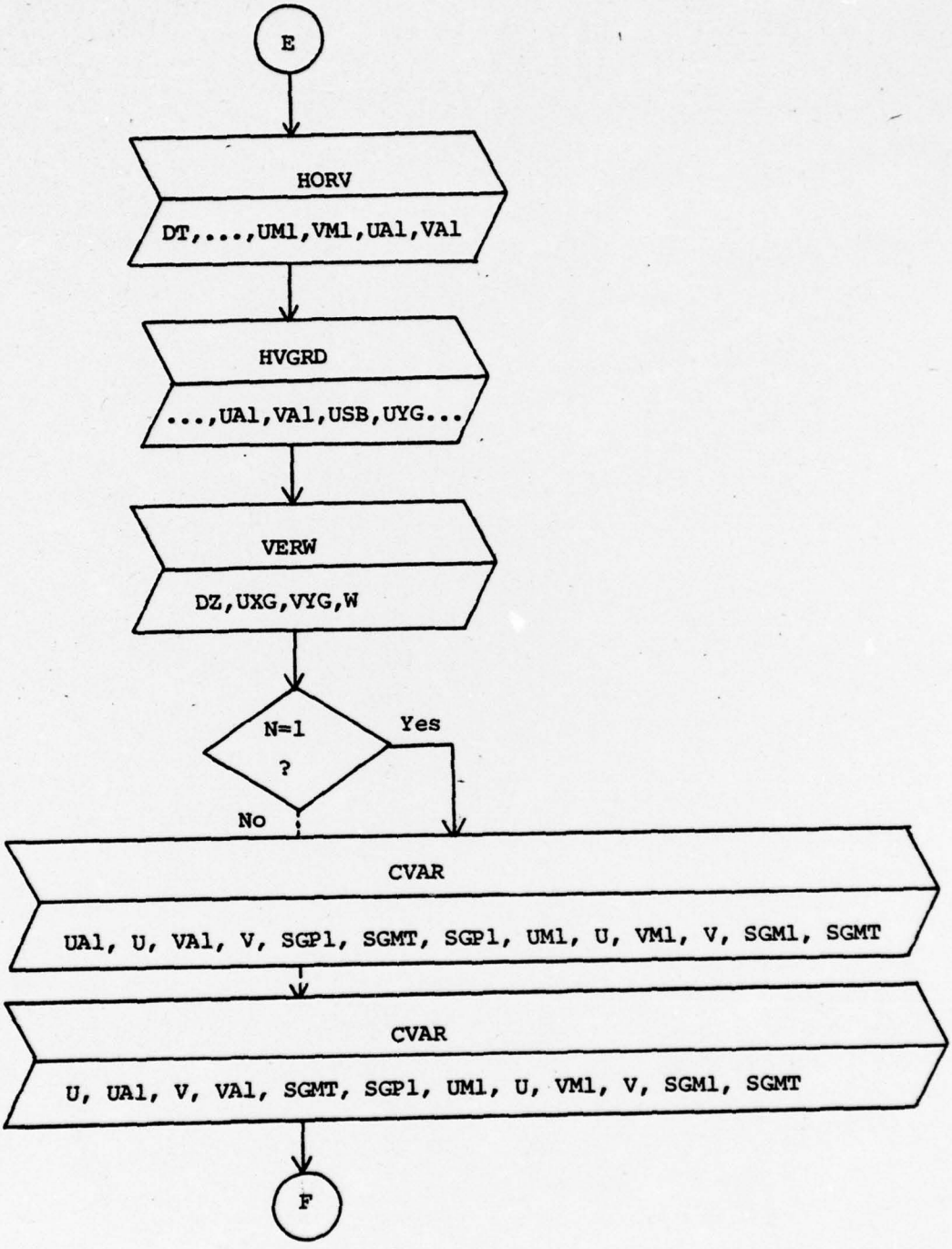

Figure 34. Continued

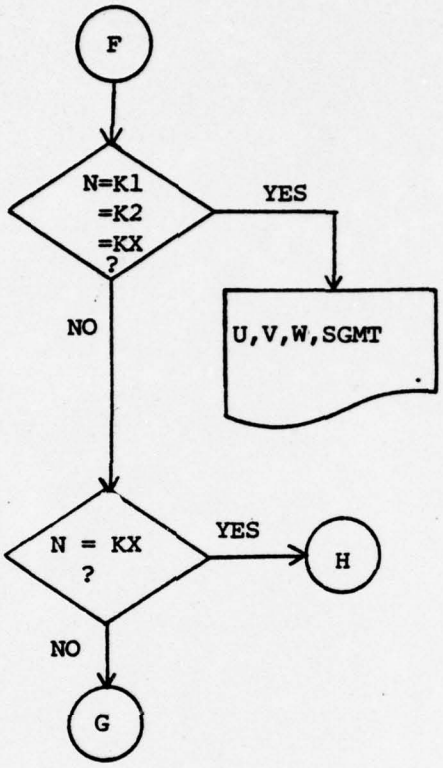

Figure 34. Continued

```
C     THIS PROGRAM IS A THREE DIMENSIONAL MODEL
C     OF THE SEA OF MARMARA, CIRCULATION IS DRIVEN
C     BY SURFACE WIND STRESS AND HORIZANTAL PRES-
C     SURE GRADIENT DUE TO INTERNAL STRAFICIATION

      DIMENSION PBAR(21,11)
      COMMON UM1(20,10,9),U(20,10,9),UA1(20,10,9)
      COMMON VM1(20,10,9),V(20,10,9),VA1(20,10,9)
      COMMON SGM1(21,11,6),SGMT(21,11,6),SGP1(21,11,6)
      COMMON SGX(22,11,6),SGY(21,12,6),SGZ(21,11,7)
      COMMON UXG(21,10,9),UYG(20,11,9),UZG(20,10,10)
      COMMON VXG(21,10,9),VYG(20,11,9),VZG(20,10,10)
      COMMON ADV(21,11,9)
      COMMON W(21,11,9)
      COMMON DZ(19)
      COMMON TX(20),TY(10),A(11)
      COMMON BO(5),CD(6),BB(5),CA(6)
    3 FORMAT(18H1 LAYER THICKNESES)
   15 FORMAT(11F5.3)
   20 FORMAT(10F7.4)
   25 FORMAT(1F8.3,2X,1F8.3)
C
C     CALCULATION OF THE LAYER THICKNESSES

C     READ THE LAYER DEPTH

      READ(5,20) (DZ(I),I=2,18,2)
      DZ(1)=(-2.0)*DZ(2)

      DO 101 K=4,18,2
      DZ(K-1)=DZ(K-2)-DZ(K)
      DZ(19)=2.0*(DZ(18)+50.0)
  101 CONTINUE
C
C     THIS DO LOOP CALCULATES INTERMEDIATE DZ

      WRITE(6,3)
      DO 102 K=2,18,2
      DZ(K)=(DZ(K-1)+DZ(K+1))/2.
      WRITE(6,25) DZ(K-1),DZ(K)
  102 CONTINUE

C     READ MERIDIONAL WIND STRESS TX

      READ(5,15) (TX(I),I=1,10)
      READ(5,15) (TX(I),I=11,20)
```

```
C     PARAMETERS OF THE MODEL

      AK=1.6
      AKV=3.2
      EH=0.5319E-2
      EV=0.851E-2
      PE1=0.1
      VV1=0.1
      RL=10.
      DX=0.1
      DY=0.05
      HH=50.

C     HORIZANTAL VELOCITY FIELD,STARTING AT REST

      DO 201 K=1,9
      DO 202 J=1,10
      DO 203 I=1,20
      U(I,J,K)=0.0
      V(I,J,K)=0.0
  203 CONTINUE
  202 CONTINUE
  201 CONTINUE

C     VELOCITIES AT THE FICTITIOUS GRID POINTS

      BB(1)=-4.
      BB(2)=-2.
      BB(3)=0.
      BB(4)=1.
      BB(5)=0.
      CA(1)=-3.
      CA(2)=-1.5
      CA(3)=-1.
      CA(4)=0.
      CA(5)=0.75
      CA(6)=0.

C     SET ZONAL WIND STRESS AND SURFACE PRESSURE
C     AS A FUNCTION OF LATITUDE

      DO 210 I=1,10
      A(I)=0.0
      TY(I)=0.0
  210 CONTINUE
      A(11)=0.0
```

```
C     INITIAL DENSITY FIELD  IN SIGMA-T UNIT
C     (SIGMA-T NORTH)-(SIGMA-T SOUTH)=4.0

      DO 106 J=1,11
      DO 107 I=1,21
      SGMT(I,J,1)=4.-0.1*(J-1)
      SGMT(I,J,2)=4.
      SGMT(I,J,3)=5.
      SGMT(I,J,4)=7.
      SGMT(I,J,5)=7.
      SGMT(I,J,6)=7.125
  107 CONTINUE
  106 CONTINUE

C     DENSITY AT THE  OPEN BOUNDARIES ARE
C     ( DEFINED OUTSIDE THE DOMAIN)

      BC(1)=3.
      BC(2)=4.
      BC(3)=5.
      BC(4)=6.
      BC(5)=7.125
      CC(1)=4.
      CC(2)=5.
      CC(3)=6.
      CC(4)=6.5
      CC(4)=7.
      CC(5)=7.
      CC(5)=7.125
      CC(6)=7.125

      INITIAL VERTICAL VELOCITY FIELD

      DO 950 K=1,9
      DO 950 J=1,11
      DO 950 I=1,21
  950 W(I,J,K)=0.

C     TIME STEP = DT

      DT=1.92E-4


      D2T=DT/2.
      D4T=DT/4.

C     WRITING INTERVAL OF THE RESULTS
      K1=90
```

```
      K2=135
      KX=180

C     PREDICTION OF U,V,SGMT AND CALCULATION
C     OF THE PRESSURE AND VERTICAL VELOCITY

      DO 52 N=1,KX
      IF(N.EQ.K1) GO TO 66
      IF(N.EQ.K2) GO TO 66
      IF(N.EQ.KX) GO TO 66
      GO TO 51
C
   66 WRITE(8) N

C     SCLUTION FOR DENSITY EQUATION

C     SUBROUTINE HDGRD CALCULATES
C     HORIZANTAL AND VERTICAL DENSITY GRADIENTS

   51 IF(N.EQ.1) GO TO 58

      CALL HDGRD(DZ,BO,CD,BB,CA,SGM1,SGX,SGY,SGZ)
      GO TO 917
   58 CALL HDGRD(DZ,BO,CD,BB,CA,SGMT,SGX,SGY,SGZ)

C       SUBROUTINE ADVEC CALCULATES ADVECTION TERM IN THE DENSITY EQUATION

  917 IF(N.EQ.2) GO TO 59
      CALL ADVEC(DZ,BO,CD,U,V,W,BB,CA,SGMT,ADV)
      GC TO 918
   59 CALL ADVEC(DZ,BO,CD,U,V,W,BB,CA,SGMT,ADV)

C     SUBROUTINE DIFFO CALCULATES DIFFUSION
C     TERM AND ADDS TO THE ADVECTION TERM THAT IS
C     CALCULATED BEFORE

  918 CALL DIFFO(DZ,SGX,SGY,SGZ,ADV)

C     SUBROUTINE SIGEQ CALCULATES NEW SGMT AND
C     ADJUST VERTICAL PROFILE FOR UNSTABLE LAPSE RATES

      IF(N.EQ.1) GO TO 61
      IF(N.EQ.2) GO TO 62
      CALL SIGEQ(DT,DZ,ADV,SGM1,SGP1)
      GO TO 920
   61 CALL SIGEQ(D4T,DZ,ADV,SGMT,SGP1)
      GO TO 920
   62 CALL SIGEQ(D2T,DZ,ADV,SGM1,SGP1)
```

```
C     SUBROUTINE PRES CALCULATES PRESSURE
C     ADV REPRESENT PRESSURE

  920 IF(N.EQ.2) GO TO 450
      CALL PRES(A,SGMT,DZ,ADV)
      GO TO 451
  450 CALL PRES(A,SGM1,DZ,ADV)
C     WRITE PRESSURE

  451 IF(N.EQ.K1) GO TO 452
      IF(N.EQ.K2) GO TO 452
      IF(N.EQ.KX) GO TO 452
      GO TO 453
  452 WRITE(8) ADV

C     CALCULATE VERTICAL AVERAGE PRESSURE

  453 DO 460 J=1,11
      DO 470 I=1,21
      SUM=0.0
      DO 480 K=1,9
      KK=2*K
      SUM=SUM+ADV(I,J,K)*DZ(KK)
  480 CONTINUE
      PBAR(I,J)=SUM/HH
  470 CONTINUE
  460 CONTINUE
C     PRESSURE  MINUS   AVERAGE PRESSURE

      DO 500 K=1,9
      DO 400 J=1,11
      DO 300 I=1,21
      ADV(I,J,K)=ADV(I,J,K)-PBAR(I,J)
  300 CONTINUE
  400 CONTINUE
  500 CONTINUE

C     SOLUTION OF U,V,COMPONENTS OF THE HORIZAN-
C     TAL VELOCITY
C
C     SUBROUTINE HVGRD CALCULATES HORIZANTAL
C     VELOCITY GRADIENTS
      IF(N.EQ.1) GO TO 54
      CALL HVGRD(BB,CA,DZ,TX,TY,UM1,VM1,UXG,UYG,VXG,VYG,UZG,VZG)
      GO TO 915
   54 CALL HVGRD(BB,CA,DZ,TX,TY,U,V,UXG,UYG,VXG,VYG,UZG,VZG)
```

```
  915 IF(N.EQ.1) GO TO 56
      IF(N.EQ.2) GO TO 57
C     SUBROUTINE HORV CALCULATES U,V, COMPONENTS
C     OF THE HORIZANTAL VELOCITIES
      CALL HORV(DT,DZ,ADV,UXG,VXG,UYG,VYG,UZG,VZG,TX,TY,UM1,VM1,UA1,VA1)
      GO TO 916
   56 CALL HORV(D4T,DZ,ADV,UXG,VXG,UYG,VYG,UZG,VZG,TX,TY,U,V,UA1,VA1)
      GO TO 916
   57 CALL HORV(D2T,DZ,ADV,UXG,VXG,UYG,VYG,UZG,VZG,TX,TY,UM1,VM1,UA1,VA1
     1)

C     SOLUTION FOR VERTICAL VELOCITY
C     CALCULATE HORIZANTAL VELOCITY GRADIENTS
  916 CALL HVGRD(BB,CA,DZ,TX,TY,UA1,VA1,UXG,UYG,VXG,VYG,UZG,VZG)

C     SUBROUTINE VERW CALCULATES VERTICAL VELOCITY

      CALL VERW(DZ,UXG,VYG,W)

C     CHANGE VARIABLES FOR NEXT TIME STEP

      IF(N.EQ.1) GO TO 65
      CALL CVAR(U,UA1,V,VA1,SGMT,SGP1,UM1,U,VM1,V,SGM1,SGMT)
      GO TO 95
   65 CALL CVAR(UA1,U,VA1,V,SGP1,SGMT,UM1,U,VM1,V,SGM1,SGMT)

C     WRITE RESULT ON A TAPE
   95 IF(N.EQ.K1) GO TO 199
      IF(N.EQ.K2) GO TO 199
      IF(N.EQ.KX) GO TO 199
      GO TO 52
  199 WRITE(8) U,V,W,SGMT
   52 CONTINUE
C
C     WRITE RESULTS

   10 FORMAT(9(1F12.6,1X))
      DO 397 I=1,20
      DO 397 J=1,10
  397 WRITE(6,10) (U(I,J,K),K=1,9)

      DO 398 I=1,20
      DO 398 J=1,10
  398 WRITE(6,10) (V(I,J,K),K=1,9)

      DO 399 I=1,21
      DO 399 J=1,11
```

```
399 WRITE(6,10) (SGMT(I,J,K),K=1,6)
      STOP
      END
```

```
      SUBROUTINE PRES(A,S,D,PR)
      DIMENSION PR(21,11,9)
      DIMENSION A(11),S(21,11,6),D(19)
C     SURFACE PRESSURE VARIATIONS ARE NEGLECTED

C     SC SIGMA-T OF THE BOTTOM WATER
C     SO  REFERENCE SIGMA-T
      SC=7.125

      SO=3.
      DO 100 J=1,11
      DO 200 I=1,21
      PR(I,J,1)=(S(I,J,1)-SO)*D(1)/2.
  200 CONTINUE
  100 CONTINUE


      DO 300 J=1,11
      DO 400 I=1,21
      DO 500 K=2,9
      KK=2*K

      IF(K.GT.6) GO TO 101

      SP=(S(I,J,K-1)+S(I,J,K))/2.-SO

      PR(I,J,K)=PR(I,J,K-1)+SP*D(KK-1)

      GO TO 500

  101 PR(I,J,K)=PR(I,J,K-1)+(SC-SO)*D(KK-1)

  500 CONTINUE
  400 CONTINUE
  300 CONTINUE
      RETURN
      END
```

```
      SUBROUTINE VERW(DD,UG,VG,W)

      DIMENSION DD(19)
      DIMENSION UG(21,10,9)
      DIMENSION VG(20,11,9)
      DIMENSION W(21,11,9)

C     W SURFACE =0 AND W BOTTOM=0

      DO 80 J=1,11
      DO 60 K=1,9
      W(1,J,K)=0.0
      W(21,J,K)=0.
   60 CONTINUE
   80 CONTINUE

      DO 90 I=2,20
      DO 70 K=1,9

      W(I,1,K)=0.0
      W(I,11,K)=0.0

   70 CONTINUE
   90 CONTINUE

      DO 100 I=2,20
      DO 200 J=2,10

      W(I,J,9)=0.0

      DO 300 K=1,8

      KK=2*K

      CD=(UG(I,J,K)+UG(I,J-1,K))/2.
      EF=(VG(I,J,K)+VG(I-1,J,K))/2.
      IF(K.EQ.1) GO TO 101

      W(I,J,K)=W(I,J,K-1)+DD(KK)*(CD+EF)

      GO TO 300

  101 W(I,J,K)=DD(KK)*(CD+EF)
  300 CONTINUE
  200 CONTINUE
  100 CONTINUE
```

```
C     CALCULATION OF THE VERTICAL VELOCITIES AT
C     THE GRID POINTS CORRESPOND TO THE OPEN BOUNDARIES

      DO 500 K=1,8
      KK=2*K
      AC=VG(1,1,K)/2.
      BC=(VG(1,1,K)+VG(2,1,K))/2.

      CB=(VG(13,11,K)+VG(14,11,K))/2.

      DB=(VG(14,11,K)+VG(15,11,K))/2.

      IF(K.EQ.1) GO TO 65

      W(1,1,K)=W(1,1,K-1)+AC*DD(KK)
      W(2,1,K)=W(2,1,K-1)+BC*DD(KK)

      W(14,11,K)=W(14,11,K-1)+CB*DD(KK)
      W(15,11,K)=W(15,11,K-1)+DB*DD(KK)

      GO TO 500

   65 W(1,1,K)=AC*DD(KK)
      W(2,1,K)=BC*DD(KK)

      W(14,11,K)=CB*DD(KK)
      W(15,11,K)=DB*DD(KK)

  500 CONTINUE
      RETURN
      END
```

```
      SUBROUTINE HVGRD(BB,CA,DD,TX,TY,UU,VV,UX,UY,VX,VY,UZ,VZ)


      DIMENSION TX(20),TY(10)
      DIMENSION BB(5),CA(6),DD(19)
      DIMENSION UU(20,10,9),VV(20,10,9)
      DIMENSION UX(21,10,9),UY(20,11,9)
      DIMENSION VX(21,10,9),VY(20,11,9)
      DIMENSION UZ(20,10,10),VZ(20,10,10)

      EV=0.851E-2
      VV1=0.1
      RL=10.
      DX=0.1
      DY=0.05
      CCN=(VV1*RL)/EV
C     DEFINE ZONAL GRADIENTS FOR INTERIOR
      DO 100 I=1,19
      DO 200 J=1,10
      DO 300 K=1,9
      UX(I+1,J,K)=(UU(I+1,J,K)-UU(I,J,K))/DX
      VX(I+1,J,K)=(VV(I+1,J,K)-VV(I,J,K))/DX
  300 CONTINUE
  200 CONTINUE
  100 CONTINUE
C     DEFINE MERIDIONAL GRADIENTS FOR THE INTERIOR
      DO 101 J=1,9
      DO 102 I=1,20
      DO 103 K=1,9
      UY(I,J+1,K)=(UU(I,J+1,K)-UU(I,J,K))/DY
      VY(I,J+1,K)=(VV(I,J+1,K)-VV(I,J,K))/DY
  103 CONTINUE
  102 CONTINUE
  101 CONTINUE
C     DEFINE GRADIENTS AT EAST AND WEST
      DO 400 J=1,10
      DO 500 K=1,9
      UX(1,J,K)=(2.*UU(1,J,K))/DX
      UX(21,J,K)=-(2.*UU(20,J,K))/DX
      VX(1,J,K)=(2.*VV(1,J,K))/DX
```

```
      VX(21,J,K)=-(2.*VV(20,J,K))/DX
  500 CONTINUE
  400 CONTINUE
C     DEFINE GRADIENTS AT THE NORTH AND SOUTH
      DO 600 I=1,20
      DO 700 K=1,9
      UY(I,1,K)=(2.*UU(I,1,K))/DY
      UY(I,11,K)=-(2.*UU(I,10,K))/DY
      VY(I,1,K)=(2.*VV(I,1,K))/DY
      VY(I,11,K)=-(2.*VV(I,10,K))/DY
  700 CONTINUE
  600 CONTINUE

C     CALCULATE GRADIENTS AT THE OPEN BOUNDARIES

      DO 80 K=1,5
   80 VY(15,11,K)=(BB(K)-VV(15,10,K))/DY
      DO 90 K=1,6
   90 VY(1,1,K)=(VV(1,1,K)-CA(K))/DY

C     CALCULATE VERTICAL GRADIENTS
C     TX AND TY ARE DEFINED VELOCITY STORAGE POINTS
C     MERIDIONAL WIND STRESS IS ZERO
      DO 20 J=1,10
      DO 10 I=1,20
      UZ(I,J,1)=CON*TY(J)
      DO 30 K=2,9
      KK=2*K-1
      UZ(I,J,K)=(UU(I,J,K-1)-UU(I,J,K))/DD(KK)
      VZ(I,J,K)=(VV(I,J,K-1)-VV(I,J,K))/DD(KK)
   30 CONTINUE
   10 CONTINUE
   20 CONTINUE
C     SURFACE AND BOTTOM BOUNDARY CONDITIONS
C     IMPLIES THAT

      DO 50 I=1,20
      DO 40 J=1,10
      VZ(I,J,1)=TX(I)*CON
      VZ(I,J,10)=(2.*VV(I,J,9))/DD(19)
      UZ(I,J,10)=(2.*UU(I,J,9))/DD(19)
   40 CONTINUE
   50 CONTINUE
      RETURN
      END
```

```
      SUBROUTINE HORV(DT,PR,UXG,VXG,UYG,VYG,UZG,VZG,TX,TY,U,V,UA,VA)

      DIMENSION D(19),PR(21,11,9)
      DIMENSION UXG(21,10,9),VXG(21,10,9)
      DIMENSION UYG(20,11,9),VYG(20,11,9)
      DIMENSION UZG(20,10,10),VZG(20,10,10)
      DIMENSION U(20,10,9),V(20,10,9)
      DIMENSION UA(20,10,9),VA(20,10,9)
      DIMENSION TX(20),TY(10)

      EH=0.5319E-2
      EV=0.851E-2
      RN=4.255E-3
      DX=0.1
      DY=0.05
      VV1=0.1
      RL=10.
      C1=0.55
      C2=0.45


      HH=50.
      T=DT**2
      CX=C1**2
      R2=RN*RN
      TT=1.+4.*((T*CX)/R2)

      DO 400 K=1,9
      DO 300 J=1,10
      DO 200 I=1,20

      KK=2*K

      PTY=-(1./RN)*(PR(I+1,J+1,K)-PR(I+1,J,K)+PR(I,J+1,K)-PR(I,J,K))/(2.
     1*DY)

      HDY=(EH/RN)*((VXG(I+1,J,K)-VXG(I,J,K))/DX+(VYG(I,J+1,K)-VYG(I,J,K)
     1)/DY)

      VDY=(EV/RN)*(VZG(I,J,K)-VZG(I,J,K+1))/D(KK)
      WI=(RL*VV1)/(RN*HH)
      WINY=-WI*TX(I)

      UN1=-(C2/RN)*U(I,J,K)
      VT=V(I,J,K)+2.*DT*(PTY+HDY+VDY+WINY+UN1)
      TVT=(C1/RN)*VT
      PTX=-(1./RN)*(PR(I+1,J,K)-PR(I,J,K)+PR(I+1,J+1,K)-PR(I,J+1,K))/(2.
     1*DX)
```

```
      HDX=(EH/RN)*((UXG(I+1,J,K)-UXG(I,J,K))/DX+(UYG(I,J+1,K)-UYG(I,J,K)
     1)/DY)
      VDX=(EV/RN)*(UZG(I,J,K)-UZG(I,J,K+1))/D(KK)
      WINX=-WI*TY(J)
      VN1=(C2/RN)*V(I,J,K)

      UT=U(I,J,K)+2.*DT*(PTX+HDX+VDX+WINX+VN1+TVT)

      UA(I,J,K)=UT/TT

      UTC=-(C1/RN)*UA(I,J,K)

      VA(I,J,K)=V(I,J,K)+2.*DT*(PTY+HDY+VDY+WINY+UN1+UTC)

  200 CONTINUE
  300 CONTINUE
  400 CONTINUE
      RETURN
      END
```

```
      SUBROUTINE HDGRD(DD,BO,CD,BB,CA,S,SX,SY,SZ)

      DIMENSION BO(5),CD(6),BB(5),CA(6)
      DIMENSION S(21,11,6),SX(22,11,6)
      DIMENSION SY(21,12,6),SZ(21,11,7)
      DIMENSION DD(19)


      DX=0.1
      DY=0.05

C     SX AND SY ARE STORED WEST AND SOUTH
C     SZ ABOVE THE SGMT STORAGE POINTS

C     CALCULATE ZONAL GRADIENT

      DO 100 K=1,6
      DO 200 J=1,11
      DO 300 I=1,20
  300 SX(I+1,J,K)=(S(I+1,J,K)-S(I,J,K))/DX
      SX(1,J,K)=-SX(2,J,K)
      SX(22,J,K)=-SX(21,J,K)
  200 CONTINUE
  100 CONTINUE

C     CALCULATE MERIDIONAL GRADIENTS

      SC=7.125
      DO 110 K=1,6
      DO 120 I=1,21
      DO 130 J=1,10
  130 SY(I,J+1,K)=(S(I,J+1,K)-S(I,J,K))/DY
      SY(I,1,K)=-SY(I,2,K)
      SY(I,12,K)=-SY(I,11,K)
  120 CONTINUE
  110 CONTINUE

C     CALCULATE VERTICAL GRADIENTS

      DO 210 J=1,11
      DO 220 I=1,21
      DO 230 K=1,6
      KK=2*K
```

```
      IF(K.EQ.6) GO TO 500
      SZ(I,J,K+1)=(S(I,J,K)-S(I,J,K+1))/DD(KK+1)
      GO TO 230
  500 SZ(I,J,K+1)=(S(I,J,K)-SC)/DD(KK+1)
  230 CONTINUE
      SZ(I,J,1)=0.0
  220 CONTINUE
  210 CONTINUE

C     CALCULATE MERIDIONAL GRADIENTS

C    AT THE GRID POINTS IN THE VICINITY OF THE STRAITS

      DO 600 K=1,6
      SY(1,1,K)=(S(1,1,K)-CD(K))/DY
      SY(2,1,K)=(S(2,1,K)-CD(K))/DY
  600 CONTINUE

      DO 700 K=1,5

      SY(15,12,K)=(BO(K)-S(15,11,K))/DY
      SY(14,12,K)=(BO(K)-S(14,11,K))/DY

  700 CONTINUE

      RETURN
      END
```

```
      SUBROUTINE ADVEC(DL,BO,CD,UX,VY,WZ,BB,CA,SI,ADV)

      DIMENSION ADV(21,11,9),DL(19)
      DIMENSION BO(5),CD(6)
      DIMENSION BB(5),CA(6),SI(21,11,6)
      DIMENSION UX(20,10,9),VY(20,10,9),WZ(21,11,9)


      DX=0.1
      DY=0.05
      SC=7.125

C     CALCULATION OF ADVECTION FOR THE INTERIOR POINTS

      DO 101 K=2,6
      DO 102 J=2,10
      DO 103 I=2,20
      KK=2*K
      C=(UX(I,J,K)+UX(I,J-1,K))/2.0
      D=(UX(I-1,J-1,K)+UX(I-1,J,K))/2.
      E=(SI(I+1,J,K)+SI(I,J,K))/2.
      F=(SI(I-1,J,K)+SI(I,J,K))/2.
      UUM1=C*E/DX
      UP1=D*F/DX
      IF(K.GT.5) GO TO 60
      G=(SI(I,J,K+1)+SI(I,J,K))/2.
      GO TO 70
   60 G=(SC+SI(I,J,K))/2.
   70 H=(SI(I,J,K)+SI(I,J,K-1))/2.
      WP1=(WZ(I,J,K)*G)/DL(KK)
      WM1=(WZ(I,J,K-1)*H)/DL(KK)
      PP=(VY(I,J,K)+VY(I-1,J,K))/2.
      Q=(SI(I,J+1,K)+SI(I,J,K))/2.
      VVP1=(PP*Q)/DY
      R=(VY(I,J-1,K)+VY(I-1,J-1,K))/2.
      S=(SI(I,J-1,K)+SI(I,J,K))/2.
      VVM1=R*S/DY
      ADV(I,J,K)=-UP1+UUM1+VVP1-VVM1+WM1-WP1
  103 CONTINUE
  102 CONTINUE
  101 CONTINUE
C     RESET B.C. FOR VELOCITY
CCC   FREE SLIP CONDITION EXIST VELOCITY TANG. TO THE BOUNDARY
C
      DO 300 K=2,6
      DO 200 I=2,20
      TLXP=UX(I,1,K)*(SI(I,1,K)+SI(I+1,1,K))/2.
```

```
      TUX1=UX(I-1,1,K)*(SI(I,1,K)+SI(I-1,1,K))/2.
      ADV(I,1,K)=(TUXP-TUX1)/DX
      TUXPN=UX(I,10,K)*(SI(I+1,11,K)+SI(I,11,K))/2.
      TUX1N=UX(I-1,10,K)*(SI(I-1,11,K)+SI(I,11,K))/2.
      ADV(I,11,K)=(TUXPN-TUX1N)/DY
      ADV(1,11,K)=0.0
      ADV(21,11,K)=0.0
  200 CONTINUE
  300 CONTINUE
C     CALCULATION OF THE ADVECTION AT THE SIDE WALLS

C     FREE SLIP CONDITIONS EXIST VELOCITY TANGENT
C     TO THE BOUNDARIES

      DO 500 K=2,6
      DO 400 J=2,10
      TVAW=VY(1,J,K)*(SI(1,J+1,K)+SI(1,J,K))/(2.*DY)
      TVMW=VY(1,J-1,K)*(SI(1,J-1,K)+SI(1,J,K))/(2.*DY)
      ADV(1,J,K)=TVAW-TVMW
      TVAE=VY(20,J,K)*(SI(21,J+1,K)+SI(21,J,K))/(2.*DY)
      TVME=VY(20,J-1,K)*(SI(21,J-1,K)+SI(21,J,K))/(2.*DY)
      ADV(21,J,K)=TVAE-TVME
  400 CONTINUE
      ADV(1,1,K)=0.
      ADV(21,1,K)=0.0
  500 CONTINUE

C     CALCULATION OF VERTICAL ADVECTION AT THE
C     GRID POINTS CORRESPONDING TO THE STRAITS

      CS=7.125
      DO 600 K=2,6
      KK=2*K
C
      UP1=WZ(1,1,K-1)*(SI(1,1,K)+SI(1,1,K-1))/2.
      UP2=WZ(2,1,K-1)*(SI(2,1,K)+SI(2,1,K-1))/2.
      UB1=WZ(14,11,K-1)*(SI(14,11,K)+SI(14,11,K-1))/2.
      DB1=WZ(15,11,K-1)*(SI(15,11,K)+SI(14,11,K-1))/2.
      IF(K.EQ.6) GO TO 65

      DC1=WZ(1,1,K)*(SI(1,1,K)+SI(1,1,K+1))/2.
      DC2=WZ(2,1,K)*(SI(2,1,K)+SI(2,1,K+1))/2.
      UB2=WZ(14,11,K)*(SI(14,11,K)+SI(14,11,K+1))/2.
      DB2=WZ(15,11,K)*(SI(15,11,K)+SI(15,11,K+1))/2.
      GO TO 75

   65 DC1=WZ(1,1,K)*(SI(1,1,K)+CS)/2.
      UB2=WZ(14,11,K)*(SI(14,11,K)+CS)/2.
```

```
      DC2=WZ(2,1,K)*(SI(2,1,K)+CS)/2.
      DB2=WZ(15,11,K)*(SI(15,11,K)+CS)/2.

   75 ADV(1,1,K)=(UP1-DC1)/DL(KK)+ADV(1,1,K)
      ADV(2,1,K)=(UP2-DC2)/DL(KK)+ADV(2,1,K)
      ACV(14,11,K)=(UB1-UB2)/DL(KK)+ADV(14,11,K)
      ADV(15,11,K)=(DB1-DB2)/DL(KK)+ADV(15,11,K)
  600 CONTINUE
      RETURN
      END
```

```
      SUBROUTINE DIFFO(DE,SXX,SYY,SZZ,ADD)

      DIMENSION ADD(21,11,9),DE(19)
      DIMENSION SXX(22,11,6),SYY(21,12,6)
      DIMENSION SZZ(21,11,12)

C     CALCULATION OF THE DIFFUSION TERM
C     ON THE R.H.S. OF DENSITY EQUATION
C     FURTHER TENDENCY TERM IS CALCULATED

      RN=4.255E-3
      EV=0.851E-2
      AK=1.6
      AKV=3.2
      DX=0.1
      DY=0.05
      PE1=0.1

      C=AK/AKV
      ZC=(C*EV)/RN

      DO 100 K=2,6
      DO 200 J=1,11
      DO 300 I=1,21

      KK=2*K
      XX=(PE1/DX)*(SXX(I+1,J,K)-SXX(I,J,K))
      YY=(PE1/DY)*(SYY(I,J+1,K)-SYY(I,J,K))
      ZZ=(1./DE(KK))*(SZZ(I,J,K)-SZZ(I,J,K+1))
      ZZ=ZC*ZZ

      ADD(I,J,K)=XX+YY+ZZ-ADD(I,J,K)

  300 CONTINUE
  200 CONTINUE
  100 CONTINUE

      RETURN
      END
```

```
      SUBROUTINE SIGEQ(DT,DD,ADD,STN,STA)
      DIMENSION STN(21,11,6),ADD(21,11,9)
      DIMENSION STA(21,11,6)
      DIMENSION DD(19)
      SC=7.125
      DO 100 K=2,6
      DO 200 J=1,11
      DO 300 I=1,21
      STA(I,J,K)=STN(I,J,K)+2.*DT*ADD(I,J,K)
      STA(I,J,1)=STN(I,J,1)
      IF(STA(I,J,6).GT.SC) GO TO 250
      GO TO 300
  250 STA(I,J,6)=SC
  300 CONTINUE
  200 CONTINUE
  100 CONTINUE

C     CONVECTIVE ADJUSMENT

      DO 400 I=1,21
      DO 500 J=1,11
      DO 600 N=1,NMAX
      DO 700 K=1,5
      KK=2*K
      A=STA(I,J,K+1)

      B=STA(I,J,K)
C
      IF(B.GT.A) GO TO 50
      GO TO 700
   50 CSM=(DD(KK)*B+DD(KK+2)*A)/(DD(KK)+DD(KK+2))
      IF(K.EQ.1) GO TO 60
      IF(K.EQ.5) GO TO 70
      STA(I,J,K)=CSM
      STA(I,J,K+1)=CSM
      GO TO 600
   60 STA(I,J,K+1)=STA(I,J,K)
      GO TO 600
   70 STA(I,J,K)=STA(I,J,K+1)
      GO TO 600
  700 CONTINUE
      GO TO 500
  600 CONTINUE
  500 CONTINUE
  400 CONTINUE

      RETURN
      END
```

```
      SUBROUTINE CVAR(UN,UNA,VN,VNA,SGN,SGNA,UM,UNN,VM,VNN,SGM,SGNN)

      DIMENSION UN(20,10,9),UNA(20,10,9),VN(20,10,9),VNA(20,10,9)
      DIMENSION UM(20,10,9),UNN(20,10,9),VM(20,10,9),VNN(20,10,9)
      DIMENSION SGN(21,11,6),SGNA(21,11,6)
      DIMENSION SGM(21,11,6),SGNN(21,11,6)

C     CHANGE HORIZANTAL VELOCITIES

      DO 100 K=1,9
      DO 200 J=1,10
      DO 300 I=1,20

      UM(I,J,K)=UN(I,J,K)

      UNN(I,J,K)=UNA(I,J,K)

      VM(I,J,K)=VN(I,J,K)

      VNN(I,J,K)=VNA(I,J,K)

  300 CONTINUE
  200 CONTINUE
  100 CONTINUE

C     CHANGE SIGMA-TS

      DO 400 K=1,6
      DO 500 J=1,11
      DO 600 I=1,21

      SGM(I,J,K)=SGN(I,J,K)

      SGNN(I,J,K)=SGNA(I,J,K)

  600 CONTINUE
  500 CONTINUE
  400 CONTINUE

      RETURN
      END
```

LIST OF REFERENCES

1. Bogdanova, A. K., 1961: The distribution of Mediterranean waters in the Black Sea, Okeanologiya, v. 1, no. 6, p. 983–991; English trans., 1963, Deep Sea Research, v. 10, p. 665–672.

2. Bogdanova, A. K., 1965: Seasonal fluctuations in the inflow and distribution of the Mediterranean waters of the Black Sea, Basic features of the geological structure of the hydrologic regime and biology of the Mediterranean Sea, Edited by L. M. Fomin, Academy of Sciences, USSR, Moscow 1965. English trans., 1969 Institute of Modern Languages, Washington, D.C. (AD 686001).

3. Bryan, K. and M. D. Cox, 1967: A numerical investigation of the oceanic general circulation. Tellus, 19, 1, 54–80.

4. Bryan, K. and M. D. Cox, 1968a: A non–linear model of an ocean driven by wind and differential heating: Part I. Journal of the Atmospheric Sciences, 25, 945–967..

5. Bryan, K. and M. D. Cox,,1968b: A non–linear model of an ocean driven by wind and differential heating: Part II. Journal of the Atmospheric Sciences, 25, 968–978.

6. Defant, A., 1961: Physical Oceanography, Vol. 1, Pergamon Press, 729 pp.

7. Gunnerson, C. G. and E. Özturgut, 1974: The Bosporus, In E. T. Degens and D. A. Ross, eds., The Black Sea – Geology, Chemistry and Biology. American Association of Petroleum Geologists, (Memoir 20), 1974.

8. Haney, R. L., 1974: A numerical study of the response of an idealized ocean to large scale surface heat and momentum flux. Journal of Physical Oceanography, 4, 145–167.

9. Levastu, T., S. Larson and K. Rabe, 1976: Numerical Models for Synoptic Analysis/Prediction of Currents and Temperature/Salinity Structure in the Oceans. Naval Research Reviews, June 1976.

10. Möller, L., 1928: Alfred Merz' Hydrographische Untersuchungen im Bosporus und Dardanelenn. Veröffentlichungen Inst. Meereskunde an der Universitat Berlin, Nue Folge A, Heft 18 Berlin 1928.

11. Pektas, H., 1956: The influence of the Mediterranean Water on the Hydrography of the Black Sea: Technical Papers, 4th Meeting Fisheries Center, Istanbul, 1956.

12. Ullyott, P., and O. Ilgaz, 1946: The hydrography of the Bosporus an Introduction: Geo. Rev., v. 36, no. 1, p. 44–60.

INITIAL DISTRIBUTION LIST

		No. Copies
1.	Department of Oceanography, Code 68 Naval Postgraduate School Monterey, California 93940	3
2.	Prof. J. B. Wickham Department of Oceanography, Code 68 Naval Postgraduate School Monterey, California 93940	3
3.	Prof. R. L. Haney Department of Meteorology, Code 63Hy Naval Postgraduate School Monterey, California 93940	1
4.	Deniz Kuvvetleri Komutanligi Personel Egitim SB. Mudurlugu Ankara, Turkey	1
5.	Dz. Kuvvetleri Seyir ve Hidrografi Dairesi Bsk. Cubuklu, Istanbul Turkey	3
6.	Istanbul Teknik Universitesi Taskisla, Istanbul Turkey	1
7.	Orta-Dogu Teknik Universitesi Ankara, Turkey	1
8.	Oceanographer of the Navy Hoffman Building No. 2 200 Stovall Street Alexandria, Virginia 22332	1
9.	Office of Naval Research Code 480 Arlington, Virginia 22217	1
10.	Dr. Robert E. Stevenson Scientific Liaison Office, ONR Scripps Institution of Oceanography La Jolla, California 92037	1
11.	Library, Code 3330 Naval Oceanographic Office Washington, D. C. 20373	1

12. SIO Library — 1
University of California, San Diego
P. O. Box 2367
La Jolla, California 92037

13. Department of Oceanography Library — 1
University of Washington
Seattle, Washington 98105

14. Department of Oceanography Library — 1
Oregon State University
Corvallis, Oregon 97331

15. Commanding Officer — 1
Fleet Numerical Weather Central
Monterey, California 93940

16. Commanding Officer — 1
Navy Environmental Prediction
Research Facility
Monterey, California 93940

17. Department of the Navy — 1
Commander Oceanographic System Pacific
Box 1390
FPO San Francisco 96610

18. Defense Documentation Center — 2
Cameron Station
Alexandria, Virginia 22314

19. Library (Code 0142) — 2
Naval Postgraduate School
Monterey, California 93940

20. Huseyin Yuce — 1
Dz. YZB
Deniz Harbokulu Egitim Uyesi
Heybeliada, Istanbul
Turkey

21. Lcdr. J. F. Pfeiffer — 1
77 Adams Place
Apt 407
Quincy, Massachusetts 02169

22. Lt. D. Henrickson — 1
Marine Sciences Branch
Commandant (G-000)
U. S. Coast Guard
Washington, D. C. 20591